VENT PROCESSES AND DEPOSITS OF A HIATUS IN A VIOLENT ERUPTION: QUILOTOA VOLCANO, ECUADOR

By Joanne A. Best

A Thesis

Submitted in Partial Fulfillment

of the Requirements for the Degree of

Master of Science

in Geology

Northern Arizona University

December 2010

Approved:

_____

Michael Ort, Ph.D., Chair

_____

Katharine V. Cashman, Ph.D.

_____

Nancy Riggs, Ph.D.

ABSTRACT

VENT PROCESSES AND DEPOSITS OF A HIATUS IN A VIOLENT ERUPTION: QUILOTOA VOLCANO, ECUADOR

Joanne A. Best

The 800 BP eruption of Quilotoa volcano, Ecuador, produced two plinian eruptions separated by a short hiatus. Units 1 and 3 (U1 and U3) of the eruption correspond to the first and second Plinian eruptions, respectively, which produced fallout and pyroclastic density currents. Unit 2 (U2) records processes during the hiatus and consists of three subunits: U2a, U2b, and U2c. This study examines uppermost U1 through to lowermost U3, with particular attention paid to U2, to determine why a dual eruption occurred.

The field relations of the units, and the grain-size distributions, componentry and surficial characteristics of the samples, were investigated. U2a is the product of pyroclastic surges, U2b a fallout unit, and U2c the result of a single vulcanian eruption immediately prior to the onset of the second plinian event (U3). The granulometry study revealed that the units share some common grain sizes, namely the modes at 1.0, 2.0 and 4.0 phi, which indicate a common fragmentation processes for all the units. Common crystal-size populations appear to be the most likely cause of these modal grain sizes. Componentry data show that the units are equally crystal rich. The volume fraction of lithic fragments remained low and the vent and conduit stable, except at the top of U1.

Low glass vesicularity, as determined through the study of the surficial characteristics of the grains, indicate that the gases that drove the eruption of U2b came from depth, and not from the fragmentation of the U2b material itself. U2b is also covered in an orange dust, the product of hydrothermal alteration. Transport processes had a very limited influence upon the characteristics of the deposits, other than a general thinning with distance.

Erosion of the country rock at the top of U1 blocked the conduit and ended the plinian eruption. The period of hiatus, as defined by less explosive, lower volume, discontinuous eruptions, began with the emplacement of U2a surges from the main vent. The vent was eventually plugged with a dome. Gas flux from depth oxidized the U2b material located in a fumarole or secondary vent, which was periodically erupted and deposited as fallout. The accumulation of exsolved gases beneath the dome pressurized the system. The release of this pressure resulted in the vulcanian eruption that produced U2c, and the second plinian eruption quickly ensued, depositing U3.

With a body of eruptable magma at depth, which would later be deposited as U3, the erosion of the conduit was enough to prevent a continued eruption and force a hiatus. This has implications for hazard mitigation, where it is necessary to determine whether a cessation of eruptive activity marks the end of the eruptive event, or is merely a short hiatus prior to a subsequent eruption of substantial magnitude.

ACKNOWLEDGEMENTS

This project was primary funded by a National Science Foundation grant, with additional funding from the Friday Lunch Clubbe.

Many individuals helped make this project possible. Firstly, I would like to thank my advisor Michael Ort for his assistance on this project, Kathy Cashman (University of Oregon) and Nancy Riggs for joining my committee and their valuable input: discussion was always lively, even if we didn‟t all agree!

I am indebted to the rest of the research team, who not only made the field season possible but also immensely enjoyable. Huge thanks to Jorge Bustillos (Escuela Politecnica Nacional, Quito) for being my wingman and tackling those crazy mountain roads, to Patty Mothes (Escuela Politecnica Nacional, Quito) for sharing her knowledge of the area, to Andrea di Muro (Observatoire Volcanologique, Reunion) for his expertise and for making us laugh, and to Mauro Rosi (Universita di Pisa, Italy) for his legendary careful insight in the field.

Once back from the Andes I had extensive support. Thanks to Minard (Pete) Hall (Escuela Politecnica Nacional, Quito) for ensuring first and foremost that I got to take my samples home. Thanks to John Donavan (University of Oregon) and Jim Wittke for training me on the SEM, to Caleb Schiff for getting me started on the Coulter Particle Size Analyser, to Dan Ruscitto (University of Oregon) and Colleen Donegan for their insight and training in the FTIR method, and to Isolde Belien (University of Oregon) for rescuing my samples!

I owe a lot to many more people and here are a few of them. Many thanks to Susan Sabala-Foreman and Meredith Michele Poggi-Jenkins for their departmental

support. You both work immensely hard, helped me navigate a multitude of obstacles, and are the glue that keeps the whole operation together. Thanks to my housemates, Megan Beach, Chris Kassel, and Keri Thornton for their patience with me at the end of each long day, and to my officemates Tenielle Gaither and Rob Ross for putting up with me during work hours! Many thanks to Matt Schmidt for getting me through that first semester, to Colleen Donegan for her wisdom and humour, to Mallory Zelawski for emergency coffees and innumerable rides home, and to the entire department for being my home for the last couple of years.

My final thanks have to go to the cornerstone that is my family. Most live many miles away but they have always encouraged me for as long as I can remember. My greatest thanks to my brother Andrew who has greatly supported me throughout this endeavour, and to my Mum and Dad, two people whom I am very fortunate to have in my life.

TABLE OF CONTENTS

LIST OF TABLES

LIST OF FIGURES

CHAPTER 1

INTRODUCTION AND BACKGROUND

INTRODUCTION

Understanding the progression of volcanic eruptions is crucial for volcanic risk assessment. Observations of recent and historical eruptions indicate that complex eruptive behavior is a common occurrence. For example, Mount Pinatubo"s climactic eruption in 1991 was preceded and followed by a series of smaller eruptions (Wolfe and Hoblitt, 1996), and at the time it was probably not possible to foresee that the larger eruption of June 15 was yet to come.

The Mount Mazama eruption, which produced Crater Lake, had two main phases of activity, the first being the single-vent phase and the second the ring-vent phase (Bacon, 1983). The first phase began with the emplacement of the "climactic pumice fall," which contributed the majority of the material of this first phase. Pyroclastic density currents followed, emplacing the Wineglass Welded Tuff, which was of a smaller volume than the preceding fallout deposit. Based on this transition from larger to smaller volumes, and from convecting columns producing fallout to collapsing columns producing density currents, it would appear that the eruption was waning. However, the collapse of the magma chamber roof instigated the second, ring-vent, phase of the eruption. Pyroclastic density currents from a number of ring vents emplaced tuff more voluminous than the Wineglass Tuff. Therefore, as a result of magma chamber processes, the eruption deviated from a linear trend of progressively weakening eruptions. Instead the eruption had a temporary reduction in activity, when the Wingelass Welded Tuff was emplaced, before the resumption of more vigorous activity.

From these two examples it is evident that eruptions can progress in different ways. Further studies will allow for models of these more complicated eruptive patterns to be produced. It is for this reason that this study examines the deposits of Quilotoa volcano, Ecuador.

Quilotoa erupted c. 800 BP and is notable for its two large plinian events (Di Muro, 2002; Mothes and Hall, 2008), which were separated by a short hiatus. By studying the units of the eruption in terms of field relations, grain-size distributions, grain componentry and surficial characteristics, and the hiatus deposits in particular, it is possible to uncover the processes that led to the two large eruptions. The results of this study reveal one way by which volcanoes can produce dual eruptions.

GEOLOGIC SETTING

The Andes

The Nazca plate is subducting below northern South America at a rate of 5.1 cm/yr and is subdivided into three distinguishable domains (Angermann et al., 1999; Hall et al., 2008). The northernmost section subducts below Colombia at 35°, producing a single volcanic chain. The central section of the Nazca plate is characterized by the Carnegie Ridge, which has been colliding with and affecting the South American continent since 2 Ma (Gutscher et al., 1999). The subduction angle is reduced to 25° as a result of buoyancy generated by the presence of the Carnegie Ridge, and produces the broader volcanic arc of the Ecuadorian Andes (Tatsumi and Eggins, 1995; Hall et al., 2008). In southernmost Ecuador, the Nazca plate dips at 14°, causing volcanism to cease within Ecuador and throughout much of Peru (van Hunen et al., 2002; Hall et al., 2008) (Figure 1.1).

The Ecuadorian Andes extend the length of Ecuador, separating the coastal region to the west from the Amazon Basin in the east. Within Ecuador, the Andes consist of two parallel mountain chains, the Western and Eastern Cordillera (or Cordillera Occidental and Real), which are separated by a 20-30-km-wide series of intermontane basins. Elevations within the Cordilleras typically reach 3500 to 4000 m, with the basins positioned at elevations of 2000 to 3000 m (Hall et al., 2008). The series of intermontane basins taper out southward and the two distinct Cordilleras join to form a single chain south of 2°30‟ S latitude.

The geology of the Western and Eastern Cordillera varies. The basement of the Eastern Cordillera is primarily Paleozoic and Mesozoic metamorphic rocks, in contrast to the Late Cretaceous oceanic basalts and volcano-sedimentary rocks upon which the

Figure 1.1. South American volcanism. The Carnegie Ridge is associated with shallow subduction beneath part of Ecuador, resulting in a broad volcanic arc. The northern, central and southern volcanic zones (NVZ, CVZ, SVZ) are separated by nonvolcanic zones, both attributed to flat subduction (van Hunen et al., 2002; Sruoga et al., 2005). After Sruoga et al., 2005.

volcanoes of the Western Cordillera are situated (Hall et al., 2008). Both chains are characterized by numerous volcanoes, of which a number have been active during Holocene time (Hall et al., 2008).

Quilotoa

Quilotoa Volcano is located within the Western Cordillera of the Ecuadorian Andes in Cotopaxi Province, 11 km north of Zumbagua (Figures 1.2 and 1.3) (Di Muro, 2002). The high point of Quilotoa‟s crater rim stands at 3914 m elevation, with the crater lake situated at 3500 m (Di Muro, 2002; Mothes and Hall, 2008). At present, the area around Quilotoa is drained by three main rivers. The Rio Zumbagua and the Rio Tigua flow southward from the south side of the volcano and then turn to merge into the Rio Toachi north of the confluence (Figure 1.3). Quilotoa‟s eruptive history has produced

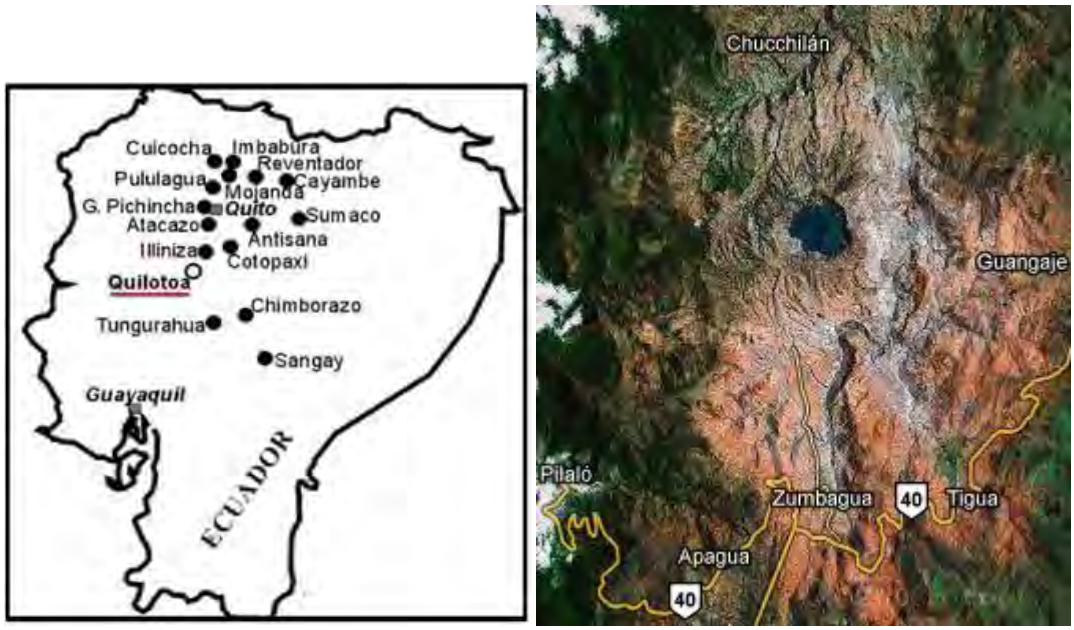

Figure 1.2. Left: map of Ecuador, its major cities (Quito and Guayaquil) and volcanoes. Quilotoa underlined. (Di Muro et al., 2008). Right: satellite image of the region around Quilotoa. Field of view approximately 20 km across. ©2010 Google – Imagery ©2010 TerraMetrics, Map data ©2010 LeadDog Consulting.

voluminous pyroclastic deposits that partially filled the antecedent topography, which produced the flat fertile plains to the north and south of the volcano. Modern fluvial activity has subsequently incised the deposits (Figure 3), which results in deep, steep-sided canyons along the rivers‟ courses.

Quilotoa is a dominantly dacitic volcano that last erupted ~800 ^{14}C years BP. This date is the best estimate as derived from six ^{14}C dates originating from organic material within the deposits and paleosol (Mothes and Hall, 2008). Sometimes referred to as a caldera, Quilotoa is perhaps best described as a volcano of shallowly dipping flanks, at the center of which is a lake-filled depression with no evidence of caldera collapse. Although the lake currently lacks an outflowing stream, the presence of breakout flood deposits and an east-facing scarp indicates that water has breached the crater rim in the past (Hall and Mothes, 2008). Structurally, Quilotoa is located on NE-SW-trending faults, as well as a now-inactive N-S fault (Hall and Mothes, 2008). The emission of gases from the alkaline crater lake has been attributed to activity along these NE-SW faults (Aguilera et al., 2000).

The eruptive stratigraphy of Quilotoa reveals a series of at least eight eruptions, of which the 800 BP eruption (Q-I) is the youngest (Hall and Mothes, 2008) (Table 1.1). The oldest event (Q-VIII) has not been dated. However, 10 m below its base is the 211 ka Chalupas pumice-flow deposit (Hall and Mothes, 2008), hence the age of Q-VIII is certainly <211 ka. The deposits of each eruption filled the valleys of the local drainage system, meaning that outcrops of older material are scarce and difficult to access. The crater is currently filled with water, and the presence of breakout flood deposits shows

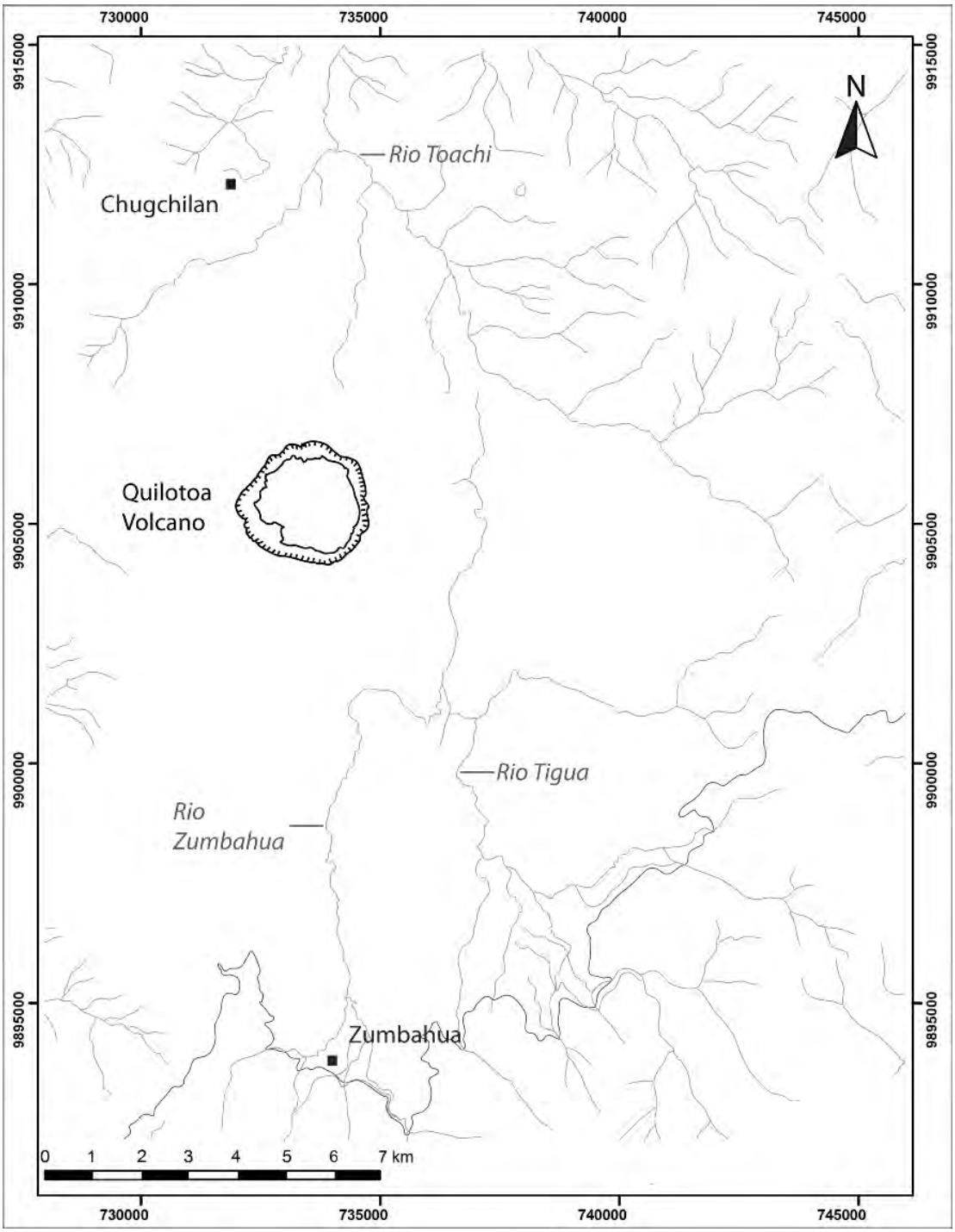

Figure 1.3. Map of Quilotoa and the surrounding area. Three rivers, Rio Tigua, Rio Zumbagua and Rio Toachi, are the main drainages in the area.

Figure 1.4. The stratigraphic succession of the units of the 800 BP eruption. Note the thickness of the eruptive units as exposed in this photograph of an incised valley. Q-I is the 800 BP eruption units, Q-II the 14,770 BP eruption units. Photograph courtesy of M. Ort.

Last eruptions of Quilotoa	
Eruption	**Age**
Q-I	800 yr BP
Q-II	14 770 yr BP
Q-III	unknown
Q-IV	33 700 yr BP
Q-V	>40 ka
Q-VI	unknown
Q-VII	unknown
Q-VIII	unknown
Marker horizon: Chalupas pumice-flow	211 ka

Table 1.1. Approximate dates of the last eight Quilotoa eruptions. (Hall and Mothes, 2008).

that the crater lake was present at a number of times during the past (Hall and Mothes, 2008).

All of the deposits of Quilotoa indicate that plinian eruptions have produced significant volumes of material time and time again. The presence of abundant free crystals in most of the eruptive sequences implies high degrees of fragmentation of a crystal-rich magma (Rosi et al., 2004; Hall and Mothes, 2008). Observations made during the January, 2009, field season show that, in this respect, the 800 BP eruption is similar to its predecessors.

The 800 BP eruption was of a smaller volume than the previous ~14 770 BP eruption (Hall and Mothes, 2008), in that the 800 BP deposits appear to be comparatively limited in extent. The 800 BP eruption deposit comprises four distinct units with a dense rock equivalent (DRE) volume of 4.9-5.5 km^3, based on proximal and medial sites and excluding distal sites (Di Muro et al., 2008).

The deposits of the 800 BP eruption are divided into four units, including two large plinian fallout deposits (Figure 1.5). The base of the 800 BP eruption deposit is marked by a contact with a well-developed black paleosol (Figure 1.5 and 1.6). Unit 1 (U1) lies upon the paleosol and is interpreted to be pyroclastic-fall,-flow and -surge material, with a bulk volume of ~7.5 km^3 (Di Muro et al., 2008). U1 is the thickest of all the four units, with isopach data indicating thicknesses of ~20 cm at a distance of ~21 km from the crater along the dispersal axis (Di Muro, 2002). U2 is a much thinner unit; at 15 km it has a maximum thickness of ~10 cm, a bulk volume of 0.12 km^3 (Di Muro et al., 2008), and can be split into a lower (U2a) and upper member (U2b). In the field, U2a

can be identified by its gray color. It is dominated by fine ash and contains small vitric fragments and oxidized lithic clasts. U2a is approximately a quarter of the thickness of U2b in medial locations, and is much more limited in its spatial extent. U2b is an orange-colored, coarser-grained unit comprising crystals and vitric material, with some oxidized lithic clasts. Ash in U2b is coarser than in U2a but is only a minor component of the unit (Di Muro et al., 2008). Overall, U2b fines upward, but in thicker proximal deposits, subunit-scale fining-upward sequences can be distinguished. U2c is a very thin unit that lies atop U2b. Even in proximal locations U2c thickness is around 2 cm or less. It is

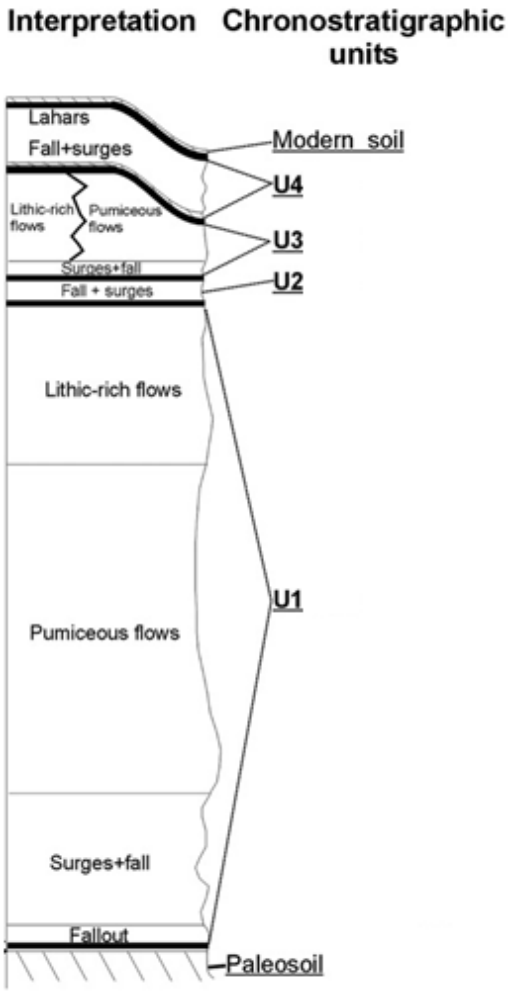

Figure 1.5. General stratigraphic column of the 800 BP eruption deposits. After (Di Muro et al., 2008).

U3 Vitric and crystal lapilli and ash. Lowest subunit is bedded. Next subunit is reverse graded to massive.

U2c Fine ash with vitric lapilli

U2b Alternating coarse and fine, laterally extensive planar beds of vitric and crystal ash.

U2a Alternating coarse and fine planar beds of vitric and crystal ash that pinch out.

U1 Vitric and crystal lapilli and ash. Bedded and matrix supported.

U1 Coarse, vitric lapilli. Massive, clast supported.

Black paleosol

Figure 1.6. The units of the 800 BP eruption, U1 through U3, visible overlying the black paleosol. U4 is the final unit of the 800 BP eruption (not pictured). Each colored interval on the ruler is 10 cm. Inset: vitric fragments are approximately 5 mm in size.

dominated by fine ash, within which vitric lapilli are found. U3 is another thick unit similar to U1 but, at ~1.3 km^3, is smaller in volume. At a distance of 17 km from the vent it has a maximum thickness of ~3 cm. U4 represents further activity that deposited more fall and surge material. As it is not adjacent to U2 and therefore not associated with the hiatus in question, it is not considered in this study. This study focuses on Units 1 through 3 of the 800 BP eruption of Quilotoa and expands upon the unit nomenclature of Di Muro (2002) with the addition of U2c. U2 is the primary focus of this work, with its relation to U1 and U3 situated above and below it also considered.

BACKGROUND: ERUPTION DYNAMICS

The dynamics of the 800 BP eruption are considered in terms of the regions of the eruptive system, in particular the vent and the conduit, as well as the process of fragmentation and the role of water. In this section, these various aspects of eruption dynamics are discussed.

The conduit

For the purpose of this study, controls on eruption dynamics are considered in terms of processes in the conduit upward toward the surface. Numerous models describe the role of conduit processes in controlling the eruption style. For example, the widening of the conduit or the vent, as reflected by an increase in the abundance of lithic fragments (Di Muro et al., 2008), can reduce the eruption velocity (Wilson et al., 1980), which in turn can result in the collapse of the eruption column. It has also been recognized that extended residence times of magma at shallow depths allows for open system degassing to progress (Jaupart, 1998), which, if all else remains equal, makes an explosive eruption less likely.

The vent

Erosion of the conduit and vent area, including any pre-existing domes, is a common occurrence during violent volcanic eruptions. The Soufrière Hills volcano of Montserrat is a contemporary example of this process, where domes are built and subsequently destroyed, sending pyroclastic flows down the flank of the volcano (Herd et al., 2005; Wadge et al., 2010). Lava domes extrude during periods of effusive activity,

and are often destroyed as a result of the resumption of explosive activity (Fink and Anderson, 2000).

The vent area may not be eroded, but instead may collapse. The stratigraphy of the 1991 Mount Pinatubo eruption includes horizons containing abundant lithic fragments, some derived from the destruction of an earlier dome and others attributed to the collapse of the vent that ultimately blocked the conduit and ended the eruption (Scott et al., 1996). At Quilotoa, U2 contains orange-colored lithic fragments (Di Muro, 2002), which may indicate the occurrence of a similar dome or vent-collapse event.

Material that has reached the vent may be immediately ejected once formed, or may remain in the vent region for a time where it may be milled, and possibly sorted, prior to its eruption and emplacement. Grain morphology and surface features can provide clues to the degree of reworking that grains have undergone, as a result of abrasion within the vent or during transport.

Studies of vitric grains have shown that it is possible to relate their morphology to the type of deposit to which they belong, either primary or reworked. Carey et al. (2000) noted that the vitric grains within reworked jökulhlaup deposits lacked the sharp edges of their primary deposit equivalent. Along with smoothing the grain edges, abrasion had damaged the vesicle walls (Figure 1.7) (Carey et al., 2000). Although the environment differs, the mechanical process of abrading vitric shards may equally apply to vent-related processes.

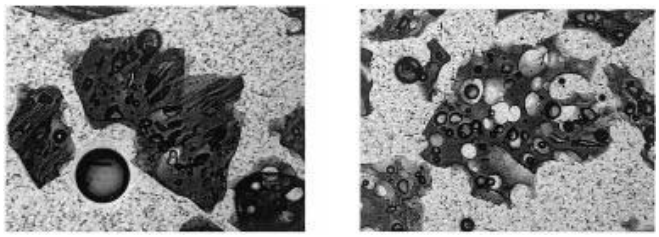

Fig. 1.7a. Primary particles. In these grains sharp edges and vesicle walls are preserved.

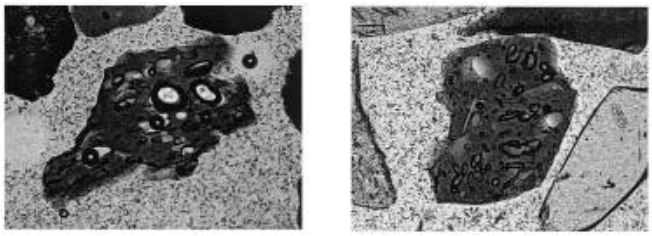

Fig. 1.7b. Reworked particles. Note the rounded edges and the lack of preservation of any delicate features. (Carey et al., 2000)

The deposits of the 1600 AD eruption of Huaynaputina, Peru, are characterized by the presence of crystal-rich layers. The production of these layers has been attributed to pyroclastic flows from a crystal-rich magma that interacted with uneven terrain, which resulted in the separation of the crystals from the finer ash through elutriation of the finer material (Thouret et al., 1999). At Quilotoa, similar crystal-rich layers are seen at the base of U1 and in U2 (Di Muro et al., 2008). For U1, the source is thought to have been a crystal-rich dome that fragmented upon the initiation of the eruption (Di Muro et al., 2008). However, for U2, the preparation of a crystal-rich deposit as a result of sorting within the vent, instead of as a result of transport, is proposed.

At Quilotoa the orange staining seen on lithic fragments, as well as on some crystals and a few grains of glass, is likely the result of hydrothermal alteration (Di Muro, 2002). Hydrothermal activity occurring within a vent may be enhanced by the exsolution

of volatiles from the magma body below. At Huaynaputina, the alteration of glass and lithic fragments was also attributed to hydrothermal activity (Thouret et al., 1999). Evidence of water interaction was observed there, but U1 to U3 of the 800 BP eruption of Quilotoa appear to be dry (Di Muro et al., 2008).

Fragmentation

Characterizing the grain-size distribution of pyroclastic deposits is one method by which to investigate the dynamics of an eruption. The deposits of explosive eruptions are dominantly fine grained (Büttner et al., 1999). Fine-grained material is produced by fragmentation, in many cases aided by magma-water interaction. However, phreatomagmatism is not required to produce deposits rich in fine material; they can be found in "dry" plinian deposits as well (Figure 1.8) (Zimanowski et al., 2003).

Brittle fragmentation has been experimentally identified as the likely mechanism for the production of fine ash, where 50 to 1000 times more energy is required to produce fine ash (<64 μm) compared to coarse ash (64-200 μm) from an equivalent body of magma (Zimanowski et al., 2003). Therefore the volume of fine ash produced can be used as a proxy for the explosivity of an eruption, and so obtaining reliable measurements of the fine ash portion is necessary to better understand the dynamics of the eruption. The secondary mechanism of milling as a source of fine ash must also be considered, where milling, either within the vent or pyroclastic density current, can reduce particle size (Rose and Durant, 2009).

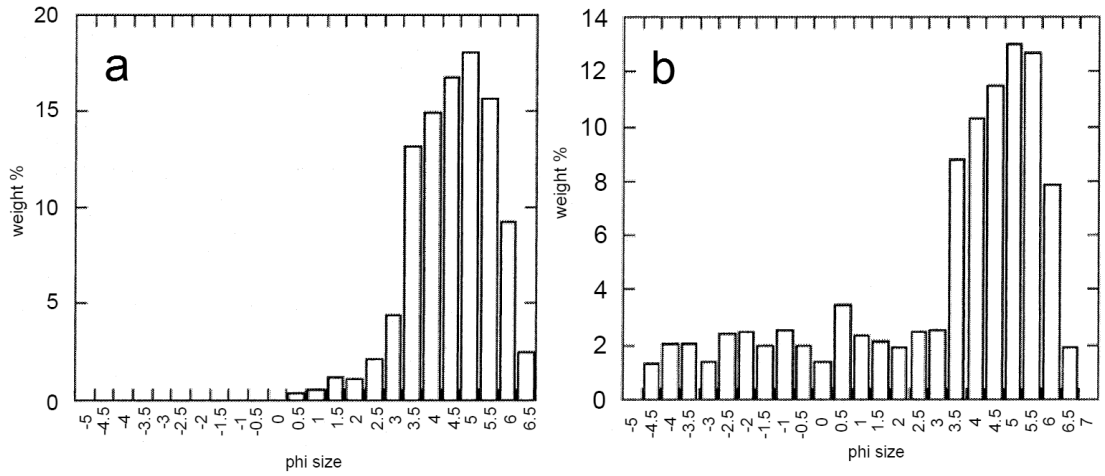

Figure 1.8. The grain-size distributions of the fine ash layer from deposits of (a) phreatomagmatic origin (b) plinian origin. Note how, in both cases, a significant proportion is fine grained, but only in the case of the plinian deposit is coarser material also present, resulting in a wider distribution. After Zimanowski et al. (2003).

Information on the fragmentation processes is primarily carried by the fine grain sizes (Büttner et al., 1999). Büttner et al. (1999) experimentally reproduced the grain shapes and sizes that occur naturally, but they also noted that the artificially produced materials were poor in fine grains in comparison to the grain-size distribution of the natural deposits. The authors inferred that many of the fine grains seen in the natural deposits were the product of particle abrasion during transport. This alternative source of fine grains, alongside those sourced by milling, needs to be considered when using the volume of fine material to infer the explosiveness of an eruption.

The role of water

As discussed in the previous section, the presence of water can assist in driving fragmentation that in turn can lead to particularly explosive eruptions. The 2010 eruption of Eyjafjallajökull in Iceland is one such example. The presence of during an eruption is

recorded in the surface characteristics of grains such as blocky grains, with surface cracks produced by sudden quenching within a water-rich environment (Figure 1.9) (see Chapter 2).

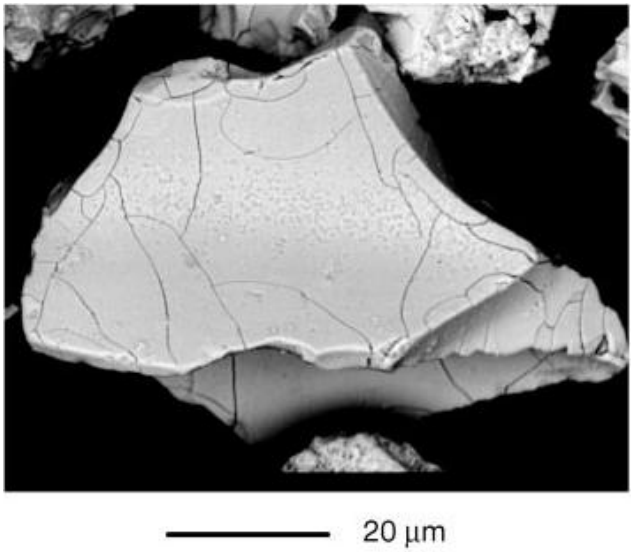

Figure 1.9. A grain exhibiting quench cracks. The equant shape, however, can be seen in grains formed in both wet and dry environments. (Büttner et al., 1999)

BACKGROUND: TRANSPORT PROCESSES

The Plume: grain-size distribution

A plinian eruption plume can be broadly divided into three parts: the jet phase, convective phase, and the umbrella region (Figure 1.10). The jet phase region lies directly above the vent and propels the ejected material skyward, driven by the kinetic energy of the eruption, derived from the exsolution of volatiles from the magma. As the eruption continues, the vesiculation and fragmentation fronts move deeper within the conduit (Mader, 1998). The rapid decompression of the system means that velocities within the jet phase region are high, on the order of 100s m/s. It is within this region, therefore, that the largest clasts are transported (Carey and Sparks, 1986).

The convective and umbrella regions are buoyancy-driven (Valentine, 1998), whereby ascent of the plume continues as long as it is less dense than the atmosphere (Mader, 1998). Buoyancy is achieved as long as the rising eruption column is hot, compared to the surrounding cold air. As a result the buoyancy of the plume changes spatially, as well as temporally. These shifts in buoyancy mean that most of the sorting of material occurs within the convective and umbrella regions. The convective region largely transfers material vertically whereas, within the umbrella cloud, once the level of neutral buoyancy is reached (H_b in Figure 1.10), particles are transported laterally until

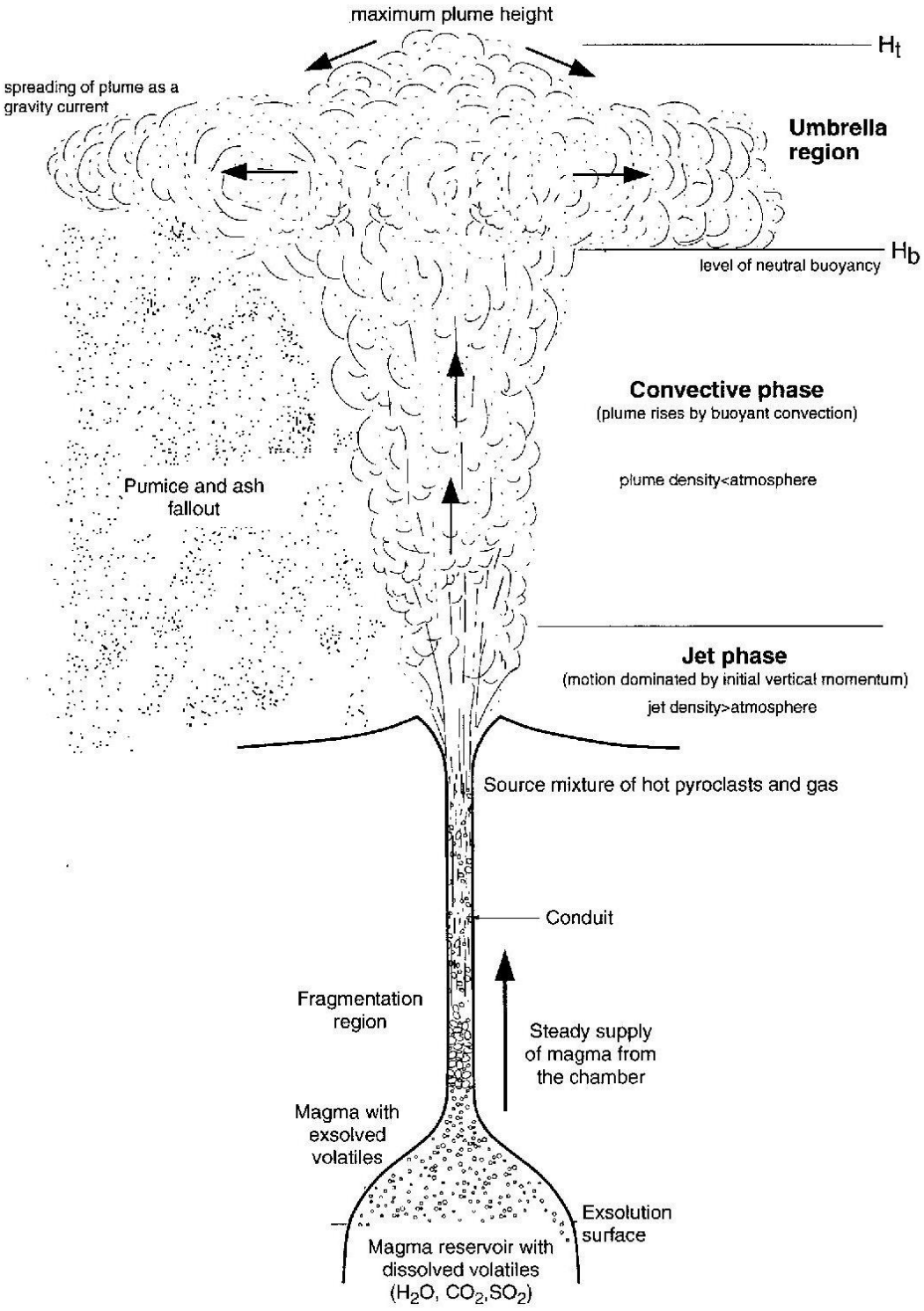

Figure 1.10. Model describing the formation of a volcanic plume. (Carey and Bursik, 2000)

they fall out of suspension once their fall velocity exceeds the lateral velocity of the umbrella cloud (Rosi, 1998).

The two main influences on the grain-size distribution of fall deposits from a plinian eruption plume are the grain size of the initial population (Walker, 1971; Sheridan et al., 1987) and the effect that settling velocities have on sorting within and beneath the umbrella cloud (Walker, 1971). The largest blocks, initially carried within the jet region of the plume, quickly fall once ejected from the vent. Fragments around 1 cm to 10 cm in diameter are entrained within the convection column but once the turbulent flow carries them to the margins of the column, where convection-driven buoyancy is reduced, they descend and are deposited. Particles finer than 1 cm in diameter tend to be entrained within the convective column and transported laterally into the umbrella cloud with the finest particles carried farthest downwind before falling out of suspension (Rosi, 1998). Thus, a negative grain-size trend with distance is usually attributed to sorting occurring as a result of transport processes.

The typical grain-size distribution of fallout exhibits a decrease in median grain size, decrease in maximum clast size, and an increase in sorting with distance from the vent. Unimodal grain-size distributions are common, due to the sorting of the deposit occurring in one location, the plume. Layer C, the most voluminous of the Mount Pinatubo horizons, exhibits such grain-size trends (Paladio-Melosantos et al., 1996).

In their study of Huaynaputina, Adams et al. (2001) noted that, within 34 km of the vent, the modal grain-size of material was 1.0 phi. At 100 km distance, however, whether the sites were located on or off the dispersal axis affected the modal grain size. At this distance, the modal grain size was 2.0 phi along the dispersal axis and 3.0 phi off

the axis. This broadly illustrates the degree to which plume-based transport influences the grain-size distribution of deposits.

The relation between grain size and distance from the vent can be more complex. Particles that fall out of suspension may be re-entrained within the plume or column (Bursik, 1998). Secondary intrusions, appearing as smaller, lower-level, umbrella regions, may form (Holasek et al., 1996), and thus complicate the deposition pattern originating from the plume. Such secondary intrusions were observed at the 1980 Mount St Helens and 1990 Mount Redoubt eruptions (Holasek et al., 1996).

Fine-grained deposits

The classic model of an ignimbrite sequence (Sparks et al., 1973) includes an upper horizon of fine ash that settles out of atmospheric suspension once eruptive activity has ceased. The identification of such a unit can therefore be used to delineate discrete phases of an eruption. At Mount Pinatubo this, along with other criteria, has been used to define individual pyroclastic fall and flow units (Paladio-Melosantos et al., 1996; Scott et al., 1996). In the case of Mount Pinatubo a notable proportion (10 wt %) of the sample was less than 4.0 phi in size. The authors attributed this to the addition of material from ash clouds, or through rain passing through the eruption plume and driving the fine material out of suspension (Paladio-Melosantos et al., 1996).

Alternatively, a fine upper unit may be co-ignimbritic in origin. A co-ignimbrite column is a secondary feature that originates from a pyroclastic density current as a result of the elutriation of fine material from the main flow due to the turbidity of the flow (Bursik, 1998; Woods, 1998). If the beds underlying the fine units are depleted of fine material the deposit is from a co-ignimbrite column (Woods, 1998), whereas if the

underlying beds are not lacking fine material this horizon is likely the result of the gradual clearing of the air after the cessation of the eruption.

Co-ignimbrite deposits have been found at Huaynaputina (Thouret et al., 1999), Mount Pinatubo (Woods, 1998), Taupo (Wilson and Walker, 1985), Toba (Woods, 1998), and in U1 at Quilotoa (Di Muro et al., 2008). Therefore, fine horizons must be carefully evaluated and their source determined before inferences can be made about the progression of the eruption.

The Plume: componentry

The shape, size and density of grains determines the way in which they are sorted (Taddeucci and Palladino, 2002). In the broadest terms, the components of a pyroclastic deposit can be split into lithic, glass and crystal fragments (Walker, 1971). The density and shape of different minerals may influence their settling velocity.

Within the fall deposit "Layer C" of Mount Pinatubo‟s 1991 eruption sequence, glass is the dominant component at grain sizes of 0 phi (1 mm) and greater, crystals are the majority at grain sizes between 0 phi and 2 phi (1 mm to 0.25 mm), and no grain-size relation is observed for the lithic fragments (Paladio-Melosantos et al., 1996). The same trend of crystals becoming more dominant than glass at smaller grain sizes to around 63 μm (4 phi) is also observed at Huaynaputina (Adams et al., 2001), Soufrière on St. Vincent (Hay, 1959), and Vesuvius (Rolandi et al., 1993).

Depositional processes

Particles within a pyroclastic density current can travel through traction, saltation, or a combination thereof. The various modes observed within the grain-size distribution

of a deposit may be attributable to the specific method of transportation (Sheridan et al., 1987; Wohletz et al., 1989; Orsi et al., 1992), since transport is a function of grain size. For surge and flow deposits, the coarsest modes represent ballistic clasts, in the next mode grains are transported by traction, the next mode by saltation, and then the finest grains are transported in suspension (Sheridan et al., 1987; Orsi et al., 1992). For fallout, modes relate only to the transport of ballistics and the suspension of grains (Wohletz et al., 1989).

Other studies, however, have challenged the significance of transport and depositional processes in influencing grain-size distributions (Gómez-Tuena and Carrasco-Núñez, 1999; Dellino et al., 2001). For example, where the grain-size mode does not vary with distance from the vent, the initial characteristics of the deposit, such as grain type and size (Gómez-Tuena and Carrasco-Núñez, 1999), are the reason for the consistency in modal grain size and the resulting grain-size distribution.

As previously mentioned, the shape of grains can indicate the type of processes that have taken place. Grains found within density current deposits are potentially subject to much greater abrasion than fall deposits. That abrasion will round the grains (Figure 1.7) so that, even if evidence of transportation is not apparent from the grain-size distribution data, the grain morphology will record the process.

THIS STUDY

Outline

This study examines the deposits of the most recent (c. 800 BP) eruption of Quilotoa volcano, which produced two large Plinian eruptions. Unit 1 (U1) and Unit 3 (U3) of the eruptive sequence are the deposits of the first and second Plinian eruptions, respectively. The emplacement of U1 and U3 was separated by a quiescent period. Unit 2 (U2) comprises the material produced and emplaced during this hiatus. The aim of this study is to elucidate the processes that led to the cessation of the first plinian eruption and then the occurrence of the second plinian eruption after a short time. The deposits of U2 should record the processes that occurred leading up to the second eruption, and therefore are the main focus of this study.

The length of the hiatus is inferred by the presence of an oxidized upper U1 surface that is observed in some localities, indicating that the surface was exposed for some time prior to the emplacement of U2. The presence, beneath U2, of deposits from phreatic blast out of the U1 ignimbrite (Di Muro et al., 2008) indicates that there were at least a few days between the emplacement of U1 and U2. Considering that strong seasonal rains are a characteristic of this locale, a hiatus of longer than about 6 months would be reflected in the erosion of U1. However, the lack of extensive erosion at the top of U1 (Di Muro et al., 2008) indicates that the period of exposure was somewhat limited, thus allowing for a postulated hiatus duration on the order of weeks to months.

The deposits of U2 are described in order to elucidate the volcanic and magmatic processes that occurred during the hiatus and produced the unit. In addition, a study of upper U1 and lower U3 illuminates the processes that drove the complete sequence of events.

The eruptive stratigraphy is studied to determine the change in style of activity as the eruption progressed. Of particular interest are the conditions under which U2 was emplaced. In addition to this temporal aspect of the eruption, isopach maps are used to determine how the extent of the units U2a, U2b and U2c vary. These trends are interpreted in terms of topography, wind direction and eruption explosivity.

The granulometric study considers the explosivity of the eruption in more detail, with particular attention paid to the proportion of fine-grained material within each unit. Grain sizes are ascertained and considered in terms of eruptive and depositional processes in order to determine which group of processes controls the characteristics of the deposits seen. Componentry of the deposits is considered in terms of the distance from the vent.

Finally, the shape and surface characteristics of the grains themselves are examined. Grain shape is quantitatively analyzed to determine whether grains have been abraded, either in the vent or during transport. The surface textures and features of the grain are also considered, such as the presence of orange staining that is likely the result of hydrothermal activity (Di Muro, 2002). Analysis of surface textures can reveal evidence of chemical pitting, which, alongside the presence of stained or coated grains, could indicate hydrothermal alteration. The presence or absence of juvenile or recycled material is important for understanding the driving forces, and limitations, of the eruptions.

This study is part of a larger effort intended to understand the processes that occurred during the hiatus at Quilotoa.

Significance

At Mount Pinatubo, the climactic eruption was preceded by a series of smaller eruptions (Wolfe and Hoblitt, 1996). Volcanic eruptions elsewhere have been known to consist of separately identifiable events, such as the various phases of the Mount Mazama eruption (Bacon, 1983; Wolfe and Hoblitt, 1996). Therefore, an understanding of the conditions under which a pause in activity can take place is critical in evaluating the probability of two temporally close eruptions occurring. Knowledge gained from studying the processes that resulted in this event at Quilotoa can be used as a framework within which similar occurrences, both at Quilotoa and at other volcanoes, can be investigated.

Field observations at Quilotoa show that the 14,770 BP eruption may have behaved in a similar way to the 800 BP event. It too is composed of two voluminous deposits separated by a lithic and crystal lapilli- and ash-rich unit that is similar in appearance to U2 of the 800 BP eruption (Figure 1.11). Therefore the findings from this study may have implications for earlier, and possibly future, activity at Quilotoa.

Although Quilotoa is not as frequently active as a number of Ecuadorian volcanoes, it is worth noting that the 800 BP eruption permanently displaced the local population (Hall and Mothes, 2008). The deposits of the 800 BP eruption of Quilotoa had a bulk volume of 27 km^3 (Di Muro, 2002). This is significantly greater than the ~8.5-10.5 km^3 estimate for the 1991 Mount Pinatubo eruption (Paladio-Melosantos et al., 1996), and so the 800 BP eruption of Quilotoa was certainly a significant event.

Being able to identify a hiatus, as opposed to a cessation of activity, has implications for volcanic hazard mitigation at any volcano. Hence this study adds to the understanding of this dual-eruption phenomenon and allow for the identification of previously unknown examples at other volcanoes.

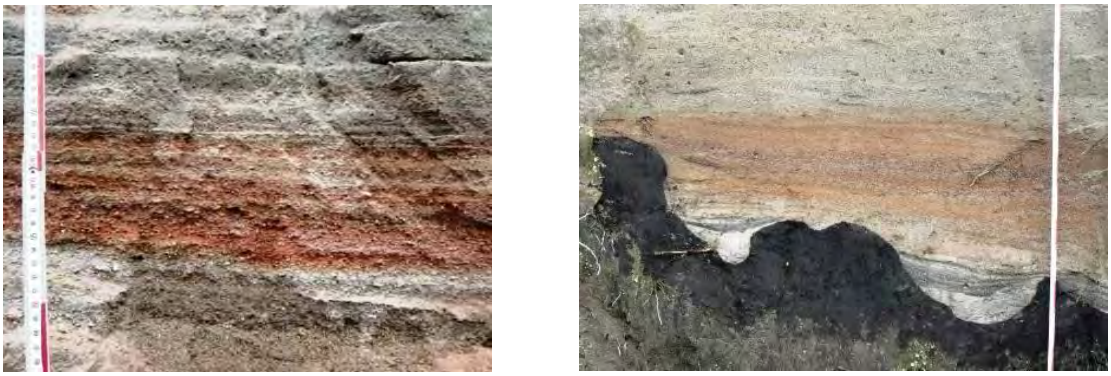

Figure 1.11. The "U2" of the 14 770 BP eruption (left) is remarkably similar in appearance to U2 of the 800 BP eruption (right). It may indicate that activity typified by two large plinian eruptions has occurred more than once at Quilotoa.

CHAPTER 2

METHODS

This research project has two main aims. The first is to fully characterize U2 and its subunits U2a, U2b and U2c. The second is two-fold: to infer a likely production mechanism for U2, and then to investigate how U2 relates to U1 and U3 in terms of the evolution of the eruption. A number of methods were employed in order to meet these research targets. Laboratory analysis was conducted in facilities at both Northern Arizona University (NAU) and University of Oregon (UO).

FIELDWORK

Previous work

The deposits of Quilotoa have been the subject of a number of studies (Di Muro, 2002; Rosi et al., 2004; Di Muro et al., 2008; Hall and Mothes, 2008; Mothes and Hall, 2008). The work of Di Muro (2002) includes field descriptions, grain-size and componentry data of the units of the 800 BP eruption, with a particular focus on U1. This study expands upon the information relating to U2, its subunits U2a and U2b, and additionally recognizes U2c.

Site selection

The deposits of previous eruptions from Quilotoa partially filled the valleys that flank it, creating a flat plain after each eruption that would then be deeply incised by rivers. The valleys are many hundreds of meters deep now, exposing thick, inaccessible sections of ignimbrites. These conditions make accessibility a major control on the sites

that can be visited, and therefore localities are predominantly road cuts, in addition to a few valley and hillside sites.

Fieldwork was conducted in January 2009 over a period of fourteen days. Units were described, stratigraphic sections measured and samples collected. A total of 37 sites were visited (Figure 2.1), at 30 of which the thickness of the units of the 800 BP eruption was measured and described. In addition, one exposure of the deposits of the 14,770 BP eruption was visited and sampled. Locality distances from the crater were measured from the center of the crater, which itself is 2.9 km in diameter (Hall and Mothes, 2008).

Sample collection

In the field, fresh exposures were obtained by scraping away the outermost layer with shovels and trowels, in order to aid unit identification. Locations were recorded on a handheld GPS unit, and unit thickness and descriptions were noted prior to sampling.

Uppermost U1 and lowermost U3 were sampled in order to bracket U2 and therefore allow inferences to be made concerning the progression of the eruption. U2 was described and sampled as subunits U2a, U2b and, where possible, U2c. A flat trowel was used to first demarcate the limit of the target horizon, and then to carefully remove the sample. In some locations, U2c was identified but was too thin to be cleanly separated from U2b and U3, and so, at localities 13 and 34, U2c was collected as part of the U2b sample.

In some places where the deposits are thicker, variations within the units were observed. For example, at some locations, U2b is characterized by a series of normally graded beds and the different parts of the unit were therefore sampled separately. Locality 17 has the thickest deposits, of which 735 cm was described and sampled. In

this case, the composite stratigraphic section were divided into subsections, depending on the similarity of the beds, or reflecting parts of the sequence bordered by post-depositional erosion.

In this thesis, samples are referred to by the label given to them in the field, which allows them to be uniquely identified.

L. 13 indicates that the *locality* number is 13,

C (for locality 17, a composite section) denotes the *subsection* the sample came from,

iii roman numerals are given to each sample *interval*. They tie into sketches, descriptions and avoid the implications of using an interpretation (such as U2b) as a descriptive tool.

In order to obtain maximum spatial coverage during the time available, samples were taken from 25 of the 30 sites where unit thickness was measured. In total, 152 samples were collected, including 147 individual tephra samples from 24 sites, and five samples that include one dome rock, one ballistic fragment, and three bulk unit samples for laboratory experiments carried out by other members of the research group.

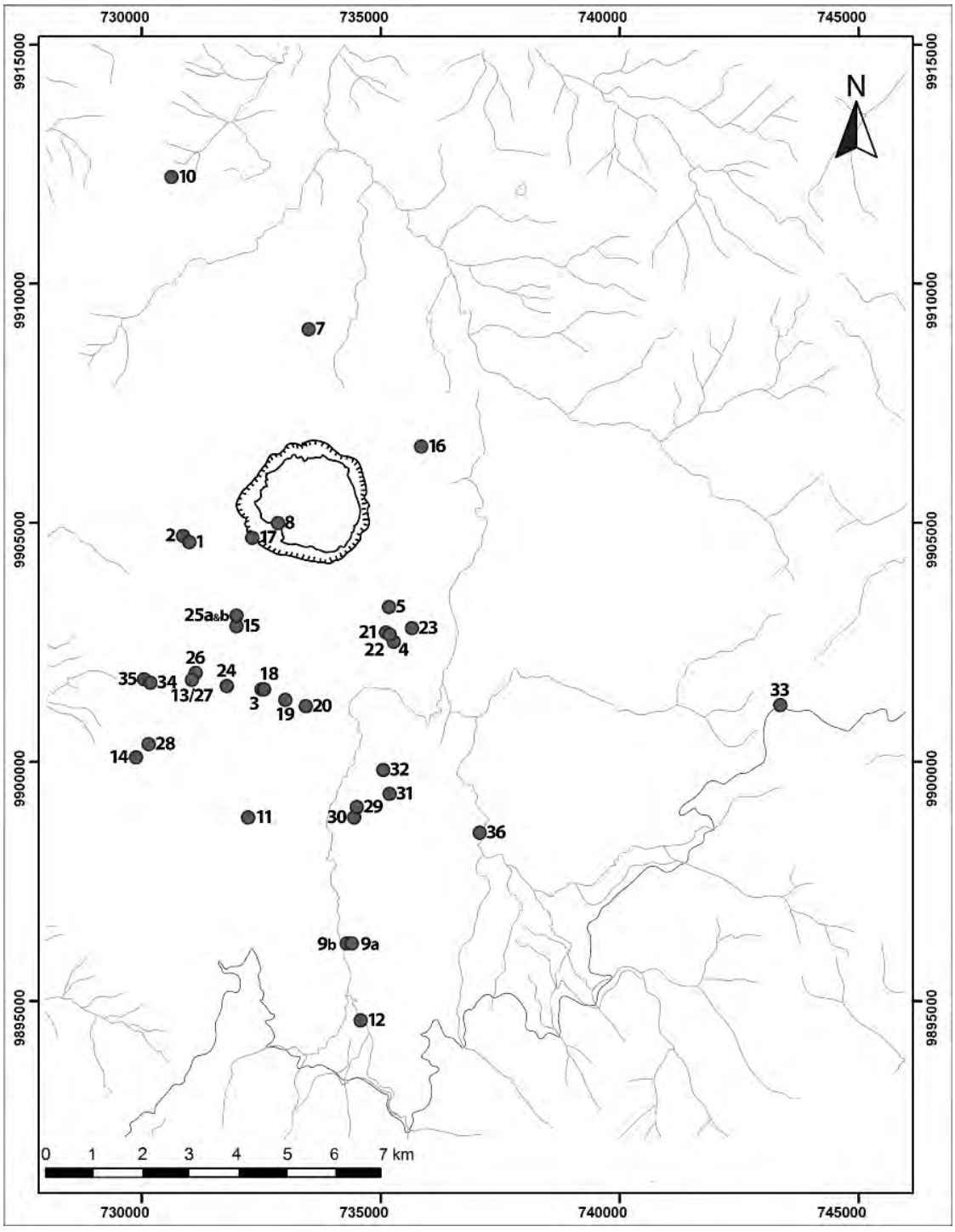

Figure 2.1. Visited localities. Gray circles correspond to all locations visited.

GRAIN-SIZE DISTRIBUTION

Previous work

In most tephra granulometric studies, the grain-size distribution of the sample is obtained though dry sieving (Walker, 1971; Orsi et al., 1992; Gómez-Tuena and Carrasco-Núñez, 1999; Adams et al., 2001; Di Muro, 2002). At small grain sizes (4.0 phi and below), the data this method yields are unreliable (Adams et al., 2001). Therefore in this study, a Coulter particle-size analyzer was used to obtain data on this finer portion.

Dry sieving

The samples were dried before sieving. Sample bags were open to Flagstaff's semi-arid climate for two months, during which time they were occasionally gently mixed to ensure that damper material near the base was exposed to the top of the bag. Larger samples were poured into trays to dry and periodically stirred to expose all material to the air in order to facilitate drying.

A total of 80 samples from 19 sites were chosen for laboratory analysis. Their selection was based on the units from which they came, with particular emphasis on U2, and their location, in order to ensure good spatial coverage of the area.

Samples were dry-sieved using a Soiltest sieve shaker at NAU. Sieves ranged from -6.0 to 4.5 phi in size, with sieves at half-phi intervals and a pan collecting grains <4.5 phi in size. Samples were sieved for five minutes in order to allow all the fine material to pass through. This sieving interval was determined after a series of test runs of varying duration. Each size fraction was weighed to the tenth of a gram.

Coulter particle-size analyzer

A Coulter particle-size analyzer at NAU was used to extend the grain-size distribution data to include the fraction of the sample between 4.5 and 10 phi in size. Twenty-nine samples, those with a significant proportion of fine-grained material (10 wt % or greater of total sample) below 4.5 phi (the „pan fraction"), were chosen for analysis by this method.

For small samples in particular, the amount of material in the pan fraction was limited. To work around this, a blend of three equal parts of grains at <4.5, 4.5 and 4.0 phi was used in order to have enough material for the Coulter analyzer to detect. In a few cases in which the sample was particularly low in volume, this blend included 3.5-phi grains. Test runs showed that no particle dispersal liquid was required to disaggregate the samples, and so small amounts of the dry sample were added to the machine and the grain-size data were downloaded to the computer. The data were then converted from microns to phi, in order to correspond to the sieve data and the SFT program (see Analysis), and grouped into half-phi intervals.

Data from the Coulter analyzer are given as a percentage of the total volume of the sample. Volume and mass are both related to grain size. Therefore volume percent, like mass percent, can be used to indicate the proportion of a sample that falls into a particular grain-size category. At such very small grain sizes (<4.5 phi or <44 μm) the different percentages mass and volume data may determine are negligible: with respect to grain size they function similarly.

Analysis

Prior to beginning analysis, the two data sets, one from sieving and one from Coulter analysis, had to be combined. The sieve data give the percent of each sample corresponding to each half-phi size interval for sizes larger than 4.5 phi, inclusive, with the pan fraction, smaller than 4.5 phi, given as a single figure but encompassing many phi sizes. The Coulter data give the percent of each sample corresponding to each half-phi size interval on grain sizes smaller than 4.5 phi. Both data sets were recorded in Microsoft Excel spreadsheets. From the sieve data, the weight percentage of material smaller than 4.5 phi is known. The Coulter data were then normalized to the weight percent of the sample corresponding to grains smaller than 4.5 phi, the pan fraction, meaning that both the sieve and Coulter data were now using the same reference. Then the two data sets were joined.

The next step was to enter the normalized data into SFT software (Wohletz, 2007). Selecting *analyze* in the program converts the histogram to a smoothed line graph. Estimates of the modal grain size of up to six subpopulations, based on where the visible peaks fell along the single line graph, were entered. *Optimize* then runs the program so that it fine-tunes the modes in terms of their distribution and phi size. The result is a series of modeled modes that, combined, closely match the natural grain-size distribution. The quality of the fit is reported and, in this study, the best model was determined to be that which produced the lowest sum of the squares of the residuals.

The purpose of using SFT to identify modes is that it recognizes subpopulations that visual observations may miss (Figure 2.2). It works on the assumption that, like sedimentary materials (Inman, 1952), each sample exhibits a broadly Gaussian distribution. This methodology has been successfully applied in other studies of

pyroclastic deposits (Orsi et al., 1992; Gómez-Tuena and Carrasco-Núñez, 1999; Taddeucci and Palladino, 2002). This study looks at the mean grain-size distribution curves for each unit created using the composite function in the SFT program, (Appendix 4.2), to identify common modes for each unit. These data allow the units to be characterized in terms of grain size, and thus compared throughout the sequence. Additionally, the modal grain size of the units was used to define the targets for the componentry study.

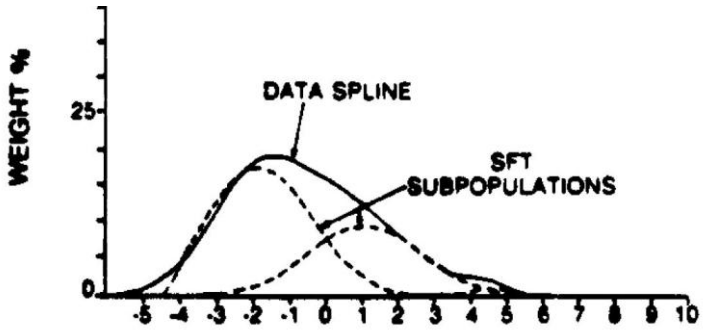

Figure 2.2. An example data set, illustrating how SFT can be used to identify two otherwise hidden subpopulations. (Wohletz et al., 1989)

SFT also provides average grain size and sorting data. Use of these Figures is again based on the assumption that the data broadly resemble a Gaussian distribution. The use of median grain size (Inman, 1952) has limitations when considering samples with bi- or polymodal distributions, which deviate from the Gaussian curve. Therefore the graphic mean (Folk, 1974) is used here. The graphic mean is calculated by taking the sum of the size of the grains of sample at the 16^{th}, 50^{th} and 84^{th} percentile and dividing by three. These percentiles bracket 68 % of the sample, which increases the chance of encompassing the peaks of bi- and polymodal samples, so the resulting graphic mean grain size better represents the sample than the median grain size.

Sorting data are also calculated by SFT, in terms of the inclusive graphic standard deviation (Folk, 1974). Ninety percent of the sample, located between the 5th and 95th percentiles, is incorporated into the calculation. The classification scheme applied to the sorting values from sedimentary samples is given in Table 2.1. Volcaniclastic deposits have a wider range of textures and densities than sediments, which results in a comparatively lower degree of sorting (White and Houghton, 2006). Also, a sample that is considered well sorted in volcaniclastic terms may be considered poorly sorted in sedimentological terms, since volcaniclastic rocks are rarely sorted by the efficient process of water, but instead by internal flow or suspension in the atmosphere.

Inclusive Graphic Standard Deviation (Sorting)	
Grain-size range(phi)	
<0.35	Very well sorted
0.35 - 0.5	Well sorted
0.5 – 0.71	Moderately well sorted
0.71 – 1.0	Moderately sorted
1.0 – 2.0	Poorly sorted
2.0 – 4.0	Very poorly sorted
>4.0	Extremely poorly sorted

Table 2.1. Sorting, as determined by the range of grain sizes within 1 standard deviation of the median grain size distribution. (Folk, 1974)

Inclusive Graphic Standard Deviation (Sorting)	
Grain-size range(phi)	
0.5 – 1.0	Well sorted
1.0 – 2.0	Moderately sorted
2.0 – 4.0	Poorly sorted
>4.0	Very poorly sorted

Table 2.2. Sorting parameters used in this thesis, as determined by the range of grain sizes within the 5th and 95th percentile (Folk, 1974).

Therefore, a classification scheme for sorting in volcaniclastic samples is proposed here (Table 2.2) and applied to this thesis, whereby the terms of Folk (1974) are attributed to materials one bracket lower in the sorting scale.

COMPONENTRY

Previous work

Componentry has been used to characterize deposits at a number of volcanoes, including Mount Pinatubo (Paladio-Melosantos et al., 1996) and Huaynaputina (Adams et al., 2001). The componentry of U1 at Quilotoa is described in Di Muro (2002) and Di Muro et al. (2008) in terms of pumice, crystals and lithic fragments. These criteria are commonly used in other studies (Walker, 1971; Rolandi et al., 1993), and are expanded upon here with the addition of holocrystalline fragments and glass-crystal-aggregates, and through the separation of felsic and mafic crystals (Taddeucci and Palladino, 2002), and, for one representative locality, quartz, plagioclase feldspar and potassium feldspar.

Sample selection

Seven sites were selected for the componentry study. One aim of this work was to examine trends in componentry in terms of distance from the vent. Therefore, the seven sites selected were located between 2.5 km and 7.5 km from the vent. In total, 101 samples were analyzed.

Process

The samples were analyzed at preselected grain sizes. The -2.5, -1.0, 1.0, 2.0 and 4.0 phi grain sizes were chosen because they are the modal sizes of the subpopulations of

the units, as determined by the grain-size distribution work. In addition, 0.0 phi grains were analyzed. The 0.0 phi size is a trough on the grain-size distribution curves, but was included in order to examine whether the grains of -1.0 and 1.0 phi were related to each other, as would be seen with a trend that holds across all three grain-sizes, or have separate sources. Grains were placed in a Petri dish and rinsed with tap water to remove surficial dust in order to aid identification. For each sample, a set of at least 200 grains was separated into the various component types using a binocular microscope.

Grain classification

The three main classes of grain are glass, crystal and lithic fragment. An additional "other" category includes holocrystalline fragments and glass-crystal aggregates (Figure 2.3). For all grains, it was noted whether or not they were coated in an orange stain, which could indicate alteration.

Glass includes pumice at the larger grain sizes, and shards at the smaller end of the range. Glass is categorized based on color, with white and grey being the most common, and brown and pink glass additionally recognized.

Of the mafic crystals, biotite and magnetite are easily identifiable, with the remaining mafic minerals being either pyroxene or amphibole. The felsic minerals include quartz, plagioclase feldspar and potassium feldspar, which, with the exception of a case study at a single locality, will not be distinguished due to the time-consuming nature of identification.

Holocrystalline fragments are also seen, as are lithic fragments, which are commonly stained orange. Glass-crystal aggregates are composed of fragments of crystal and glass, commonly of more than one color, stuck together with fragile glass. In

addition to these classifications, the presence of adhering glass was noted. A crystal with adhering glass is defined as one in which at least 50% of the entire grain is a mineral. The componentry data are represented as a series of bar charts, and combined with grain-size distribution data in order to examine spatial and temporal trends.

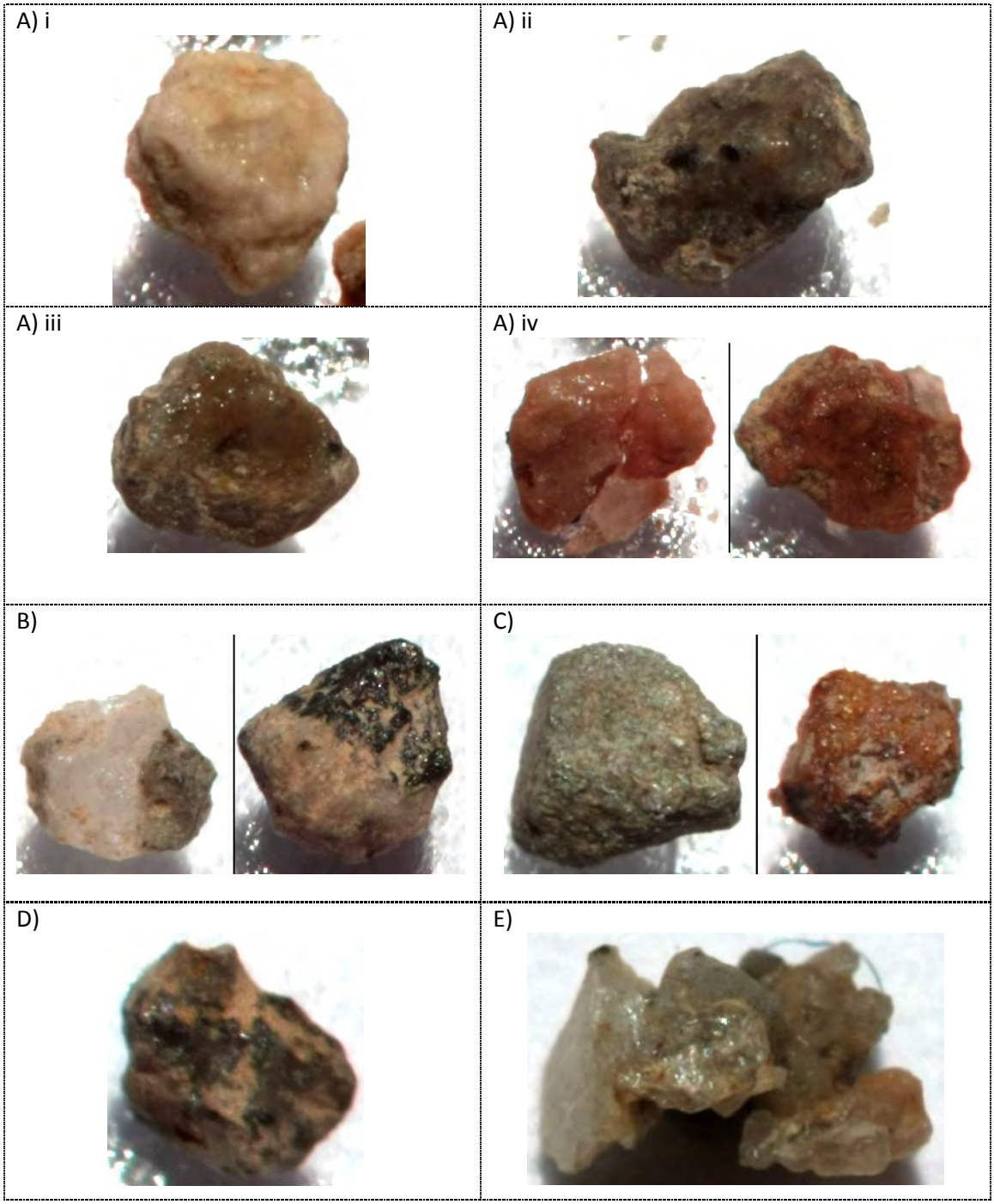

Figure 2.3. Components of the Quilotoa tephra. A) Glass, i – white, ii – grey, iii – brown, iv – light and dark pink. B) two crystals with adhering glass. C) non stained and stained lithic fragments. D) Holocrystalline fragment. E) Glass-crystal aggregate.

GRAIN MORPHOLOGY AND SURFICAL CHARACTERISTICS

This part of the study examines grain shape, texture, and staining and coating. These characteristics can be used to infer the conditions and processes that were operating at the vent and during the transport and deposition of the grains. These data, in concert with field relations, componentry and grain-size distribution information, allow for the comprehensive description of U2.

Previous work

Grain shape

The assessment of grain shape is commonly carried out in order to describe phreatomagmatic products, or to distinguish between those and grains of magmatic origin (Dellino et al., 1990; Dellino and La Volpe, 1996; Hooten, 1999; Dellino and Liotino, 2002; Austin Erickson, 2007). Blocky grains and shards are generally associated with magmatic eruptions (Dellino and La Volpe, 1996). Blocky grains with surface cracks and other features resulting from interaction with water (Dellino et al., 1990; Büttner et al., 1999), as well as moss-like shapes and grains with a fluidal form (Heiken and Wohletz, 1985; Dellino and La Volpe, 1996; Büttner et al., 1999), are associated with phreatomagmatism. Therefore, blocky grain shapes are not diagnostic of the type of eruption, and 8surface textures must be examined. In this study, differences in grain shape are used to determine the nature of syn- and post-production processes, and possibly discriminate between the deposits of the different units.

Grain shape was considered in order to quantify the degree to which the grains had been abraded, based on the assumption that the grains in question were formed from the same fragmentation process (Dellino and La Volpe, 1996). Subsequent abrasion can

occur due to transport processes, where an increase in roundness should be seen with increasing distance from the vent. Grains may also be milled within the vent, in which case grain roundness would be independent of distance from the vent.

Grain texture, staining and coating

One indicator of eruption processes is preserved in grain texture. Surface cracks, for example, may indicate quenching (Heiken and Wohletz, 1985; Büttner et al., 1999), or hydration (Heiken and Wohletz, 1985). Vesicularity can also vary between grains of a deposit, where different fragmentation conditions are reflected in the vesicular texture (de Rosa, 1999). Pumice fragments from the 800 BP Quilotoa eruption exhibit different textures (Rosi et al., 2004). Elongate and spherical vesicles are associated with white pumice, and more homogenous vesicle textures are typical of grey pumice. Both pumice types are geochemically similar and so physical processes, the effects of conduit shear, were invoked by Rosi et al. (2004) in order to explain the observed differences.

Samples from this study were examined to see if such a trend between grain type and vesicular texture could been seen. Back-scattered images were obtained from the SEM. Vesicularity was qualitatively assessed using charts of modal proportions (Best, 2003) of the type usually employed in igneous petrology, to assist in the visual assessment of the percentage of the grain consisting of vesicles. The vesicles themselves were then classified as either equant or elongate in shape (Rosi et al., 2004; Houghton et al., 2010).

The presence of orange-stained grains is likely the result of alteration, possibly under hydrothermal conditions, and so the SEM can be used to determine the elemental characteristics of such staining. Images from the SEM can also reveal some interesting

surface textures, such as the presence of a coat of vesicular glass over a grain. The presence of these, and similar, features can illuminate the processes that occurred after the grain was formed, and thus introduce more evidence on the evolution of the eruption.

Sample selection

Localities

The primary locality for SEM-based grain analysis, locality 13/27, was chosen because all five units were individually sampled, and because, at 4.5 km from the vent, the site is centrally located in comparison with the rest of the localities. In addition, samples from localities 1 and 2, situated 2.5 km from the vent, and locality 30, located 6.5 km from the vent, were analyzed for grain shape only. This was so that grain shape could be considered in terms of distance from the vent. If a trend is evident, then transport-based processes are a controlling factor on grain shape. Conversely, if no trend is seen, then vent processes likely dominated.

Grain size selection

The dominant modes are 1.0 and 2.0 phi, and 1.0 phi was selected for grain shape and surface analysis because it is larger in size and grain features, such as the presence of orange staining, are thus more easily identified and can be compared with SEM observations. In all, 97 grains were analyzed in terms of grain shape, and 78 grains from across all 5 units were examined to determine grain texture, staining and coating.

Process

Grains were mounted onto a glass slide using double-sided tape (Cioni et al., 2008) and then imaged using the JEOL JSM-6480LV Scanning Electron Microprobe (SEM) at NAU. Operation was under low vacuum conditions, with an accelerating voltage of 20 kV and at a working distance of 10 mm. Back-scattered images were collected first, and then the elemental analysis of the grains and their coatings was carried out, utilizing the Energy Dispersive Spectrometer (EDS) on the SEM.

Grain shape

Only the3 shape of the glass was considered. Crystals were excluded because their shape is partly controlled by their habit, and lithic clasts were omitted since, by definition, they were formed and therefore affected by processes prior to the eruption.

Grains of glass were compared in terms of their circularity, in order to assess the amount of abrasion that had occurred. Circularity is a dimensionless parameter (Dellino and La Volpe, 1996) that allows grains to be compared independent of their actual dimensions. Circularity is defined as:

$$Circularity = \frac{Particle\ perimeter}{Perimeter\ of\ the\ circle\ with\ the\ same\ area\ of\ the\ particle}$$

(Dellino and La Volpe, 1996)

Lower values are indicative of a rounder grain, which can be inferred as having formed as the result of transport (Dellino and La Volpe, 1996) or vent processes. This parameter has been successfully applied to sedimentary particles (Dellino and La Volpe, 1996), where the influence of transport, usually fluvial, is commonly important, as well

as pyroclastic grains such as those at Vesuvius (Cioni et al., 2008) and the Monte Pilato-Rocche Rosse sequence on Lipari, Italy (Dellino and La Volpe, 1996).

SEM images of the grain were first converted into monochrome using Adobe Photoshop so that the grain was filled black and lay upon a white background. Then the image was imported into ImageJ (Rasband, 1997-2009), where the perimeter and area of the grain were calculated, thus allowing for the circularity of the grain to be quantified and comparisons made between samples.

CHAPTER 3

RESULTS: FIELDWORK

In the field the stratigraphy and thickness of sections were recorded, and in the laboratory the maximum grain size obtained. This fieldwork was carried out so that spatial variations within the units, and the temporal progression of the eruption, could be examined.

Stratigraphic information can be used to infer whether an eruption was intermittent or continuous, shown by the presence of one thick bed or several thinner beds, and whether the eruption was strengthening or weakening, as recorded by grading and maximum clast size. Whilst these up-sequence data record the intensity of the eruption, spatial data, namely unit thickness, gives information related to the magnitude of the event. Also, data on the areal distribution of the units in relation to topography provide evidence on the emplacement mechanism of the deposits. In addition, distance-dependent variations within the unit can be identified.

These approaches were applied to Quilotoa so that the relation between the two voluminous units, U1 and U3, with the hiatus deposit, U2, could be thoroughly examined. The progression of the activity that preceded the second plinian eruption is recorded in the stratigraphy of U2, which is examined in detail here for the first time. In the first part of this chapter the units are described and a composite stratigraphic column is presented, and in the second part the isopach and isopleth maps of U2a, U2b and U2c are analyzed.

STRATIGRAPHY

To consider the eruptive sequence as a whole, from upper U1 to lower U3, a composite stratigraphic section is used. Localities selected for inclusion in this composite stratigraphic section were selected for the extent of the deposits exposed (Figures 3.1 and 3.2). U1 thickness data are from locality 30 with additional descriptions from locality 13. Data on U2a are derived from locality 1, U2b from locality 2, and U2c from locality 26. U3 thicknesses are from locality 15, with addition descriptions from localities 13 and 16. This approach allows for the consideration of details gathered from a number of sites across the field area. In addition, the changes in stratigraphy with distance from the crater are explored along an approximately north-south transect, with sites either side of the crater (Figure 3.3). Individual stratigraphic columns for each locality are in Appendix 3.2. The unit descriptions that follow use the grain-size classification scheme of Thorpe and Brown (2003) (Table 3.1).

Grain Size		**Pyroclastic fragments**
phi	mm	
≥ -8.0	≥ 256	Coarse blocks and bombs
< -8.0	< 256	Fine blocks
< -6.0	< 64	Lapilli
< -1.0	< 2	Coarse ash
< 4.0	< 0.0625 or 1/16	Fine ash

Table 3.1. Grain size classification scheme (Thorpe and Brown, 2003).

Below U1, in most locations, is a dark paleosol (Figure 3.2). The contact between U1 and the paleosol is erosive in some places. U1 is a gray vitric- and crystal-rich lapilli and coarse ash unit, where the coarsest components are white pumice (Figure 3.4). U1 is

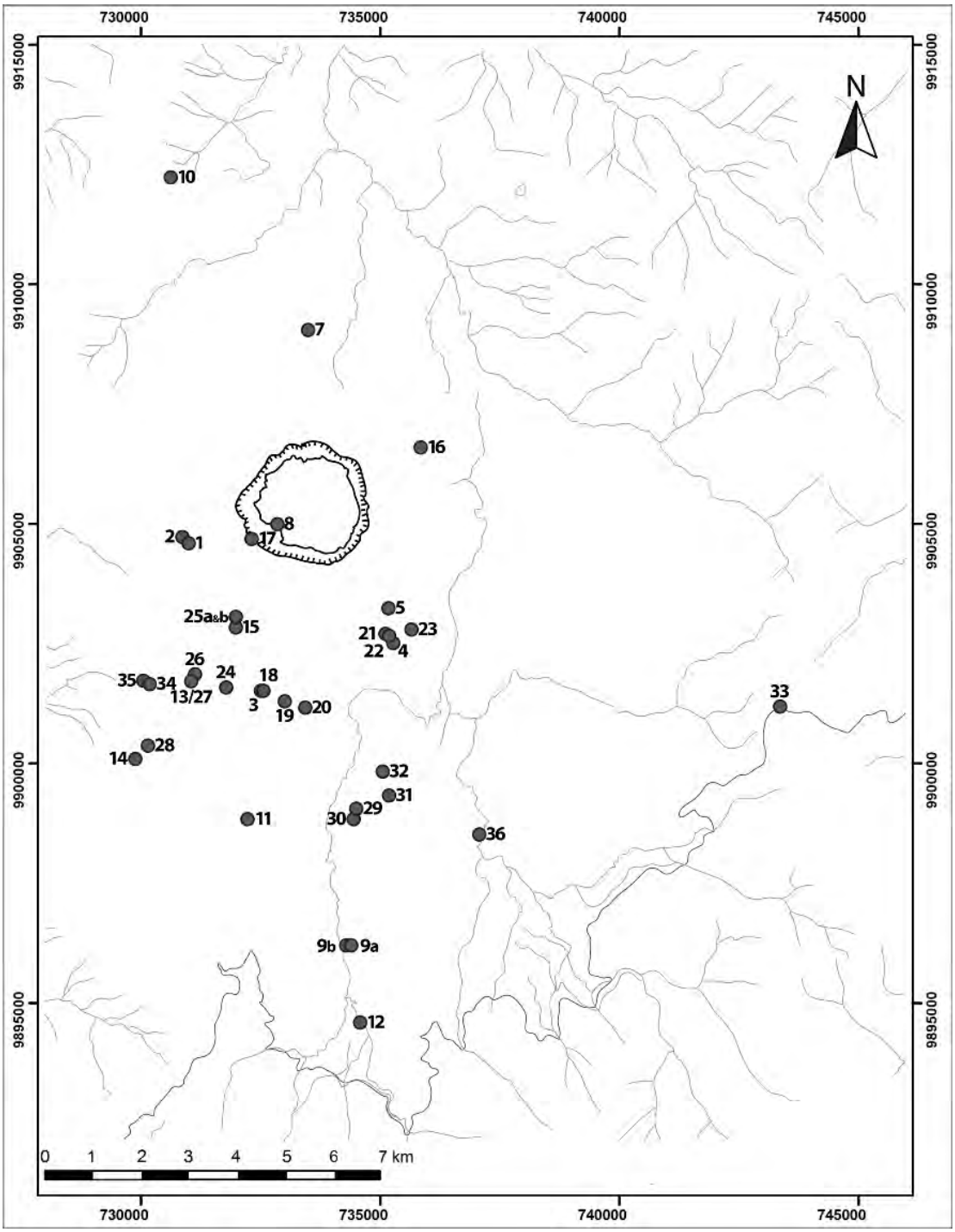

Figure 3.1. Map of all the locations, positions indicated by gray circles, visited during the course of this study.

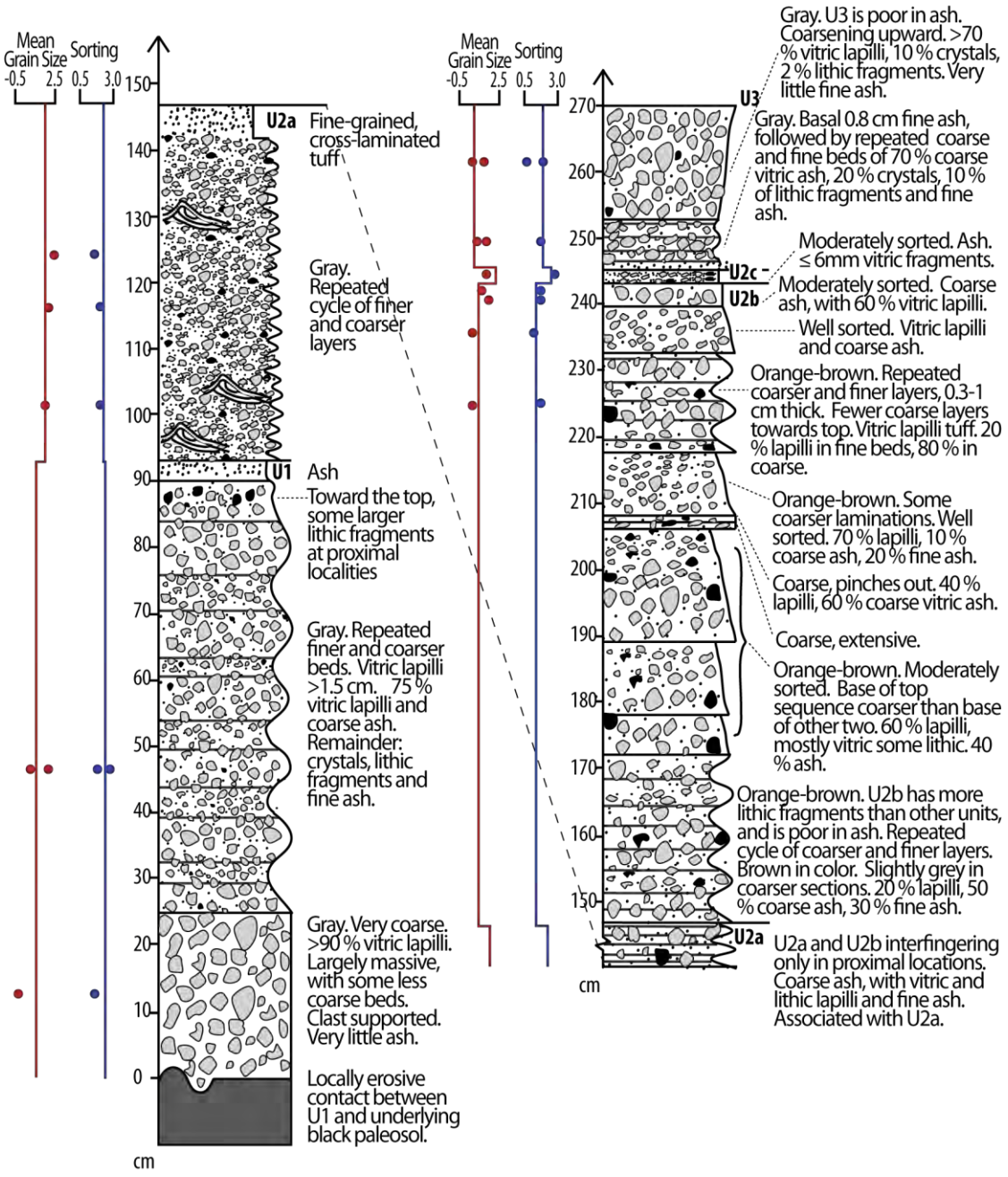

Figure 3.2. Composite stratigraphic section from upper U1 to lower U3. *Mean grain size* is the graphic mean grain size (Folk, 1974) (Chapters 2 and 4), and is given in phi. *Sorting*, is the inclusive graphic standard deviation (Folk, 1974) (Chapters 2 and 4), where low values indicate better sorting. For both sorting and mean grain size, the line represents the mean value for the unit and, in order to see sub-unit variations, the dots are the values from samples upon which this composite stratigraphic column is based.

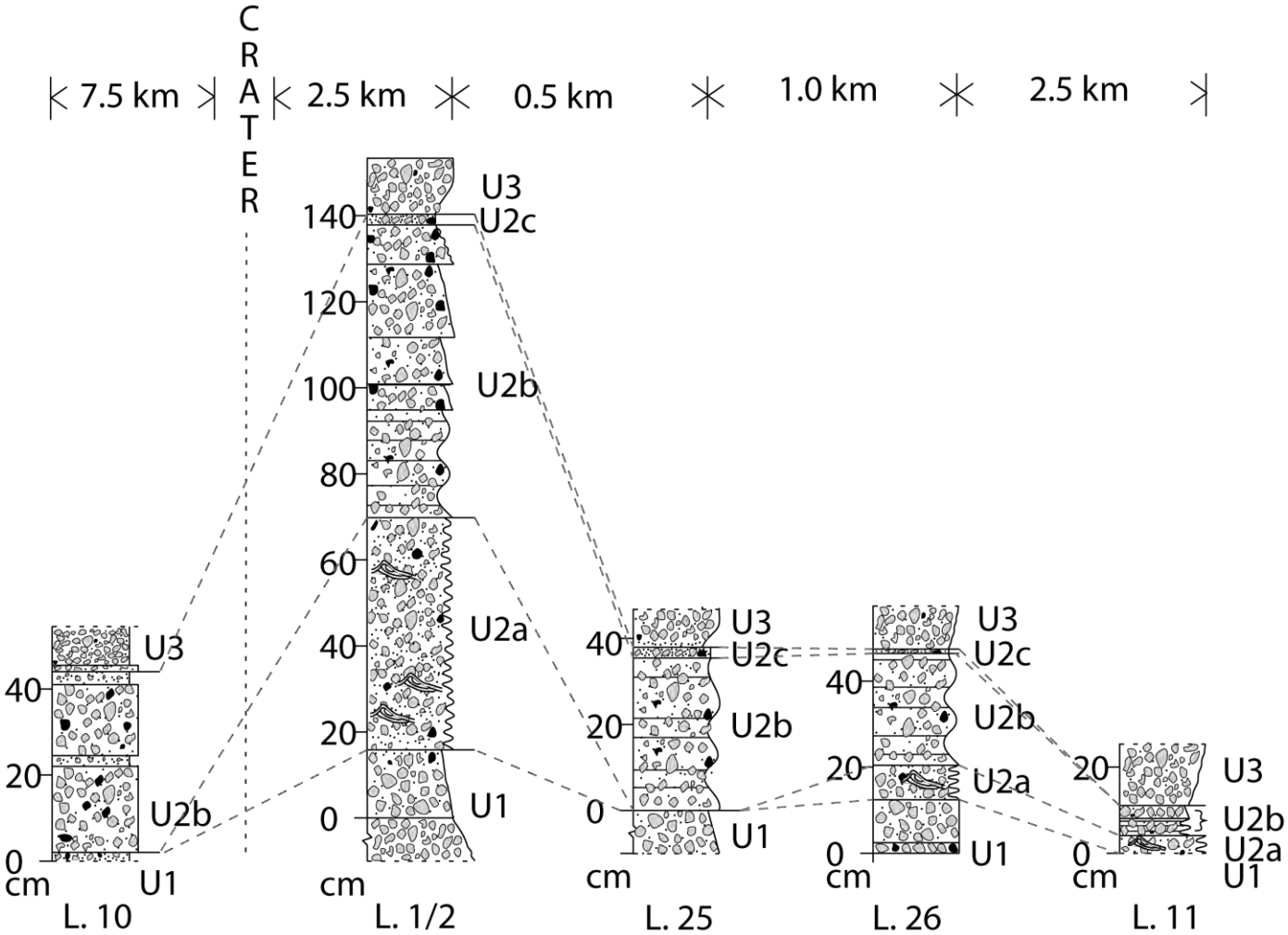

Figure 3.3. Stratigraphic columns of sites along an approximately north-south transect, including the crater. See Figure 3.1 for site locations. Figure not to horizontal scale. Locality 11 is 6.5 km from the crater and locality 10 is 7.5 km from the crater.

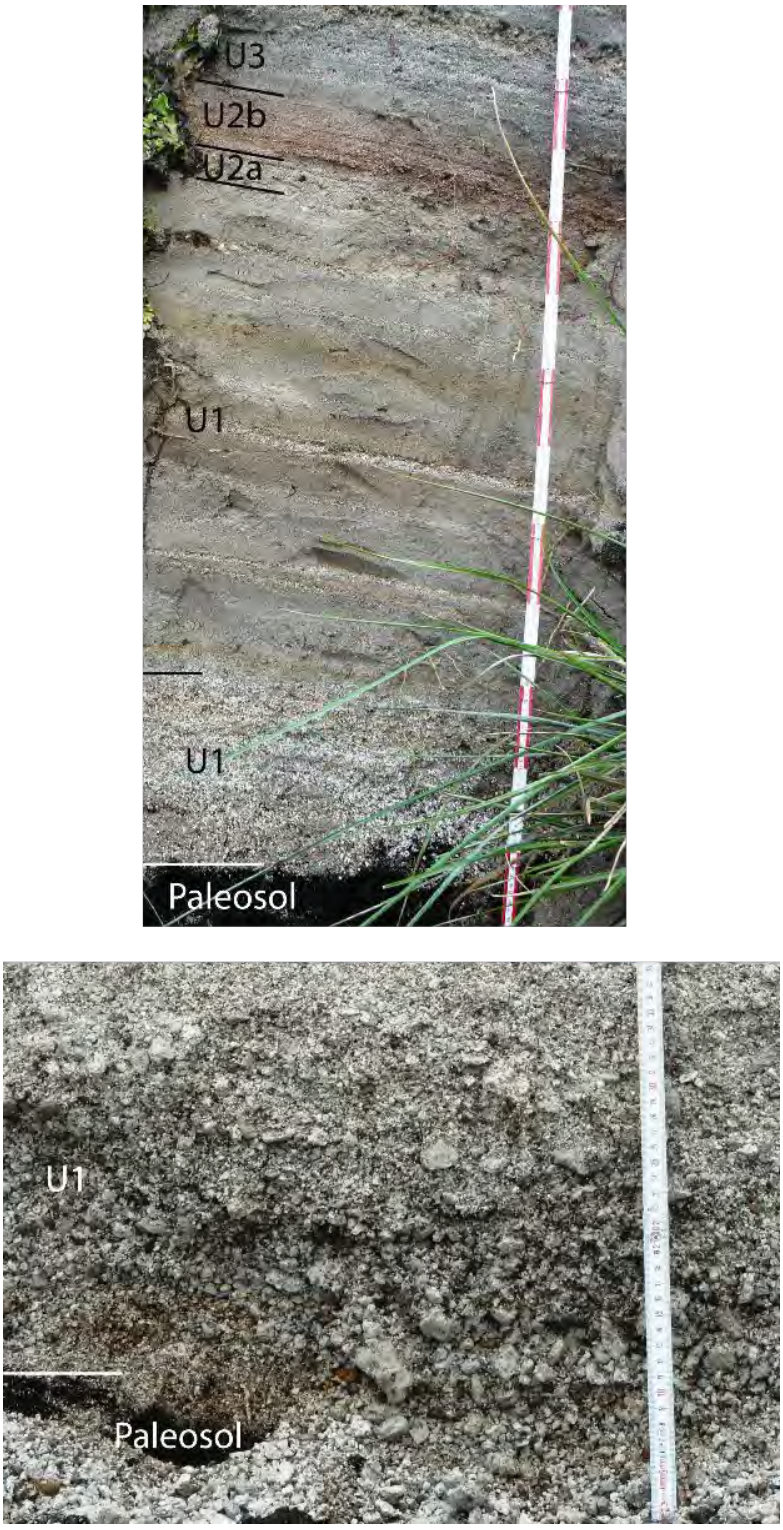

Figure 3.4. The gray, coarse vitric lapilli of U1. Uppermost U1 is a sequence of alternating coarse- and fine-grained beds (Top: Locality 30). The subunit below is massive (Top: Locality 30. Bottom: Locality 10). Note the non-erosional contact between U1 with the underlying black paleosol (Top).

f

poorly sorted, with an inclusive graphic standard deviation of 2.35 phi, and has a graphical mean grain size of 1.23 phi (Chapter 4). Upper U1 is laterally extensive, mantles topography, and is split into two gray subunits (Figure 3.2 and 3.4). The upper subunit is a repeated sequence of finer- and coarser-grained planar beds, the lower of the two a massive coarse-grained bed. Overall upper U1 is normally graded. Neither subunit has evidence of reworking.

The lower subunit is dominantly (>90%) vitric lapilli (Figure 3.4). This massive subunit is clast-supported, dominated by lapilli-sized pumice and poor in fine and coarse ash. The upper subunit is a repeated cycle of coarser and finer-grained beds, where vitric lapilli still dominate (~75 %) but the subunit is matrix supported and the deposit is bedded. The remaining ~25 % of the unit is a matrix of crystals, fine ash and sparse lithic fragments. Toward the top of this subunit, at some proximal localities, lithic fragments become larger and more abundant. Evidence of erosion is seen at some sites.

The U1/U2a contact is noted by the increase in the proportion of ash, the lack of larger pumiceous lapilli, and therefore by the finer grain size of the deposit (Figure 3.5). Additionally, the beds of U2a pinch out, unlike the laterally extensive beds of U1.

U2a is a gray vitric- and crystal-rich ash unit, characterized by a repeated sequence of finer- and coarser-grained layers that, as particularly well exposed at proximal localities, are not laterally extensive (Figures 3.2 and 3.5). The individual beds, which form the dune structures within the unit, are no thicker than a few cm. Based on field observations the coarser beds appear to be more poorly sorted than the finer beds.

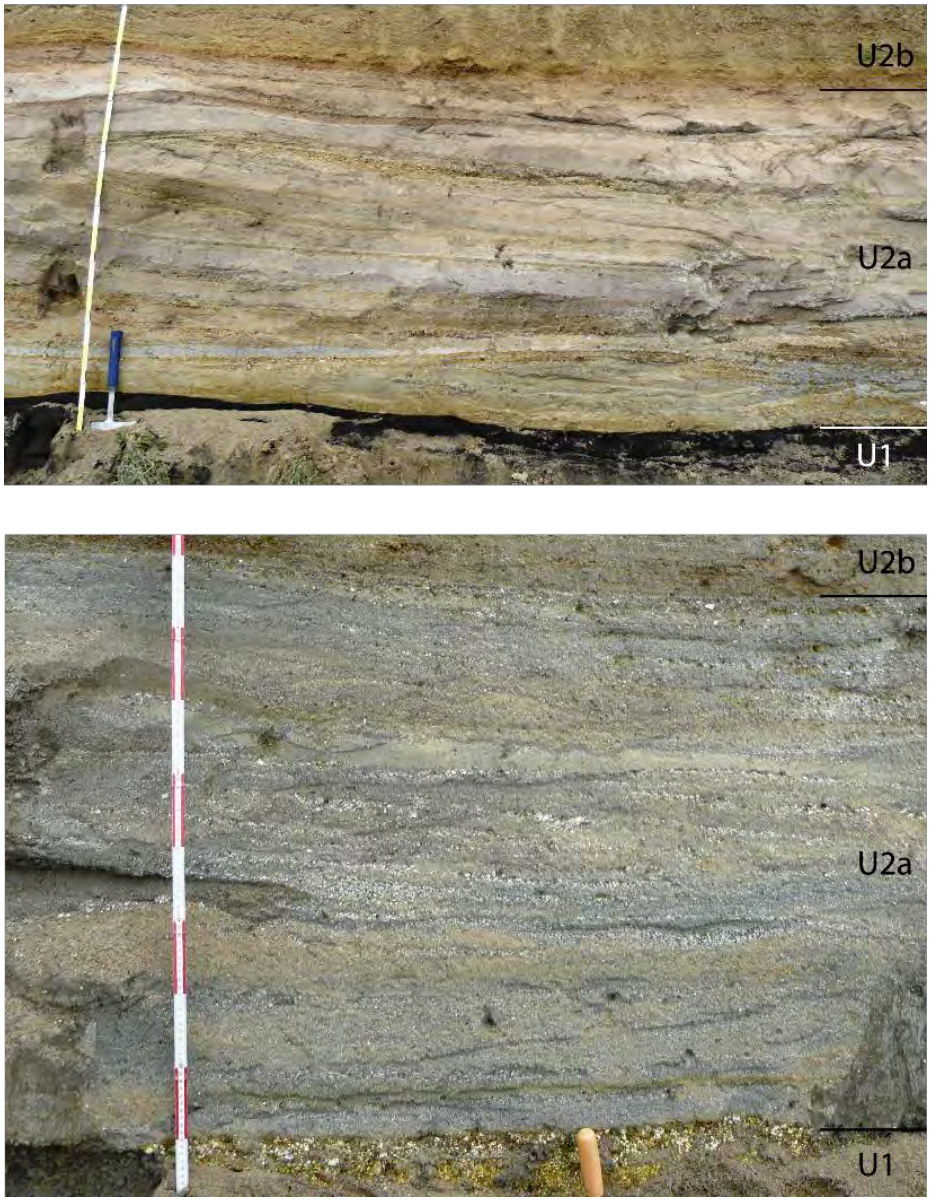

Figure 3.5. The fine and coarse-grained beds that pinch out and characterize the main body of U2a. Colored divisions on the rulers are 10 cm; the hammer is approximately 35 cm long. Note the different scales of the features in each photograph. Upper U1 is just visible in the lower few cm of the bottom image, the boundary marked by the trowel handle. (Both photographs locality 1).

The proportion of fine and coarse vitric ash and crystals means U2a is matrix supported, with vitric lapilli and sparse lithic fragments that are smaller than those of U1. The top of U2a is predominantly ash. Overall U2a is normally graded and the beds show no evidence of reworking. With a graphical mean grain size of 1.80 phi and an inclusive graphic standard deviation of 2.21 phi, U2a is finer-grained than U1 but is similarly poorly sorted (Chapter 4).

The U2a/U2b contact is gradational in that up to 2 beds of U2b material occur within the uppermost U2a beds at proximal sites, including localities 1 and 17 (Figure 3.6), where the U2a beds form dune structures and pinch-out laterally. In this instance, the boundary between the two units is defined as being where U2a material ceases and U2b material becomes the sole deposit type. Elsewhere the contact is sharp, where gray,

Figure 3.6. Part of the region of overlap between U2a and U2b, as seen at Locality 17, the former crater rim site. Section J lies between the tools. Coarser and finer units are visible and distinct within this section. Colored divisions on the ruler are 10 cm.

ash-rich U2a is replaced by coarser, orange-brown, ash-poor U2b.

U2b is a sequence of orange-brown, finer- and coarser-grained beds of vitric and crystal-rich coarse ash (Figure 3.7). The exposure at locality 2 shows that U2b can be divided into a number of these discrete beds (Figure 3.2), but fewer divisions are present at more distal locations. The beds of U2b are between 1 and 17 cm thick, either showing no grading (massive) or normal grading, and are planar and laterally extensive. U2b mantles topography, with no evidence of reworking.

The following subunit descriptions are derived from locality 2, where the most subunits have been identified. The lower part of U2b is richer in fine ash than the rest, with ~30 % fine ash and ~50% coarse ash (Figure 3.1). Above this lower bed are three moderately sorted, normally graded beds, composed of ~60 % lapilli, of which most are vitric and some lithic, and ~40 % ash. These beds are overlain by two thin massive beds of coarse material with similar componentry to the underlying beds. A well sorted, normally graded bed, poorer in ash than those below, overlies this. Repeated ≤1-cm-thick laminations of finer and coarse ash form the bed above this. Finally, a well sorted, normally graded bed of ~60 % vitric coarse ash is topped by a few cm of massive, moderately sorted, vitric coarse ash at the top of U2b.

Overall, U2b is moderately sorted and has the second largest mean grain size of the units, after U3, with an inclusive graphic standard deviation of 1.43 phi and a graphical mean grain size of 0.97 phi, derived from the mean of beds of U2b sampled at different localities (Chapters 2 and 4).

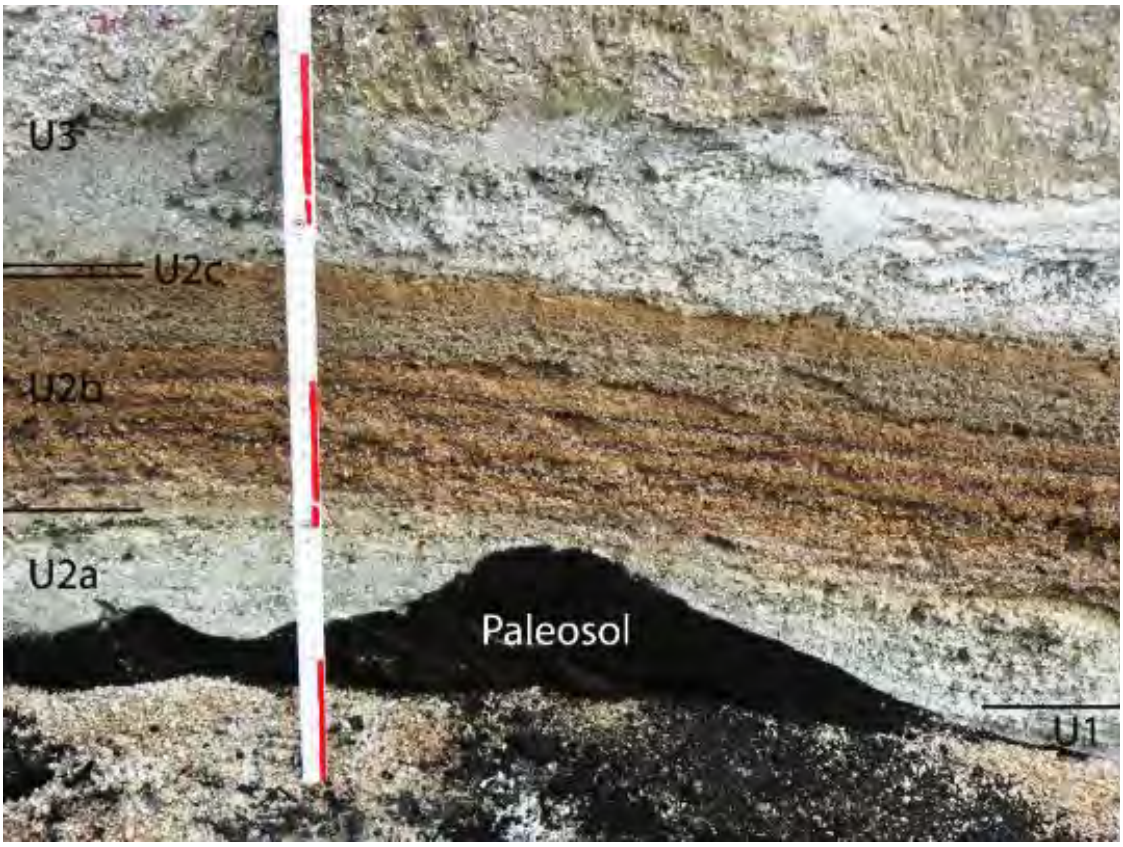

Figure 3.7. The fine and coarse-grained sequences and normally graded beds of U2b, the orange-brown colored unit in the center. Colored divisions on the ruler are 10 cm. Also note the less common erosional contact between U1 and the underlying black paleosol (Locality 13 (27)).

The U2b/U2c contact is defined by the appearance of a matrix of abundant fine ash, punctuated by rounded vitric lapilli (Figures 3.7 and 3.8). The limited thickness of U2c (≤ 2 cm) and the brown color means that, whilst the contact between the two units is

sharp, its identification requires the examination of sub-cm transitions within the deposits.

U2c is a brown colored vitric and crystal-rich ash unit, with rounded vitric lapilli ≤ 11.5 mm (Figure 3.8). Composed of a single bed no more than 2 cm thick, U2c is a massive, laterally extensive planar bed that is matrix supported and shows no signs of reworking along either contact (Figure 3.2). U2c is the most poorly sorted unit, with an inclusive graphic standard deviation of 2.54 phi, and also, at 2.33 phi, the smallest graphical mean grain size (Chapters 2 and 4).

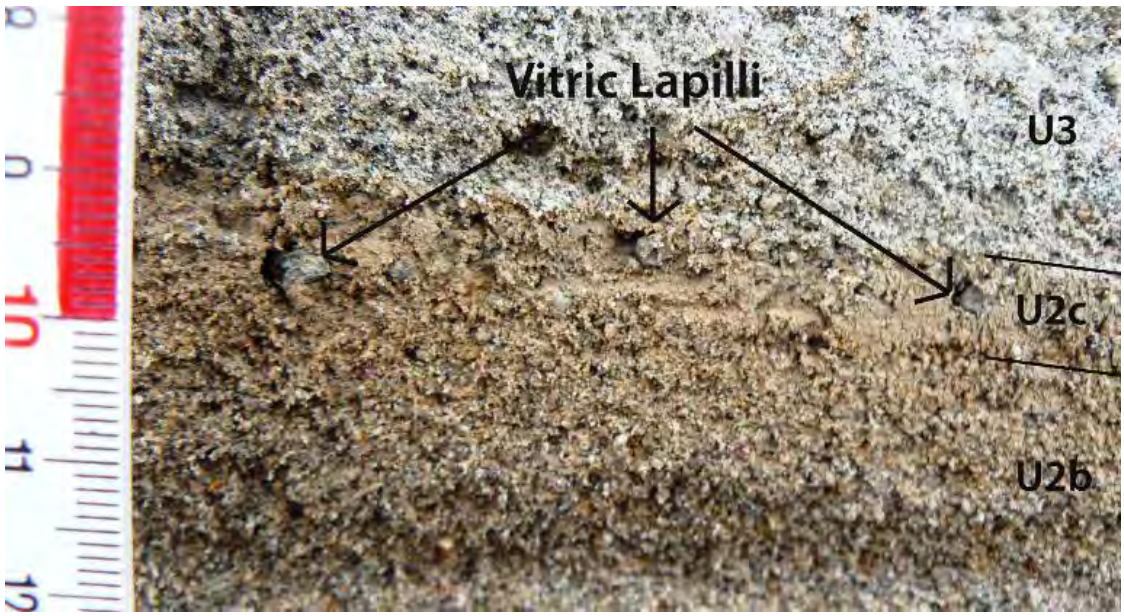

Figure 3.8. U2c is poorly sorted, composed of ash and vitric lapilli. Black lines mark the top and bottom of U2c where it is sandwiched between U2b and U3 (Locality 27(13)). See Figure 3.7: the upper 8 mm light brown bed is U2c, pictured here.

The U2c/U3 contact is sharp, planar (no evidence of erosion) and distinguished by a reduction of ash and a color change, from orange-brown to gray (Figure 3.8). In addition, the vitric lapilli that characterize U2c are also present in lower U3.

U3 is a gray vitric- and crystal-rich lapilli and coarse ash unit, where the coarsest components are white pumice (Figure 3.9). Lower U3 is laterally extensive and matrix supported, mantles topography, and is split into two subunits (Figure 3.2). The lower subunit is a repeated sequence of finer- and coarser-grained planar beds and the thinner of the two subunits, and the upper is reversely graded. Overall, lower U3 is reversely graded, and neither subunit has evidence of reworking.

U3 begins with a very thin <1 cm layer of ash that quickly gives way to a set of repeated fine- and coarse-grained beds composed of ~70 % vitric ash (Figures 3.2 and 3.9). Then the deposit coarsens upward, composed of >70 % vitric lapilli and less ash than the previous bed. Large ballistic fragments are also found in lower U3. A lithic bomb measuring 10 cm was found at locality 22, 3.4 km from the vent, and another measuring 40 cm was found at locality 17 along the former crater rim. Overall, with a graphical mean grain size of 0.64 phi and an inclusive graphic standard deviation of 1.84 phi, lowermost U3 has the largest mean grain size of the deposits and is moderately sorted (Chapters 2 and 4).

As fully discussed in Chapter 7, uppermost U1 is a fallout deposit, in which the lower massive subunit records a strong, sustained eruption column, and the upper bedded subunit a pulsatory eruption column. U2a was emplaced by surges, as evidenced by the thin, discontinuous beds. U2b is the product of fallout from a pulsatory eruption column, based on the internal bedding of the unit. The lapilli of U2c are the pieces of a destroyed dome and the fine ash likely the product of the fragmented U3 vanguard magma. The laterally extensive lower subunits of U3 are the product of fallout, where bedded

lowermost U3 records a pulsatory eruption column and the reverse graded subunit above the establishment of a sustained eruption column.

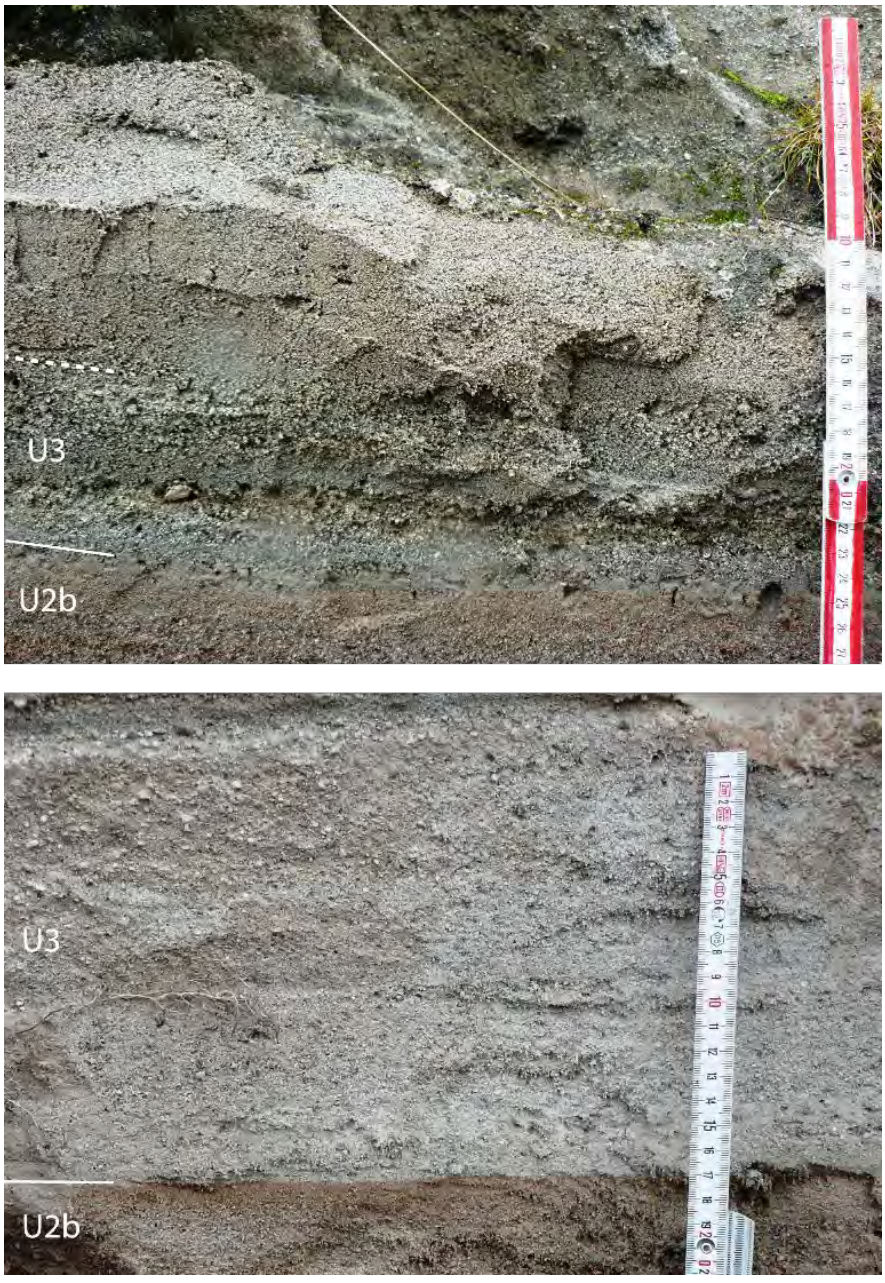

Figure 3.9. U3 has alternating fine and coarse beds at its base (top photograph, limit of alternating beds marked by dashed line), before becoming reverse graded (bottom photograph). The black line marks the lower limit of U3. (Top is locality 15, bottom locality 11).

ISOPACH AND ISOPLETH MAPS

The isopach maps presented here are used to show the areal extent of the units, in particular in relation to topography. With a lack of evidence indicating significant erosion of the deposits, except perhaps for U2a as discussed below, these values can be treated as original thicknesses. The isopleth maps are based on the maximum clast size found at each site as derived from sieve data.

U2a

The isopach map of U2a illustrates how the areal distribution of the unit is constrained by topography (Figure 3.10). Directly south and down slope of the crater is the catchment area of an ephemeral drainage system, the watershed for which trends roughly north-south along two margins approximately 2 km west of and 200 m east of the crater. U2a is constrained within this area. The presence of these stream valleys coincide with some unit thicknesses that are lower than their surrounding values. This includes measurements of 0, 3 and 3.3 cm in a region close to the crater, and measurements between 0 and 5 cm that are positioned along the 10 cm isopach. The thickness of U2a at the former crater rim site is, at 47.7 cm, less than that of locality 1, 1.1 km farther away. Overall, the isopach map indicates a southerly distribution of U2a that is constrained both to the east and west. The isopleth map of U2a (Figure 3.11) mimics the distribution of the isopach map, so that the thickest deposits are correlated with the largest clast sizes.

U2b

U2b is not topographically constrained like U2a, in that U2b is found at locations outside of the drainage area that holds the U2a sites (Figure 3.12). The isopach map

shows a north-south elongation in the thickness of U2b, although more than one data point north of the crater is needed to confirm the possibility that U2b reaches farther north than it does south. U2b is narrowly distributed in the east-west direction. At locality 25b and locality 21, along the 30 cm and 40 cm isopach respectively, lower thicknesses are recorded. The isopleth map of U2b indicates that maximum grain size is also unrelated to topography (Figure 3.13). Maximum grain size has a general north-south distribution, but the isopleth map also shows the presence of a minor westerly axis. However, more data points to the east of the vent would be required to confirm this feature.

U2c

U2c has a limited number of data points (Figure 3.14). This is partly due to the recognition of U2c partway through the field season after some sites had already been visited. Locations where this applies are indicated as having no data. Sites where U2c was known to be absent are labeled as such. From the information available, U2c has a southerly distribution, similar to U2b, with thinner deposits to the east and west. This could be a result of the limited spatial coverage of the data points, but is similar to the trend seen in U2a and U2b. U2c is not as extensive as U2b. U2b is present at three localities in the SE where U2c is absent.

U2c is not topographically constrained in the manner of U2a, in that U2c is present at two sites, localities 14 and 28, where U2a is absent. These localities are situated in the southwest corner of the field area along the margins of the drainage watershed, at higher elevations, beyond the extent of U2a. At any given site where both units are present, U2a is thicker than U2c. Therefore, if both were equally

topographically constrained, U2c would be unlikely to reach greater distances than U2a. Therefore the emplacement of U2c has to be independent of topography. Additionally, whereas the thickness of U2a varies on a local basis, thicknesses of U2c are much more consistent, indicating the emplacement process was not one that is channeled or constrained by topography.

The thinness of U2c made it difficult to sample separately from U2b and U3. Therefore, the isopleth map has only five data points (Figure 3.15). With the exception of the 8 mm data point, a trend for smaller maximum grain sizes with distance from the crater is seen.

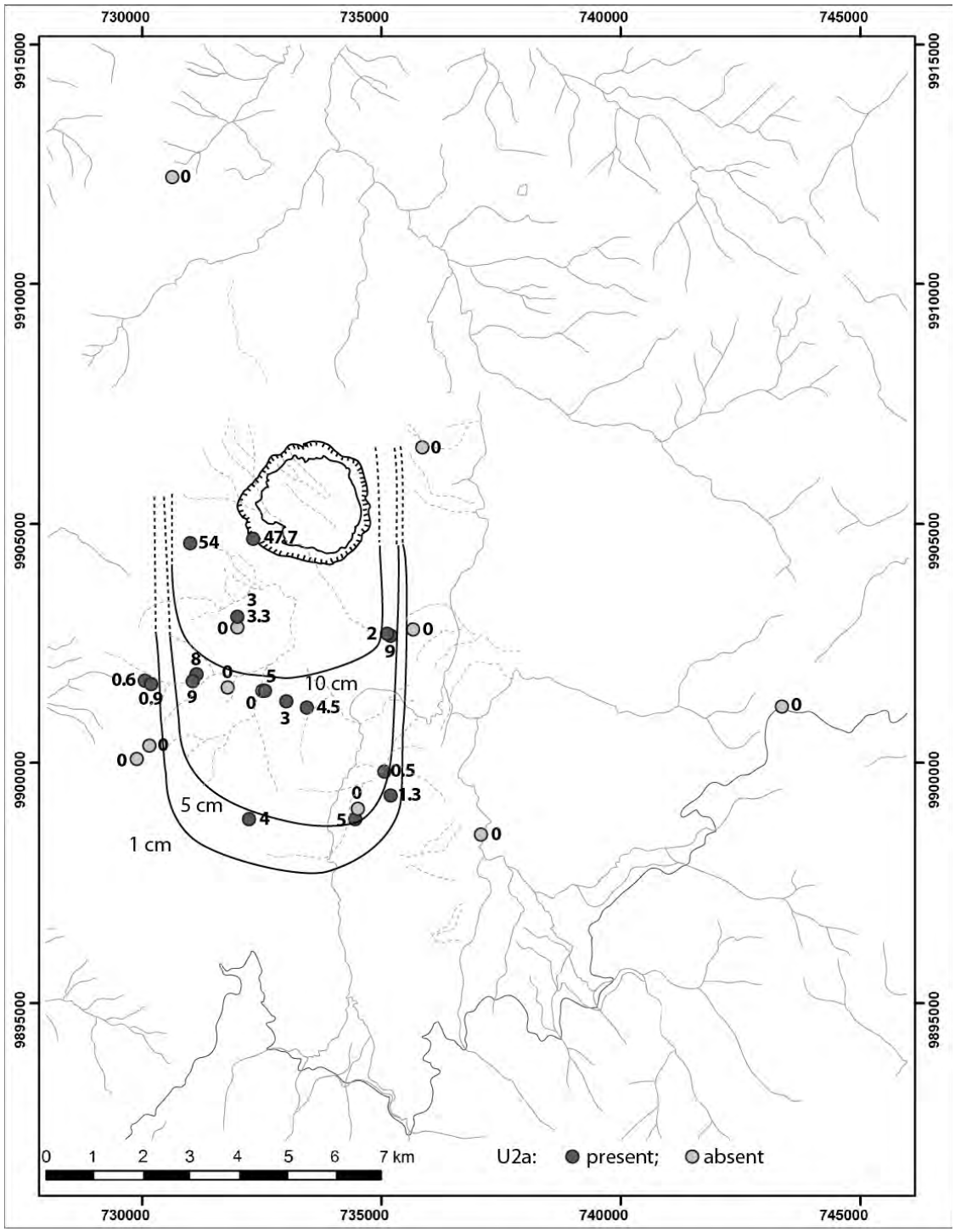

Figure 3.10. Isopach map of U2a. Ephemeral streams in the region of U2a marked as dashed lines.

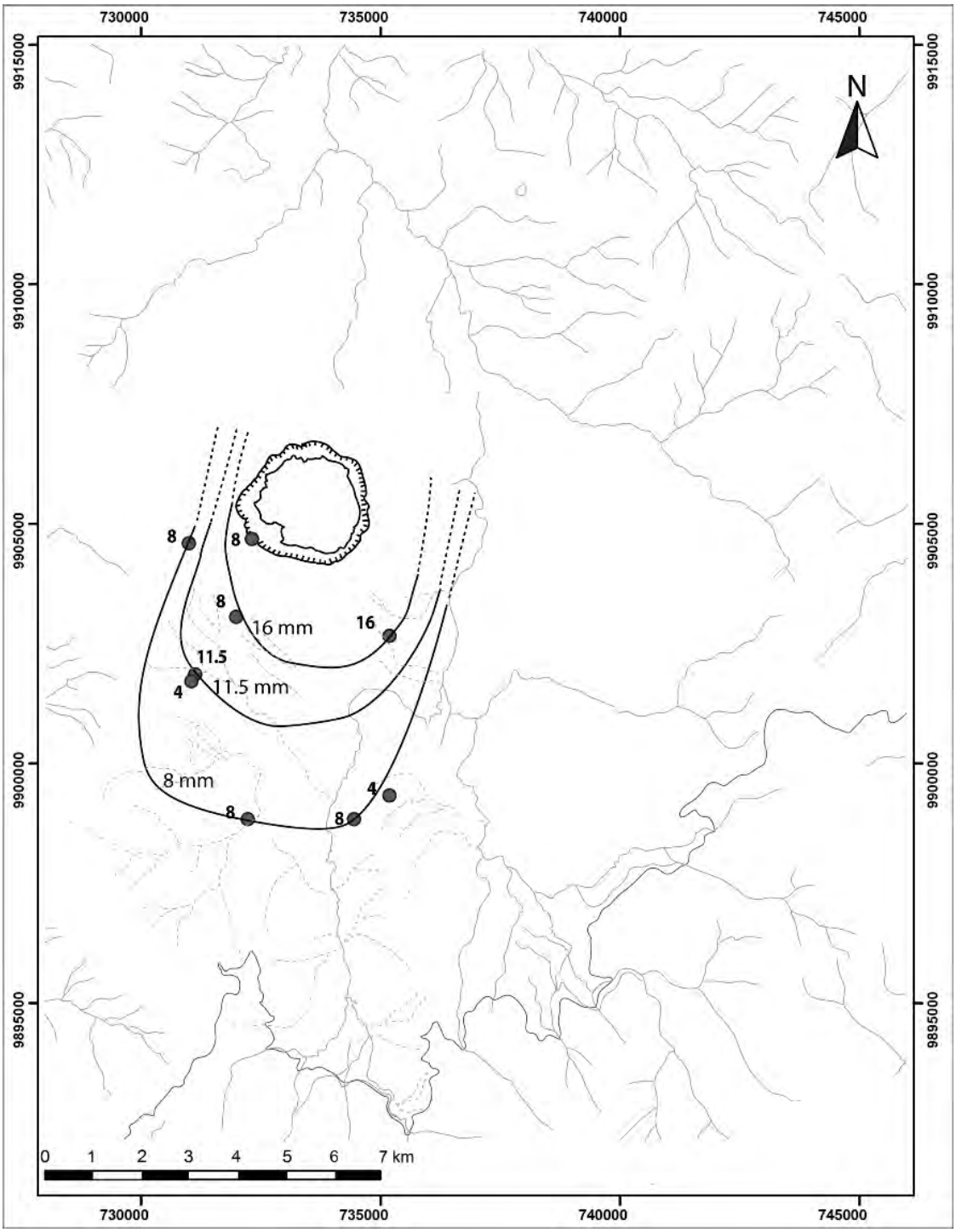

Figure 3.11. Isopleth map of U2a. Ephemeral streams in the region of U2a marked as dashed lines.

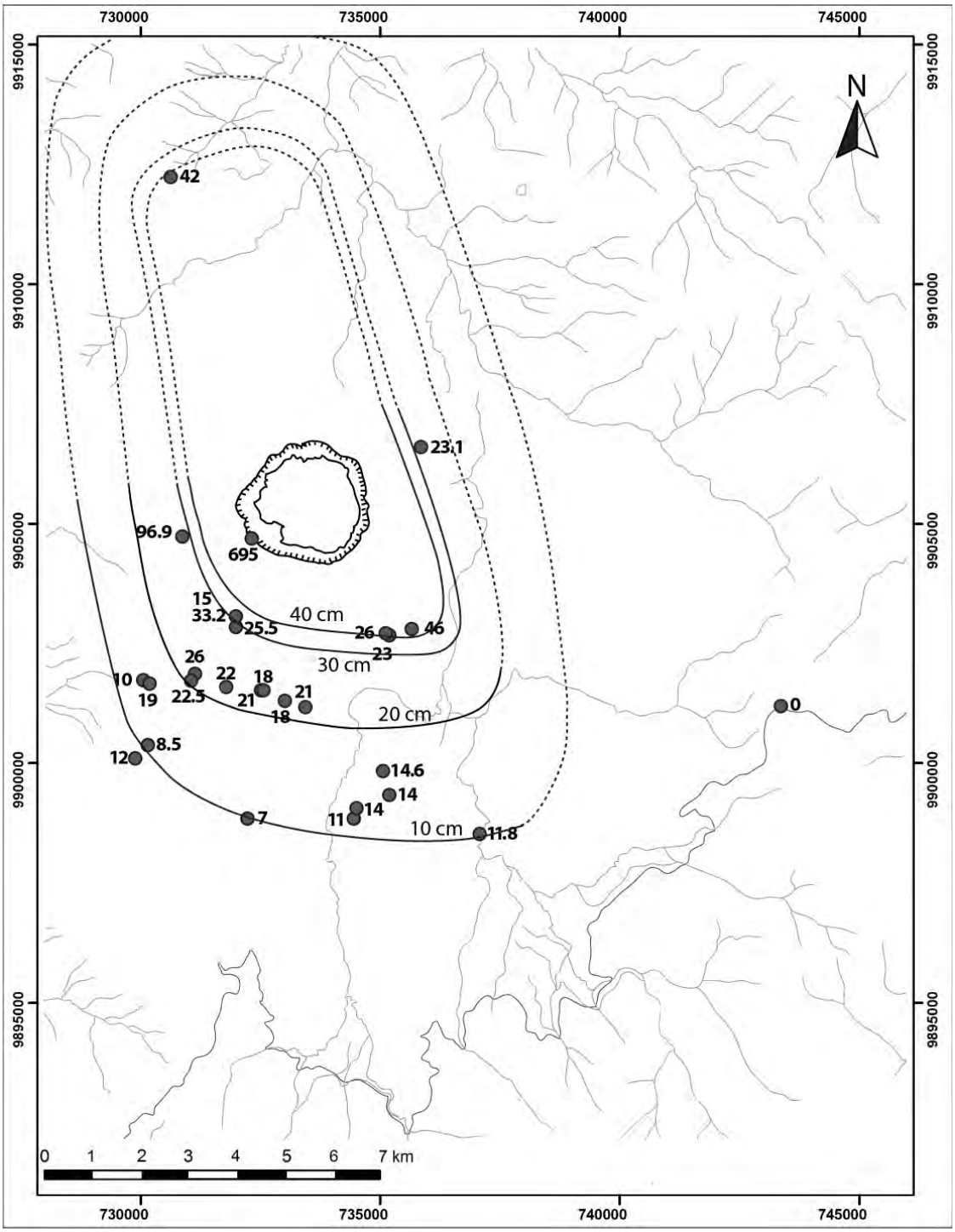

Figure 3.12. Isopach map of U2b.

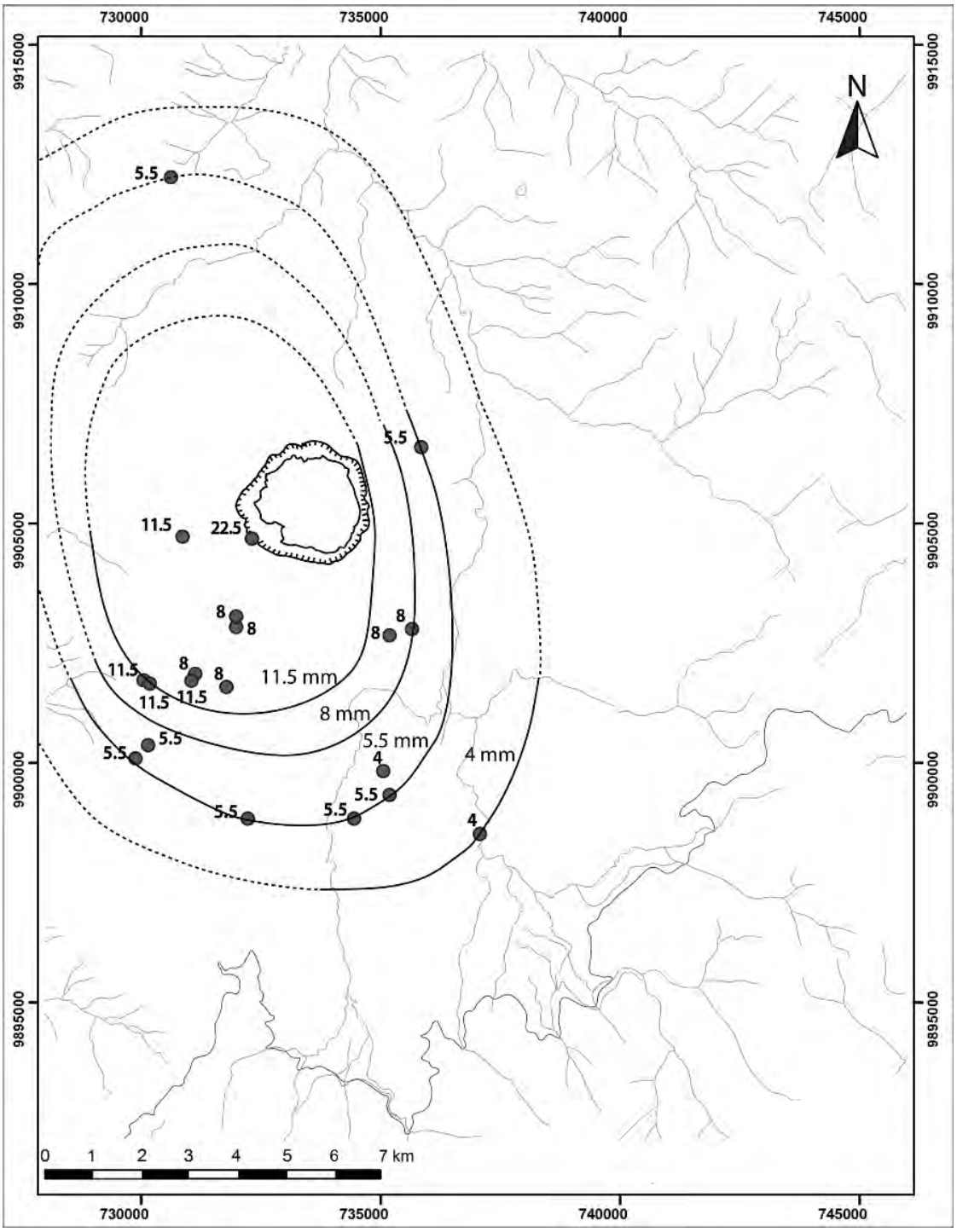

Figure 3.13. Isopleth map of U2b.

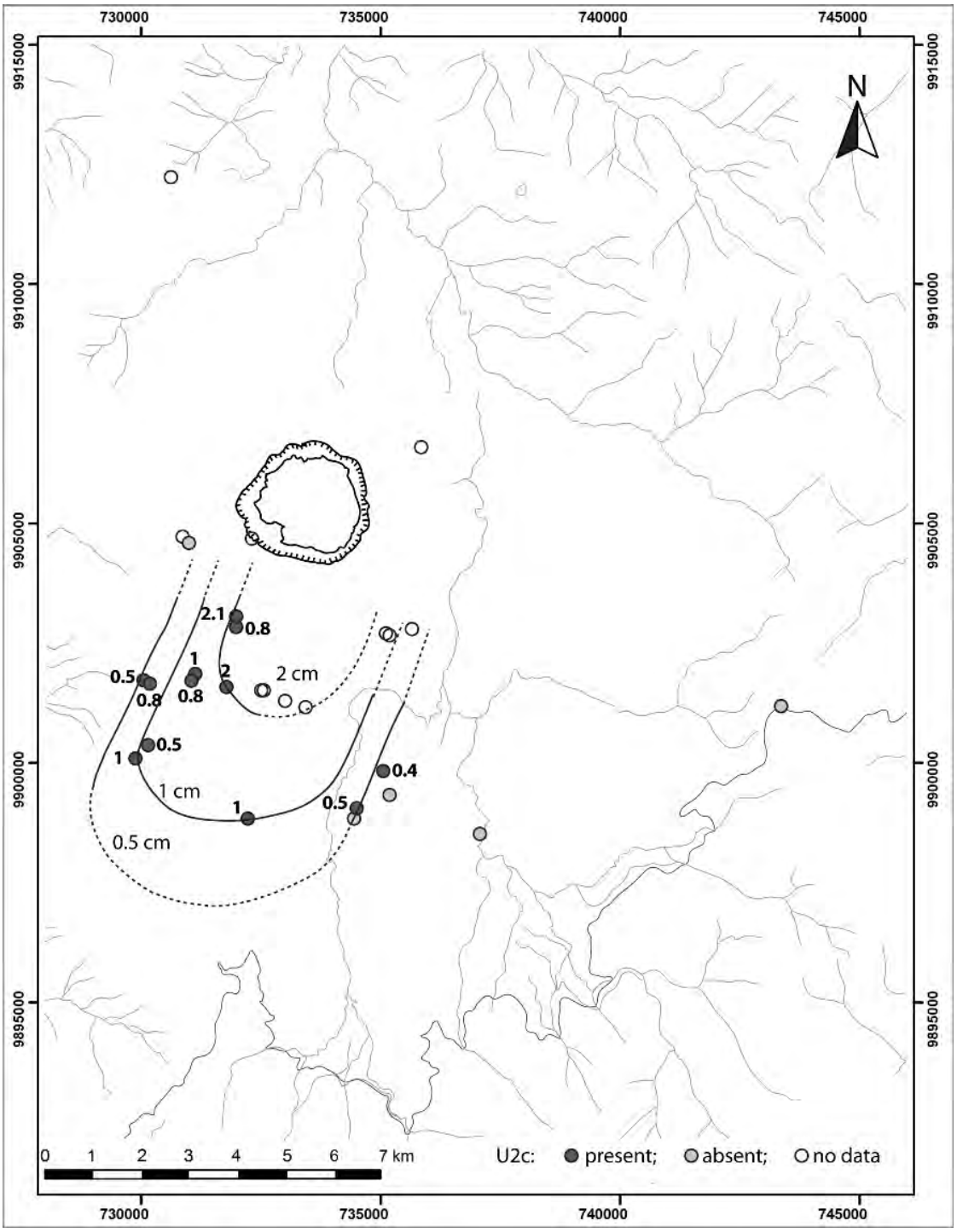

Figure 3.14. Isopach map of U2c.

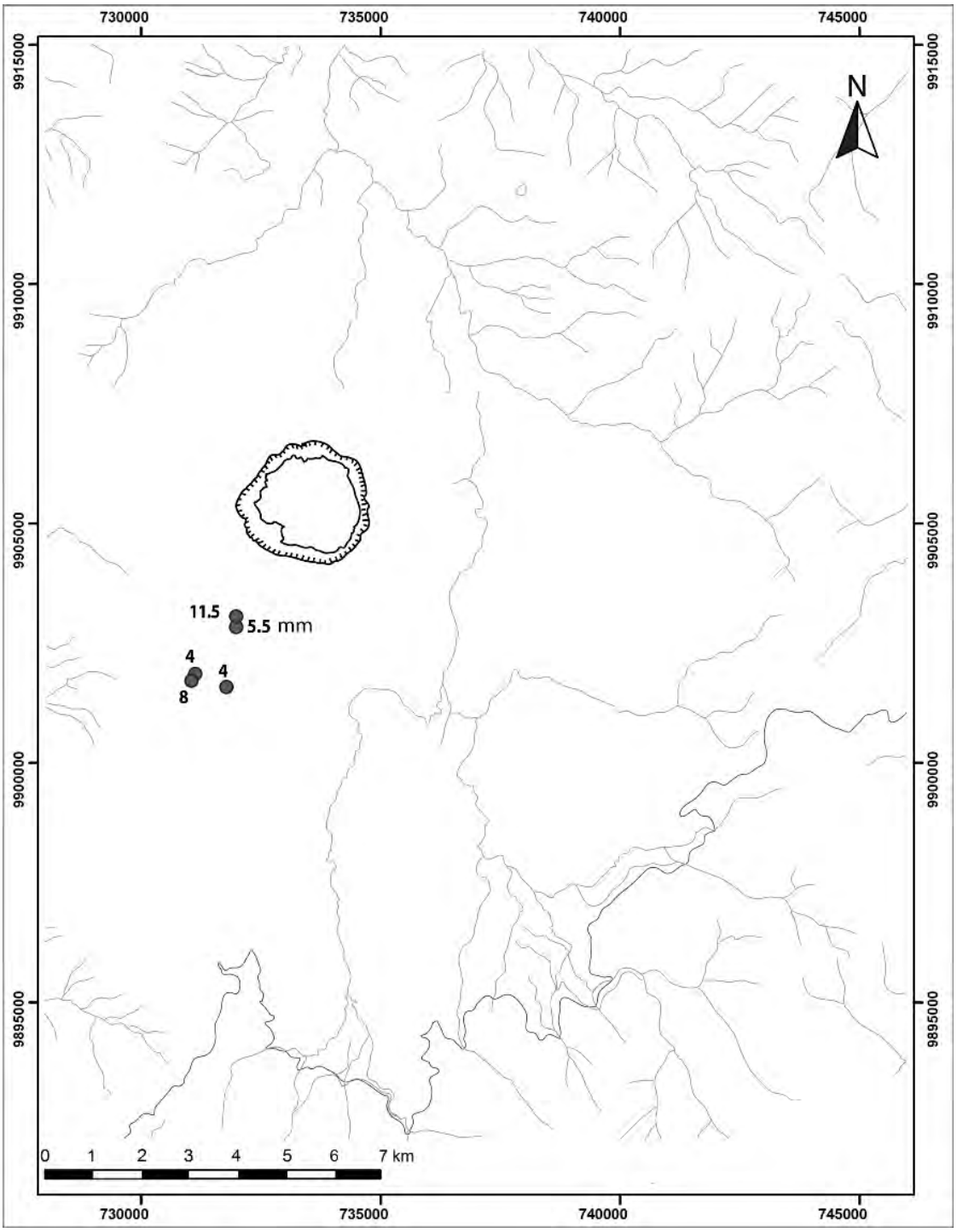

Figure 3.15. Maximum clast sizes in U2c.

CHAPTER 4

RESULTS: GRAIN-SIZE DISTRIBUTION

This chapter begins by examining the overall grain-size distribution trends of each of the units, based on all of the analyzed samples. Thereafter, the mean distributions of the units are used to first compare modal grain sizes visually and then with the use of SFT, and then to consider grain-size distribution trends in terms of the localities' distance from the vent. Finally locality 17, the site closest to the vent and correspondingly with the thickest deposits of U2, is discussed. To close, I describe the way in which the data presented here direct the componentry study.

THE DATA

A total of 80 samples from 19 different localities were sieved, and 29 of those had a significant proportion (≥10 wt %) of fine-grained material that warranted further investigation using the Coulter particle-size analyzer (Figure 4.1). At some sites, the main units were split and sub-sampled. For example, the coarser and finer beds seen within U2a at some sites were sampled separately.

Uppermost U1 has a broad grain-size distribution and exhibits a moderate degree of variability within its samples (Figure 4.1). Two samples, which correspond to the lower, coarser, massive subunit of U1, have grain-size peaks at the coarsest end of the scale (Figure 4.2). At sizes around -5 phi, the presence or absence of a few pumice fragments can significantly change the weight of the sample. U1 has very little material smaller than 4.5 phi in size. Overall, U1 is poorly sorted (inclusive graphic standard deviation of 2.35 phi (Chapter 2)), with a mean grain-size of 1.23 phi (Table 4.1).

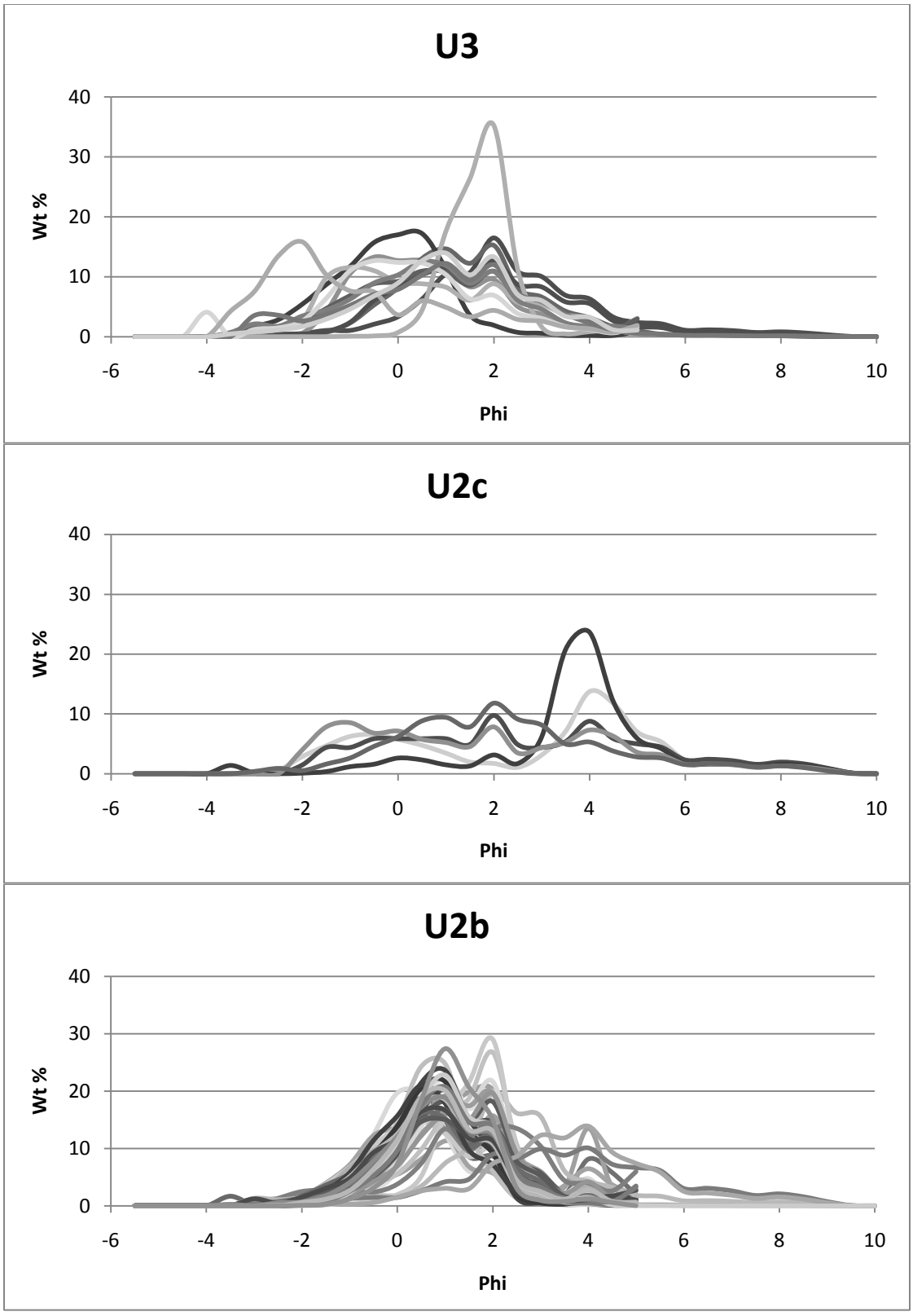

Figure 4.1. Grain-size distributions of samples from each unit. U3 is at the top of the sequence, U1 at the base.

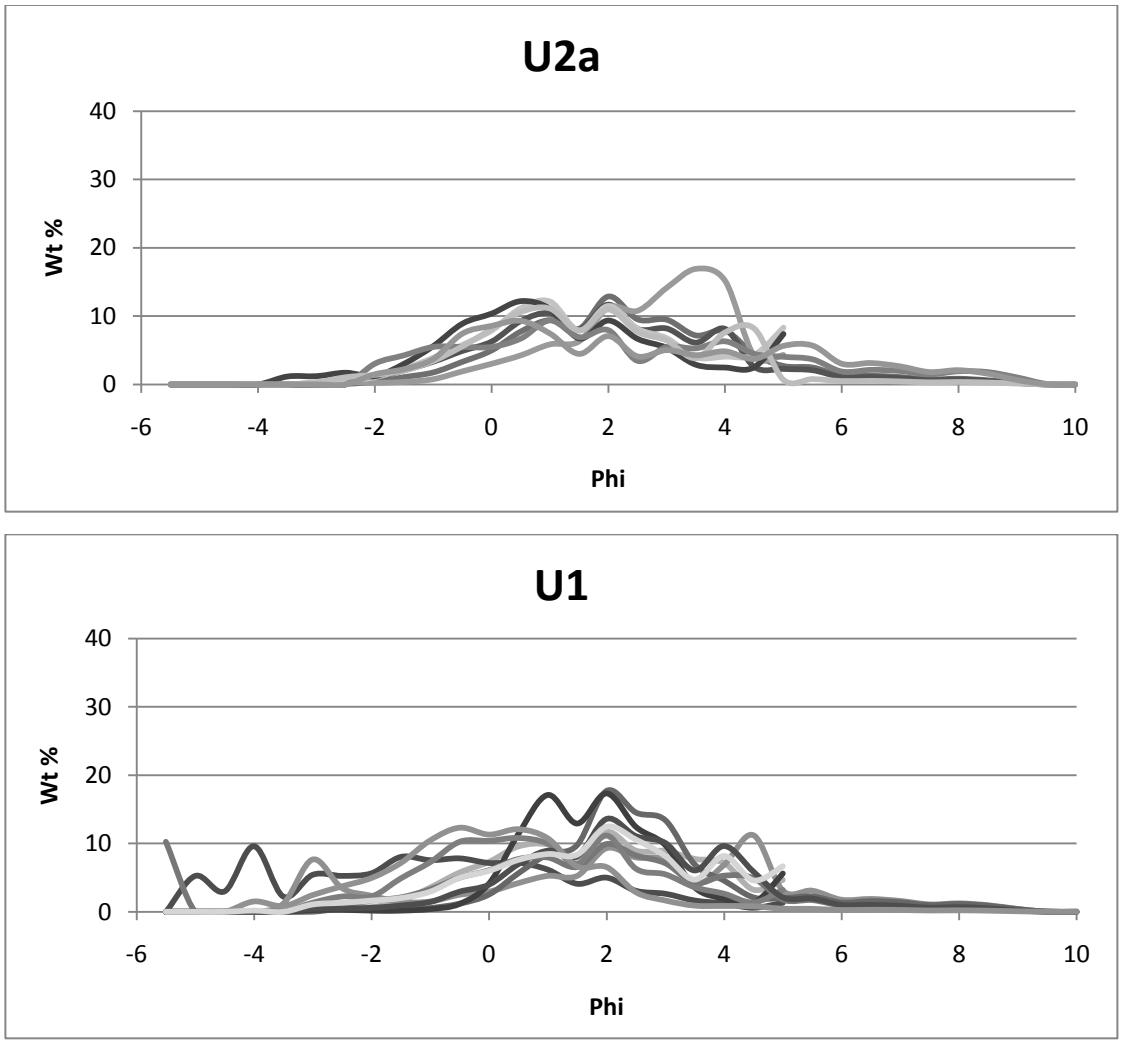

Figure 4.1 continued.

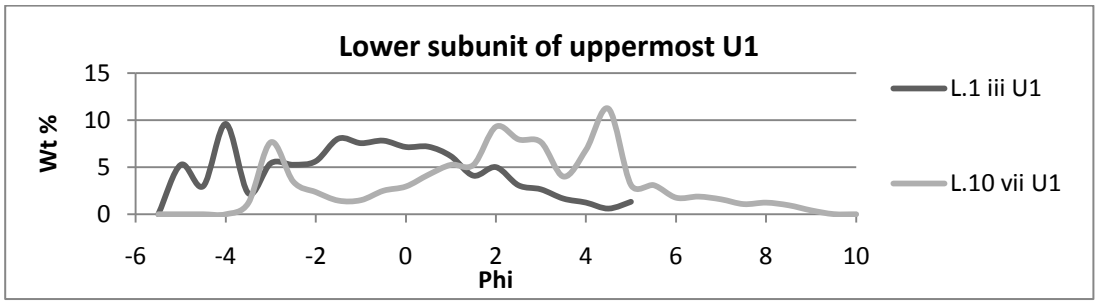

Figure 4.2. Grain-size distribution of the lower subunit of uppermost U1.

	Grain-size distribution statistics					
	Graphical Mean Grain-size (phi)	**Inclusive Graphic Standard Deviation (Sorting)** (σ_1)		**Inclusive Graphic Skewness**	**Graphic Kurtosis**	
		Grain-size range (phi)				
U1	1.23	2.35	poorly sorted	-0.06	1.19	leptokurtic
U2a	1.80	2.21	poorly sorted	+0.12	1.01	mesokurtic
U2b	0.97	1.43	moderately sorted	+0.08	1.19	leptokurtic
U2c	2.33	2.54	poorly sorted	-0.17	0.88	platykurtic
U3	0.64	1.84	moderately sorted	-0.02	1.06	mesokurtic

Table 4.1. Statistical data on the units, as output from SFT. Graphical mean grain size and sorting (Folk, 1974), with the interpretation of sorting values as described in Chapter 2. Skewness and kurtosis data (Folk, 1974) provide a quantitative data description.

With an inclusive graphic standard deviation (σ_1) of 2.21 (Table 4.1) U2a is poorly sorted with a distribution similar to U1, except for a lack of material coarser than -2.0 phi and a slightly greater proportion, up to 5.5 wt%, of material finer than 4.5 phi (Figure 4.1). Correspondingly, U2a has a mean grain-size of 1.80 phi. The eight samples show some agreement in their distributions, particularly in the positioning of the peaks along the graph (individual sample skewness and kurtosis data, detailed in Appendix 4.1.2).

Whereas the other units are distinctly polymodal, samples of U2b tend toward bimodality (Figure 4.1). U2b has the narrowest grain-size distribution of the analyzed units, with samples being moderately sorted (σ_1 1.43) (Table 4.1) and the bulk of the material falling between -2.0 and 4.5 phi, with a mean grain-size of 0.97 phi. With the exception of two samples, in which the grain-size patterns are similar but finer grained than the rest, U2b samples have similar grain-size distributions.

Sample U2c was sampled in five locations (Figure 4.1). In two other cases where the unit was identified, the beds were too thin to be physically separated for sampling. U2c is poorly sorted (σ_1 2.54) with a grain-size distribution that is the most fine grained of all the units, with a mean grain-size of 2.33 phi (Table 4.1). Very little material is coarser than -2.0 phi and the fine material begins to taper at around 6 phi. Within the eruptive sequence, the appearance of U2c marks a return to the broad, polymodal grain-size distributions associated with U1 and U2a.

Lowermost U3, like uppermost U1, has a wide grain-size distribution that lacks material finer than 4.5 phi (Figure 4.1). U3 is moderately sorted ($\sigma_1$1.84), with a mean grain-size of 0.64 phi (Table 4.1). The grain-size range extends to -4.0 phi, with the coarser fraction dominated by pumice and subordinate lithic fragments, as in U1. Some repetition of trends among the samples is evident, but the level of similarity seen in the U2 samples is not replicated here. The most notable example of similarity in U3 samples is the presence of the modal peak centered at ~2.0 phi. The unimodal sample with a pronounced peak around 2.0 phi, L16 i U3, is a U3 sample and not U2b, as confirmed by field observations.

MEANS AND MODES

Inspection of the mean grain-size distribution of each unit (Appendix 4.2.3) reveals that similar modes are repeated across the units (Figure 4.3). These modes include 0.73, 1.82 and 3.70 phi, with some units exhibiting smaller modes or inflections at other phi sizes.

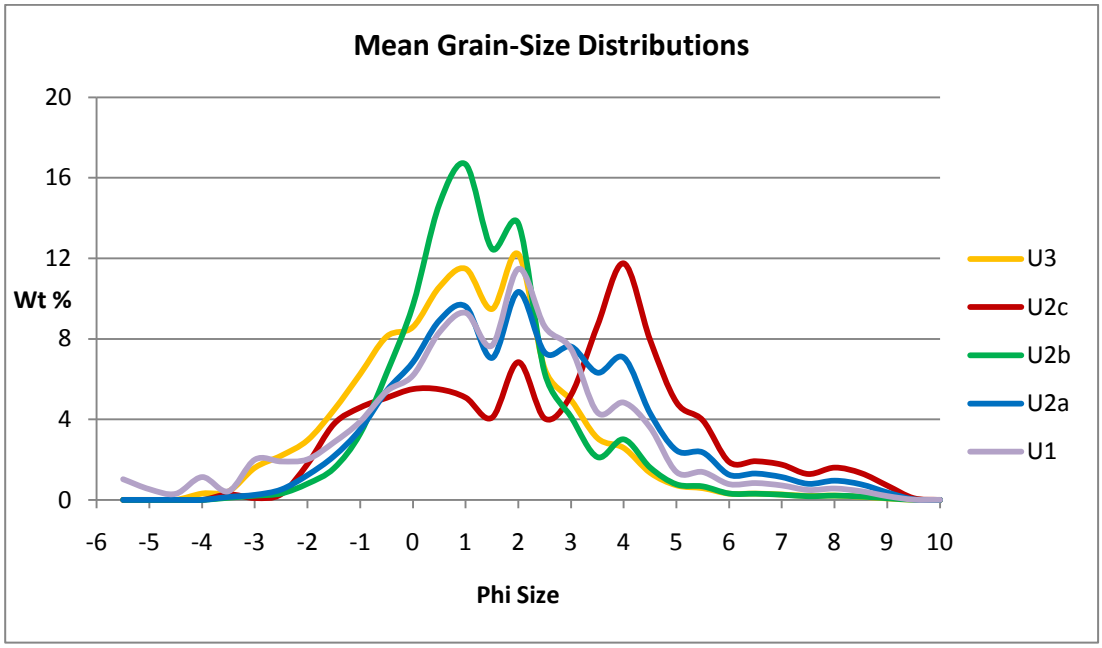

Figure 4.3. The mean grain-size distributions of each unit.

U1, U2a and U3 all have their highest peaks at around1.82 phi, followed by ~0.73 phi (Figure 4.3). They also have shoulders around -0.39 phi and either peaks or inflections at 2.71 and 3.70 phi. Overall the distribution of the three units mirror each other, but with different peak heights. U3 is the coarsest of this group of three and U2a the most fine grained, with U1 falling between the other two.

U2b is distinct from the rest (Figure 4.3). The peak at 0.75 phi is the greatest in height, followed by 1.75 phi. The mode at 3.78 phi is present but 4.5 and 5.5 times

smaller than the other two peaks. U2b has both the least coarse and least fine material of any of the units.

The greatest peak in U2c falls at 3.68 phi (Figure 4.3). Like the other units, a mode at around 1.8 phi is present, but is minor in comparison to 3.68 phi. The well-defined peak at around 0.73 present in the other units is not apparent here. Instead, a broad shoulder between -1.5 and 1.0 phi is seen.

In order to accurately identify the subpopulations of each unit, the data were entered into the SFT program (Wohletz, 2007), described in Chapter 2. Five to six subpopulations were used to describe the grain-size distribution of each unit (Figure 4.4) (Appendix 4.5). The modal parameters that best fit each unit were compared to determine the similarity of the values across the units (Table 4.2). Six modes are shared by more than one unit, but the modes common to all five units are 0.64-, 1.82- and 3.70-phi. In addition, all but U2c exhibit modes at around -0.39 and 2.71 phi and, as is clearly shown graphically (Figure 4.4), U1 has notably more >-2.5-phi material than the other units. The proportion of each deposit falling under each mode varies, but the units share many grain-size distribution patterns. Clearly, some similar grain-forming processes occurred in all the eruptive episodes represented by these deposits. The question, therefore, is whether these processes occurred before material reached the vent, in the vent, during transportation within the eruption column, or as a result of depositional processes. The influence of the latter two processes should be present in distance-related grain-size-distribution trends.

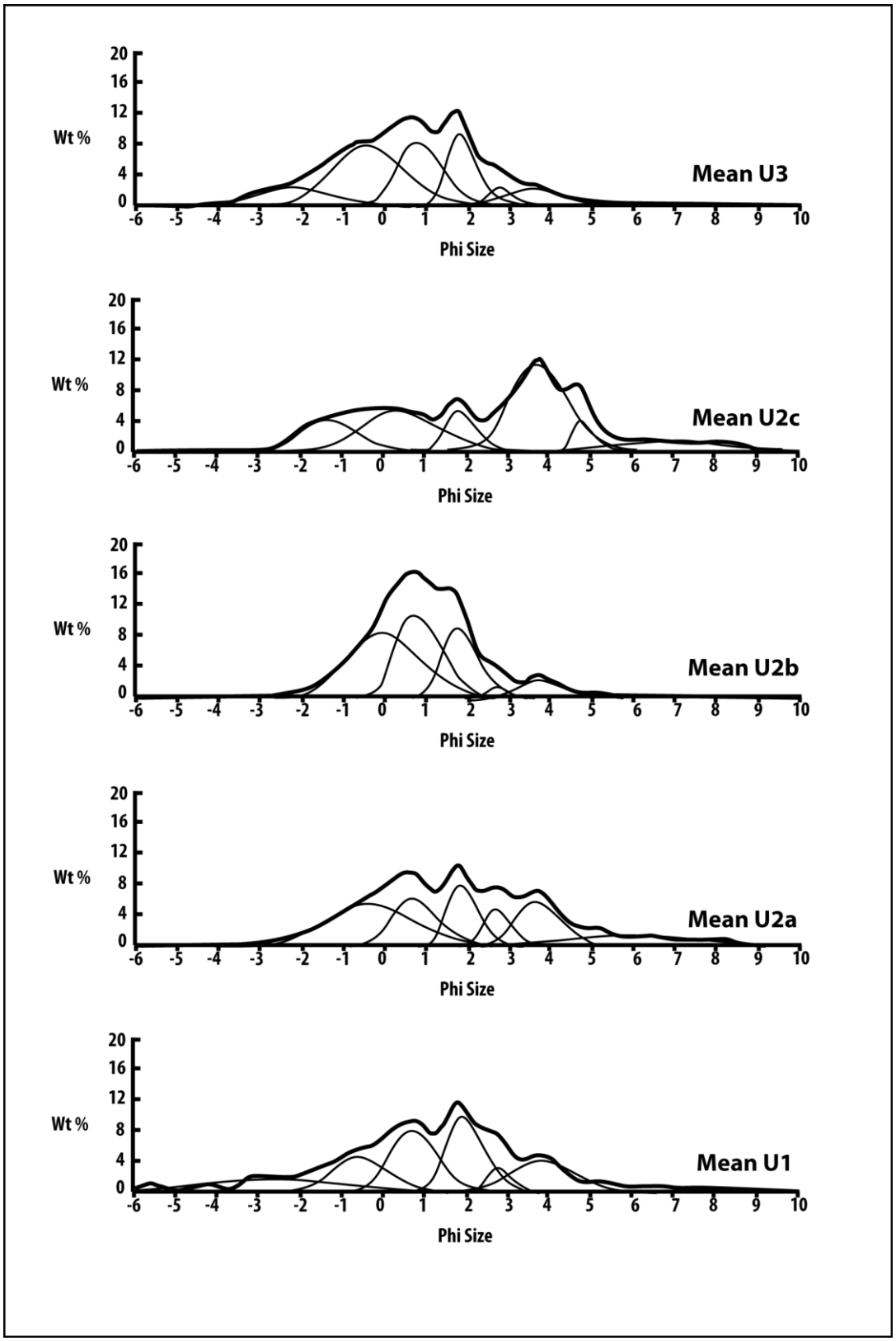

Figure 4.4. SFT plots showing mean grain-size distribution and subpopulations of each unit.

	Modes									
U3	-2.3		-0.45		0.79	1.8	2.73	3.59		
U2c		-1.41		0.32		1.8		3.68		6.96
U2b			-0.11		0.75	1.75	2.71	3.78		
U2a			-0.37		0.7	1.85	2.69	3.67	5.83	
U1	-2.7		-0.63		0.66	1.9	2.7	3.8		
Mean phi size	**-2.50**	**-1.41**	**-0.39**	**0.32**	**0.73**	**1.82**	**2.71**	**3.70**	**5.83**	**6.96**

Table 4.2 Modes of the subpopulations, as determined by using SFT for data analysis.

DISTANCE

The next stage is to consider whether grain-size distribution correlates with the distance a site is located from the vent. This is so that the effects of transport, and any associated processes such as sorting and particle abrasion, on grain-size distributions can be assessed. The localities are grouped by distance (Figure 4.5), and samples from each are compared to see if any trend is apparent (Figures 4.6 and 4.7). It may be expected that grain-size distribution data from the farthest sites should show a shift toward finer grain sizes as a result of transport within a plume or pyroclastic density current, but no such trend exists for any unit: proximal and distal sites have very similar distributions (Figure 4.6). This is also reflected in the modal grain sizes (Figure 4.7), where there is no relation between the distance a site is from the crater, and the modal grain sizes present (Appendices 3.1 and 4.5). For U2a and U2c, larger clasts are more abundant at greater distances (Figure 4.6), which does not correlate with transport controlling sorting and abrasion.

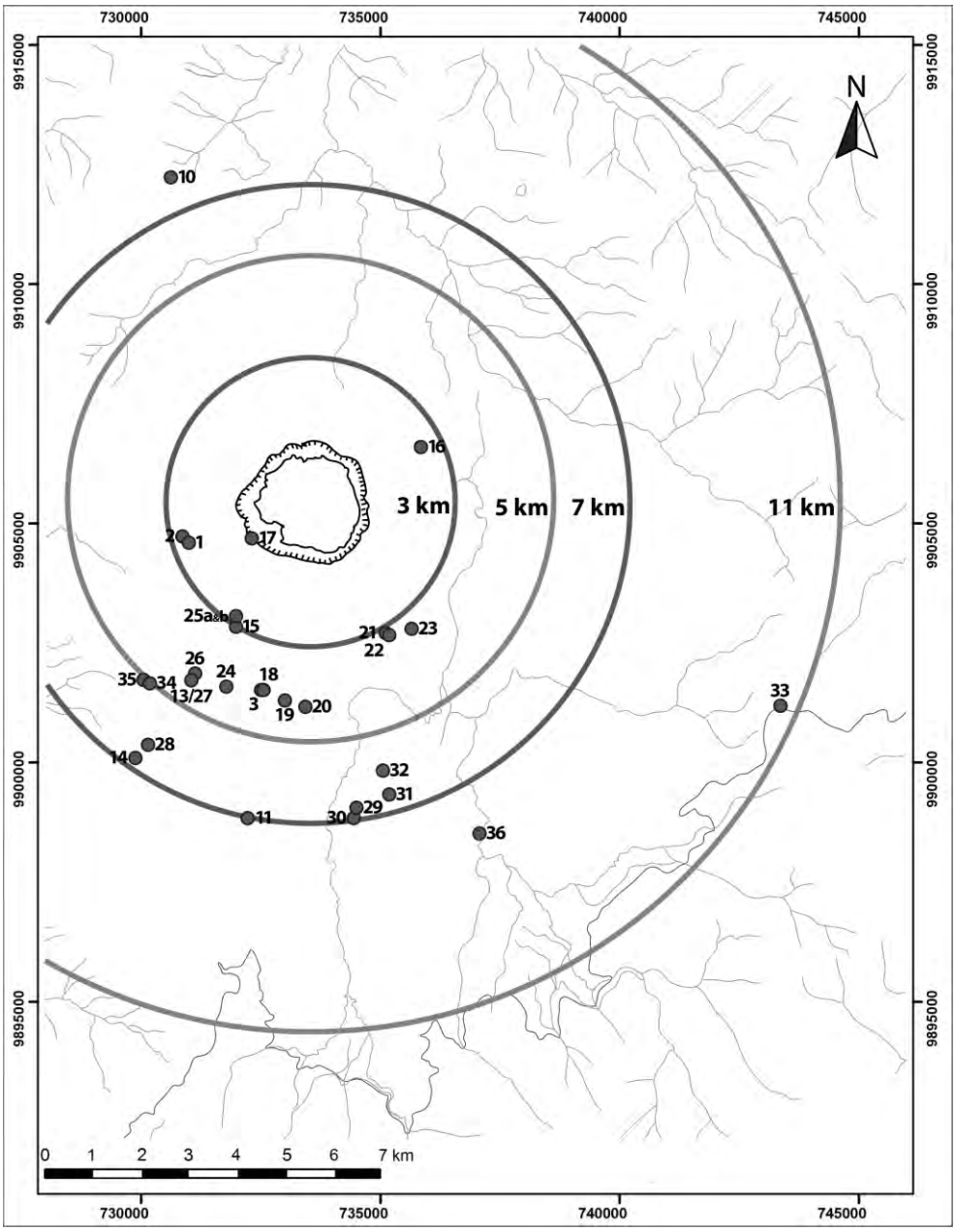

Figure 4.5. Distances from the vent for each of the localities, bracketed for comparison in Figure 4.6

Figure 4.6. Grain-size distributions of samples from each unit, in terms of distance from the vent. U3 is at the top of the sequence, U1 at the base.

Key: distance from the vent

Red	1 - 3 km
Orange	3 - 5 km
Blue	5 - 7 km
Purple	7 - 11 km

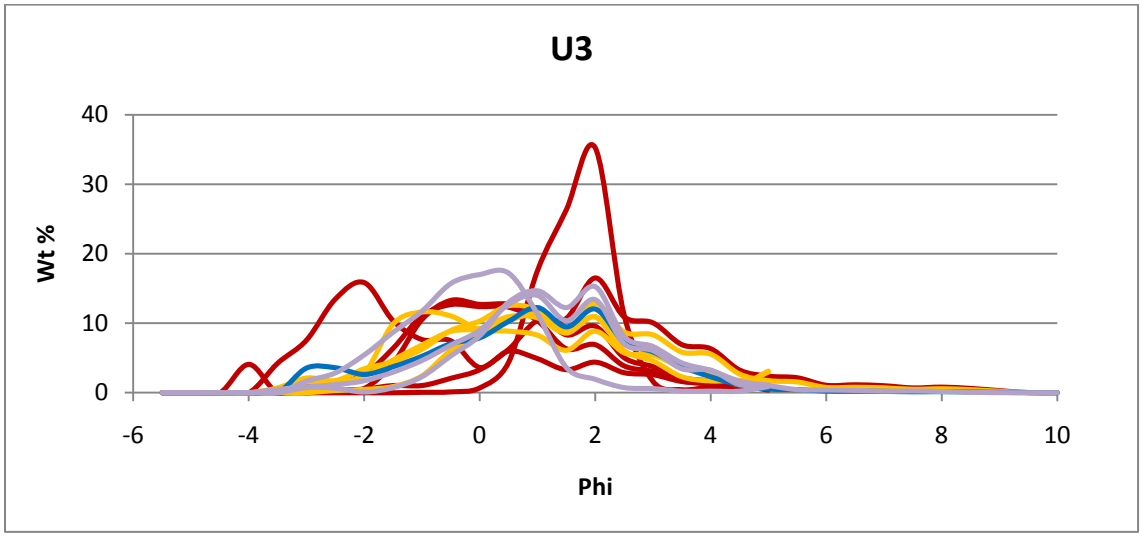

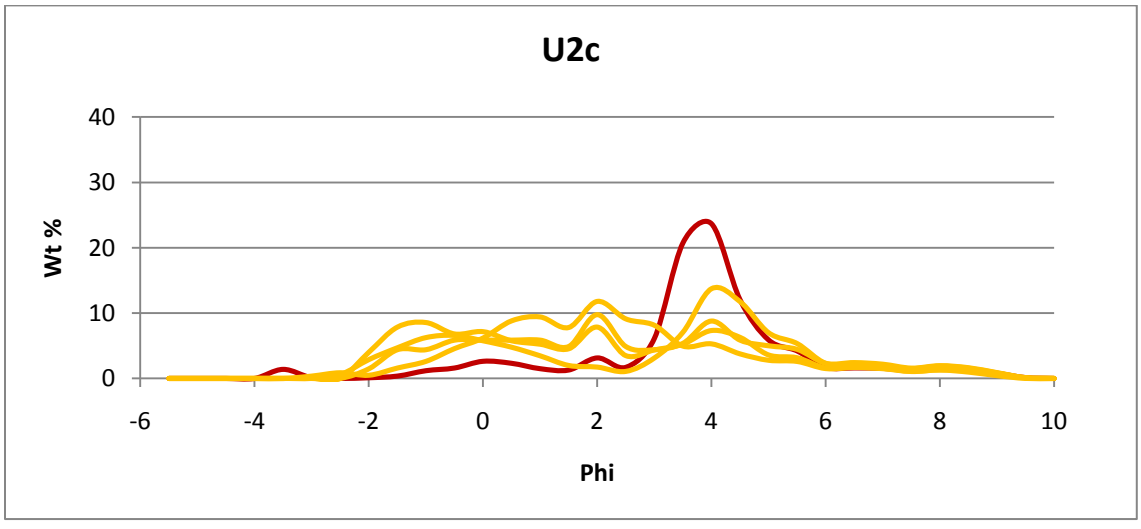

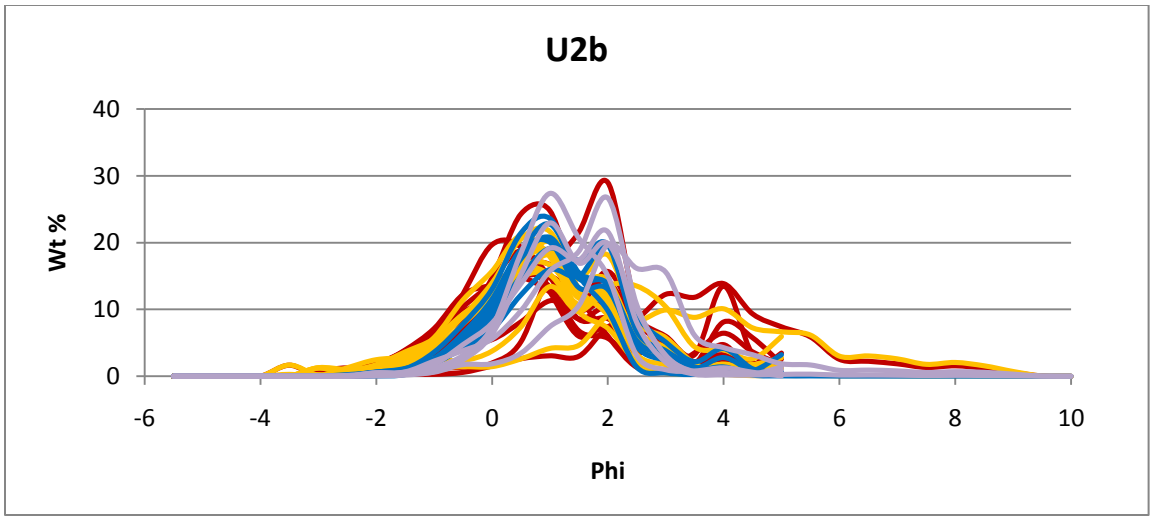

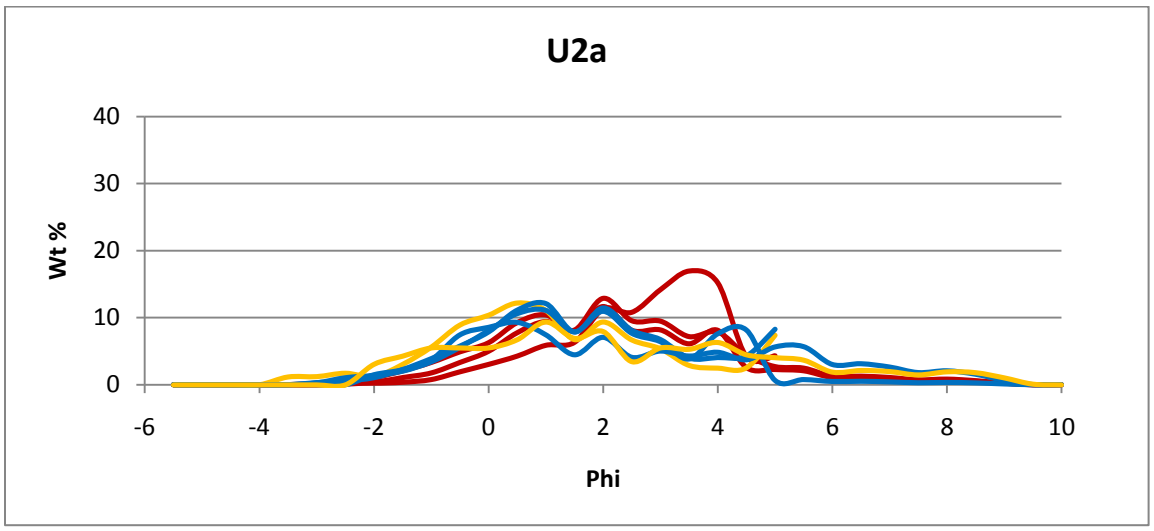

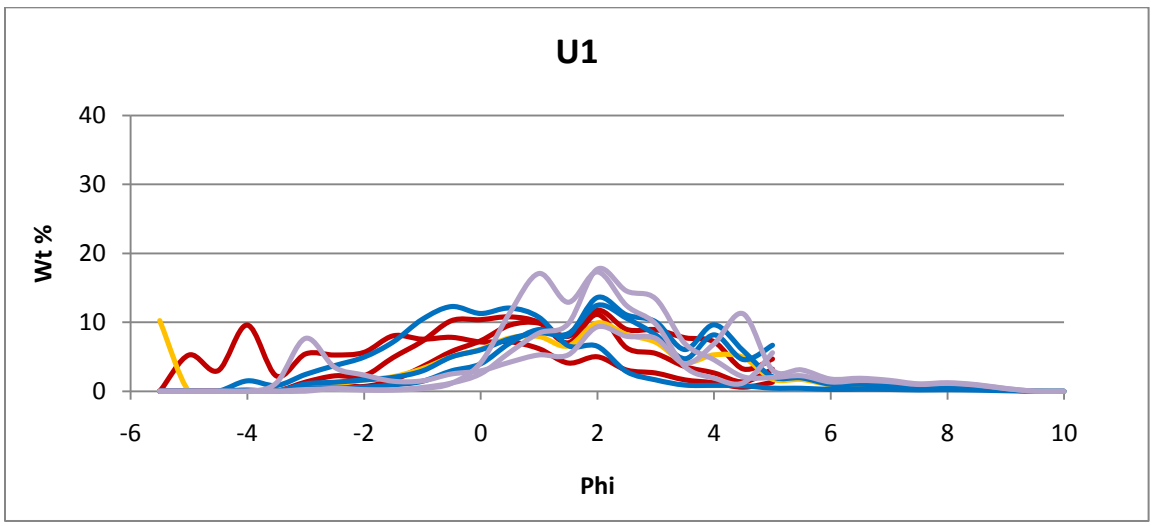

Figure 4.6 continued

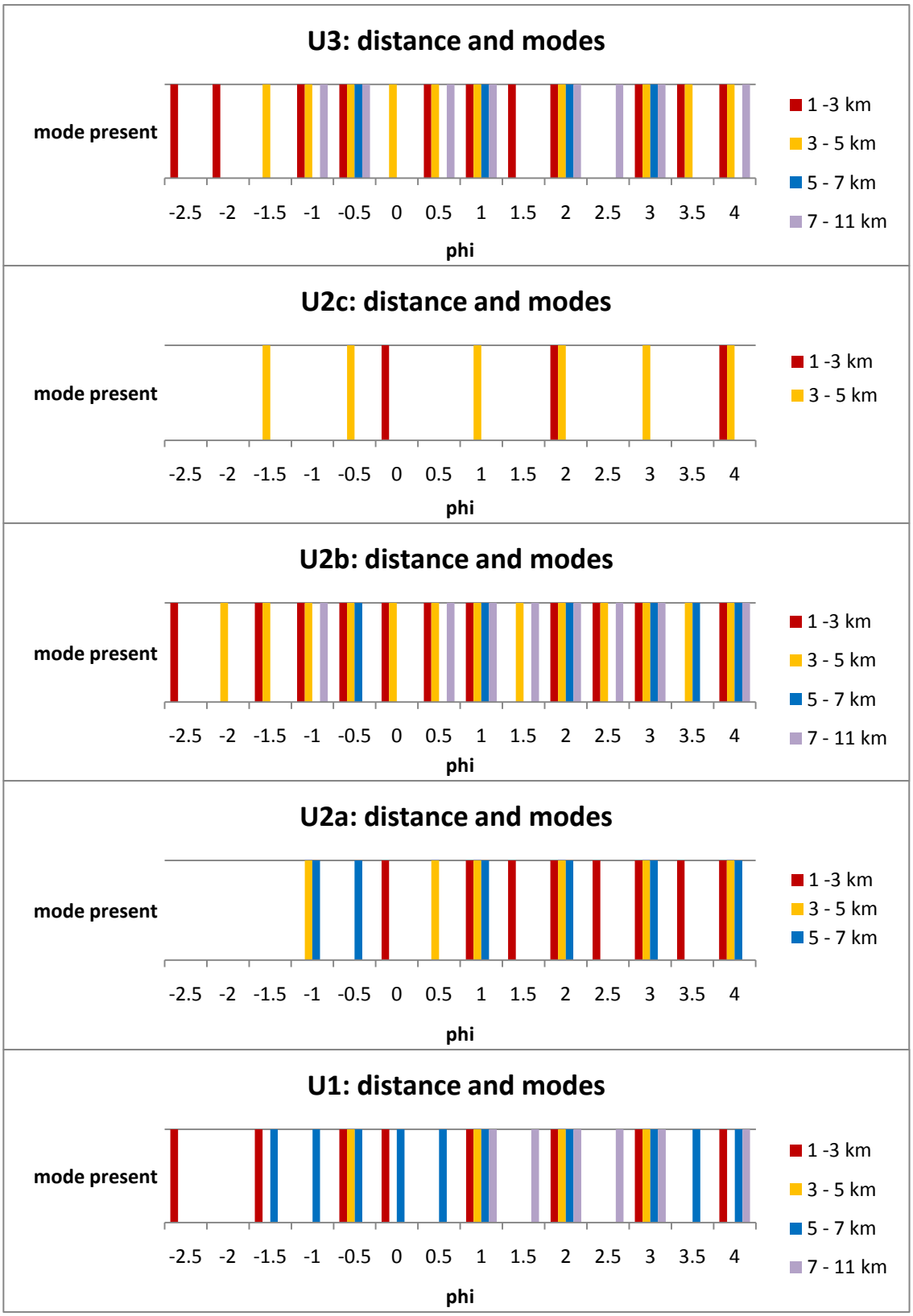

Figure 4.7. The modes that are present in each of the units, with respect to distance.

Aside from grain-size distributions and modal populations, trends concerning the finer grain fractions can be examined. F1 is the weight percent of material <0.0 phi (1 mm) and F2 <4.0 phi (63 μm) in diameter (Walker, 1983; Papale and Rosi, 1993; Di Muro et al., 2008). Both F1 and F2 in U1 increase in wt% with distance (Figure 4.8), by ~30 wt% and ~11 wt%, respectively, over ~5 km. In U2a, the proportion of F1 decreases by ~13 wt % across ~4 km, whereas F2 increases by ~8 wt % over the same distance. F1 of U2b increases by ~13 wt% over ~5 km, whereas F2 decreases by ~5 wt%. F1 and F2 of U2c both decrease over ~1.5 km, both by ~13 wt%. There is little to no change in the values of F1 and F2 for U3, over the ~5.5 km covered.

The question of trends with distance can also be considered statistically. Using the grain-size and sorting parameters as defined by Folk (1974) (Chapter 2), some subtle trends are seen (Figure 4.9). The mean grain sizes (M_z) of U2a, U2b and U3 are independent of distance: there is no relation between the two (Figure 4.9). U1 shows a steady reduction in mean grain size with distance, and U2c an increase. For all units, sorting (σ_1) is independent of distance (Figure 4.9), with very little to no change in sorting with distance.

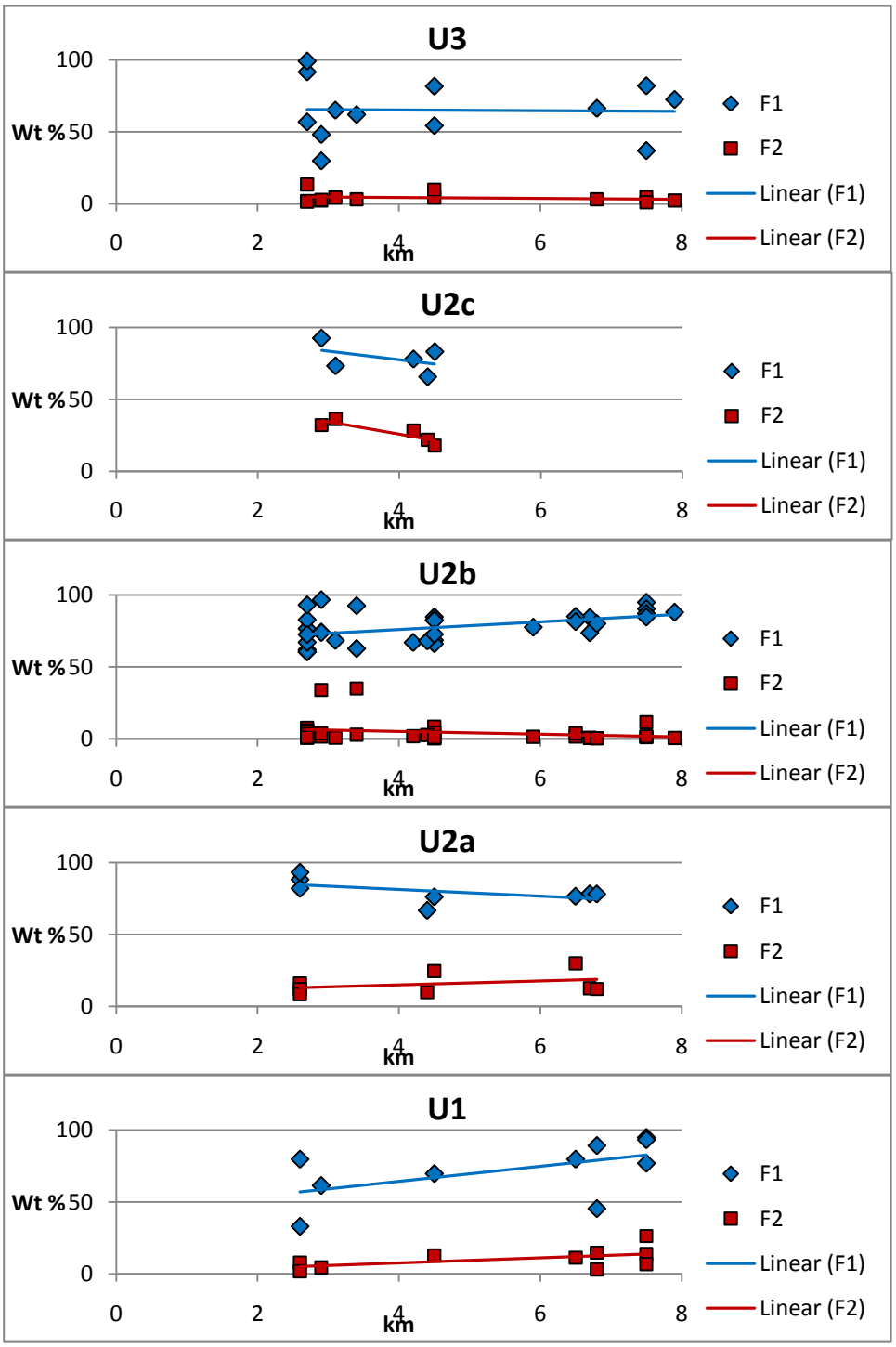

Figure 4.8. Weight percent of the finer grain-size proportions. F1 is material <0.0 phi (1 mm) and F2 <4.0 phi (63 µm).

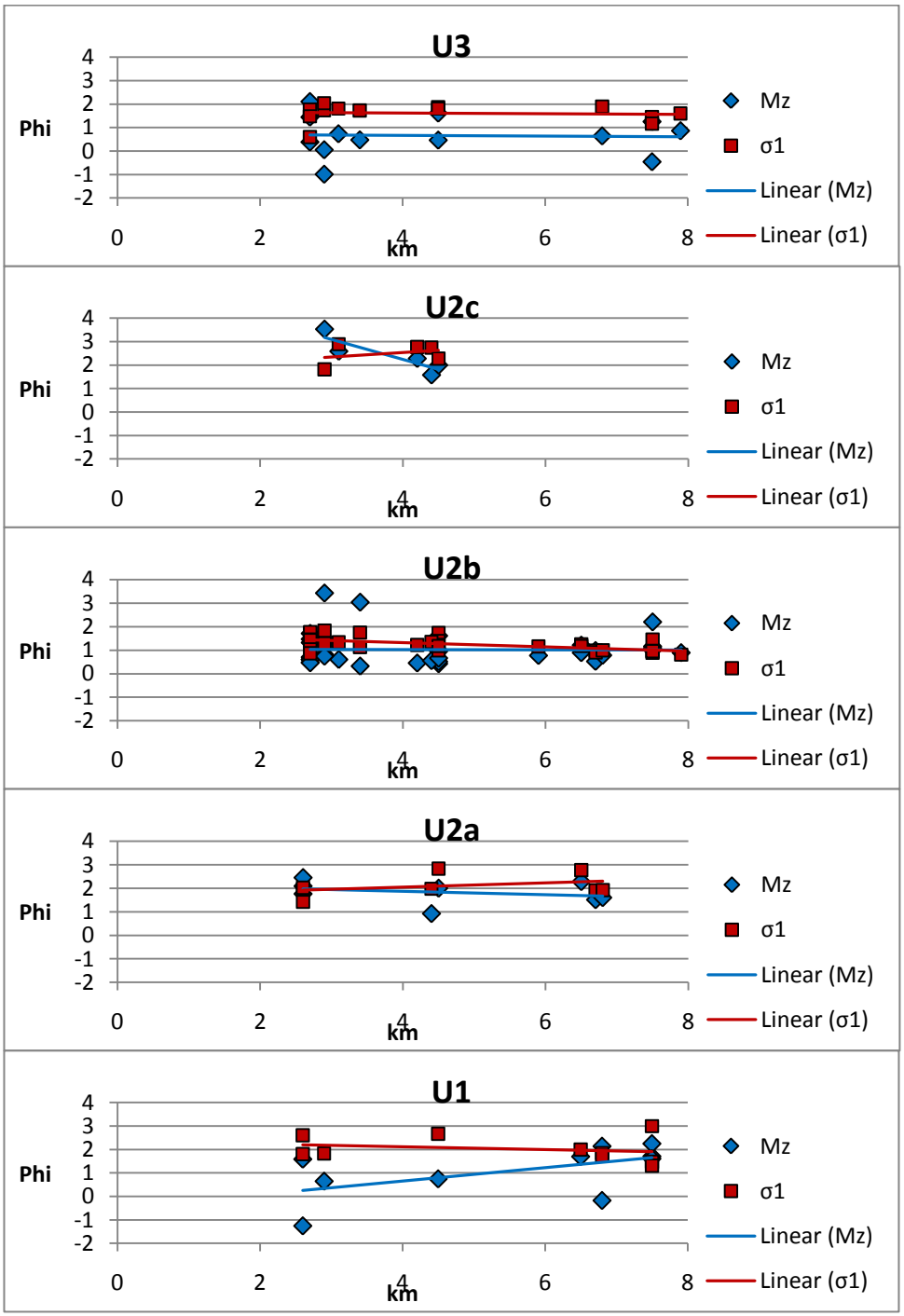

Figure 4.9. Graphical mean grain size (M_z) and sorting (σ_1) (Folk, 1974) with respect to distance. For sorting, lower values, reflecting a tighter range in grain sizes, indicate better sorting.

LOCALITY 17

Locality 17, positioned on the former crater rim and the closest site to the crater center, permits a closer look at the relation between U2a and U2b (Figure 4.10). At other sites, with the exception of Locality 1, U2a and U2b have a single distinct contact. At Locality 17, however, beds with characteristics of each are interstratified. Due to the significance of U2a and U2b to this study, the relation between them is studied in more depth.

U2b is notably different from U2a (and all the other deposits) in that it is better sorted and poorer in fine-grained material (Figure 4.3). In the field the units are also distinguished by color, with U2a characteristically grey, and U2b brownish-red due to the dust that coats many of the U2b grains (see Chapter 1). At locality 17, alternating beds of finer and coarser material occur in the interval of overlap between U2a and U2b. Six samples were collected from this interval, with an additional two samples analyzed from U2a below it (K iv and K v) and two samples from U2b above it (H and J i), bracketing the interval. The sequence of interest is 179 cm thick and includes ten subunits that exhibit grain-size distribution trends that repeat (Figure 4.10). Two of the samples have distributions that resemble that of the mean U2a, as derived from the samples collected elsewhere in the field area (Figure 4.3). Five samples have distributions that resemble U2b, and three other samples are similar to each other but are not like those of any previously described unit.

Of note is sample K iv, one of the four samples bracketing the interval of overlap between U2a and U2b. Field observations based on color indicated an U2a affinity, but grain-size distribution data (Figure 4.10) show that it resembles U2b. The grain-size

distributions of the other bracketing samples, H, J i for U2b and K v for U2a, match the mean trends of those units (Figure 4.10).

The samples similar to U2a at locality 17 have modal grain sizes at around 0.98, 1.82, 2.77, and 3.74 phi, the same as other U2a samples (Figure 4.11). With respect to the mean U2a, locality 17 has more material 0.98 to 3.74 phi, and less outside of this range.

The five U2b-like samples at locality 17 are coarser than the mean U2b, with some material at -4.0 phi. The modal grain-sizes, however, are identical to those of the larger data set. The mean of three non-associated locality 17 samples, labeled "other," do not closely mirror a previously described unit. The grain-size distribution is broadly bimodal, with peaks around 3.20 and 3.87 phi, and in this respect is similar to U2b, albeit at a finer grain size.

With similarities between the grain-size distributions of locality 17 samples and the rest of the data established, the stratigraphic order of the different beds of U2a- and U2b-like material can be considered (Figure 4.12), with sample K v at the bottom and H at the top. Overall, the sequence becomes coarser upward, but median grain size fluctuates. U2a-like material begins the sequence with sample K v. U2b-like tephra was then deposited for the first time, followed by the non-associated fine-grained unit. U2a-like deposits were produced one last time, and thereafter the sequence records the deposition of U2b inter-bedded with the non-associated fine-grained units.

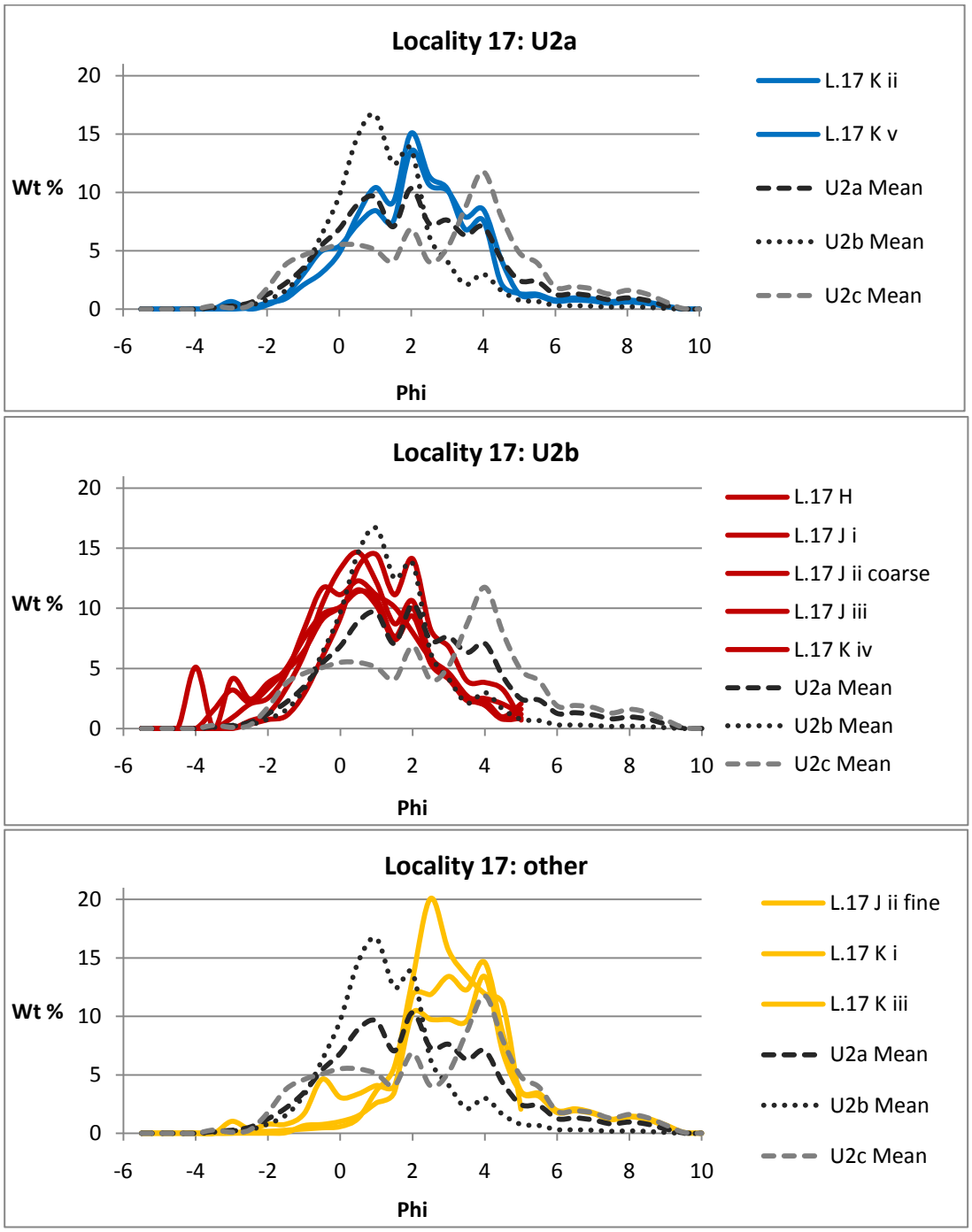

Figure 4.10. The grain-size distributions of samples taken from the former crater rim, where U2a and U2b overlap. Some of the samples exhibit similar grain-size distributions, and are denoted by bold colored solid lines (blue, red and orange). Similar samples are grouped and shown on separate graphs above. The top graph shows samples that closely resemble U2a, as determined from the mean of the other sites (Figure 4.3); the middle graph, samples that resemble U2b; and the bottom graph, samples that are similar to each other, but do not relate to either U2a or U2b.

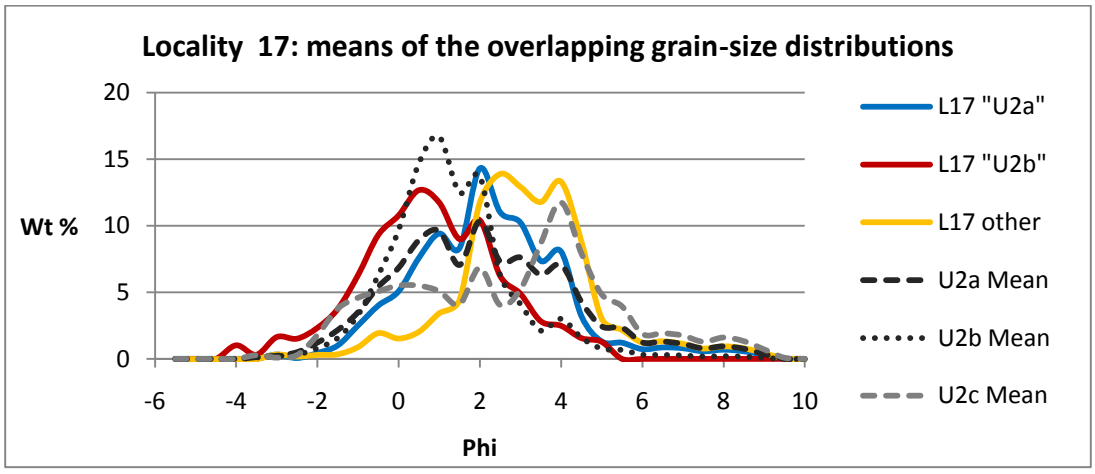

Figure 4.11. The mean grain-size distributions of the samples of the overlap sequence at locality 17. Similarities with mean U2a and U2b, as determined from other sites, are apparent.

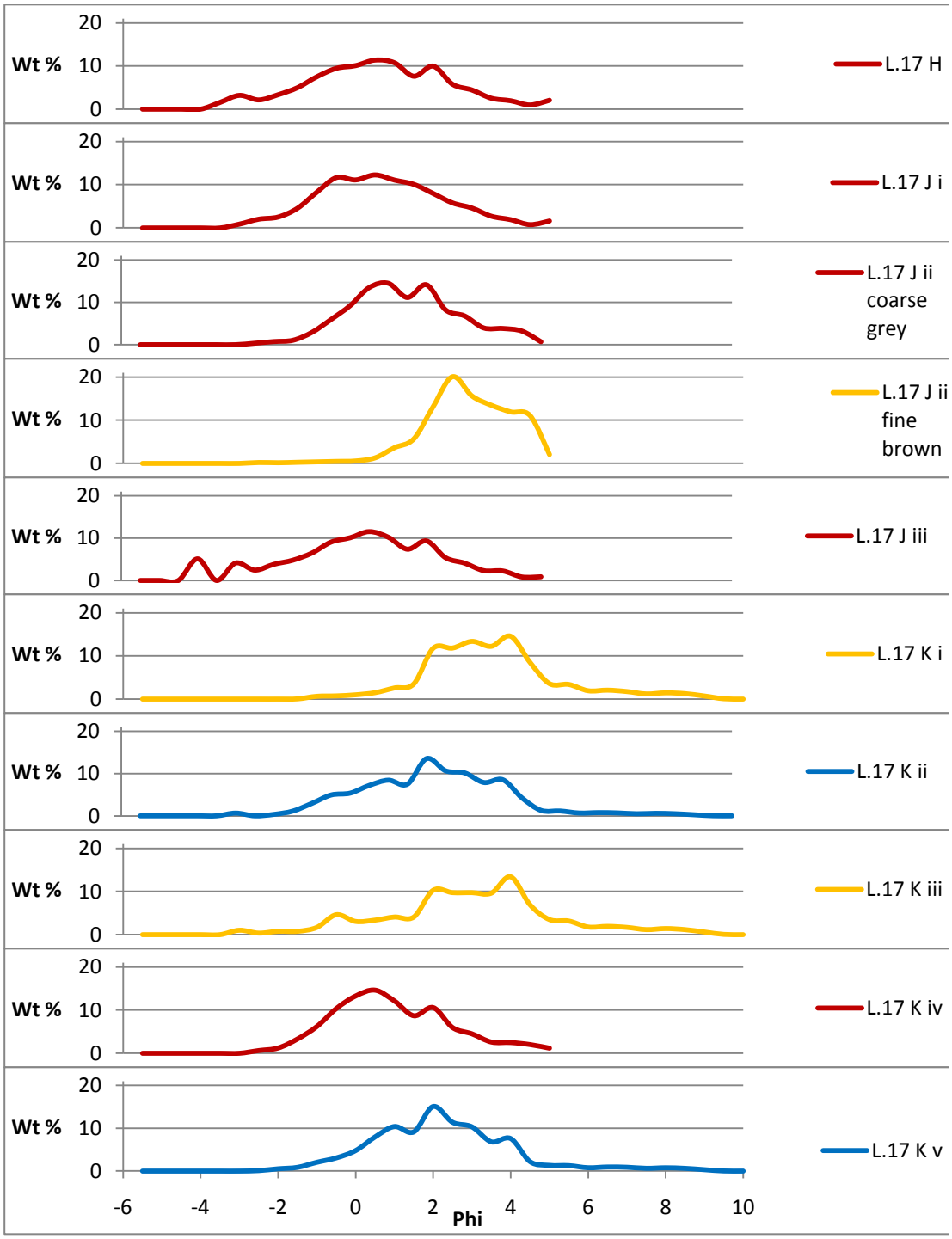

Figure 4.12. The grain-size distributions of the ten samples that lie within the overlap sequence. Sample K v is at the bottom of the sequence; H at the top. Colors are as for Figures 4.10 and 4.11. Blue denotes U2a-like samples; red U2b-like samples; orange non-associated samples. Samples of similar grain-size distribution are not necessarily stratigraphically adjacent.

GUIDANCE FOR COMPONENTRY SAMPLE SELECTION

The five stratigraphic units considered here, U1 through U3, are only partly distinguished by their grain-size distributions. U2b tends toward a bimodal distribution whereas U1 and U3 have more variable polymodal distributions. The five units are similar in their modal grain sizes, with common subpopulations at 0.64, 1.82 and 3.70, albeit in varying proportions. Analyzing the data in terms of distance does not reveal any trends for any of the units. Therefore the next step is to look at the components that make up these modes in order to see whether their compositions vary. For componentry the closest half-phi interval of the common subpopulations, 1.0, 2.0 and 4.0 phi, are used in order to look for differences. Particular attention is paid to the componentry of the 1.0 and 2.0 modes: these are the most significant subpopulations in all but U2c and, despite being close in size, clearly define individual modes.

CHAPTER 5

RESULTS: COMPONENTRY

The componentry of the deposits was examined to determine the proportions of glass, crystal and lithic fragments in each unit and each modal grain-size population. These data are important for understanding if physical processes were occurring that could, for example, produce free crystals directly from the magma and/or milled pumice. In addition, the proportion of lithic fragments indicates the degree to which vent and conduit erosion were occurring during the eruption. Comparisons can then be made between units to discover how eruption processes differed during the various stages of the eruption.

A more detailed approach to componentry, where glass and crystals are separated into various types, can highlight differences in the source magma of the units. This could be reflected in both the glass type and the overall composition of the free crystal assemblage. This approach also allows for trends relating to a site‟s distance from the vent to be examined.

The componentry study was carried out on the closest half-phi size to the modes identified from the grain size analysis (Chapter 4). Grain-size populations of -2.5, -1.0, 0.0, 1.0, 2.0 and 4.0 phi in size were categorized. Glass was categorized by color, and crystals by mineral type. Lithic fragments, holocrystalline fragments, and glass-crystal-aggregates were also classified. The analyzed samples were collected from six sites: locality 1/2, locality 13 (also known as 27), locality 30, and locality 10, situated 2.5 km, 4.5 km, 6.5 and 7.5 km from the crater, respectively, and locality 15 and locality 24, situated 3 and 4 km from the crater, respectively, for U2c (Figure 5.1).

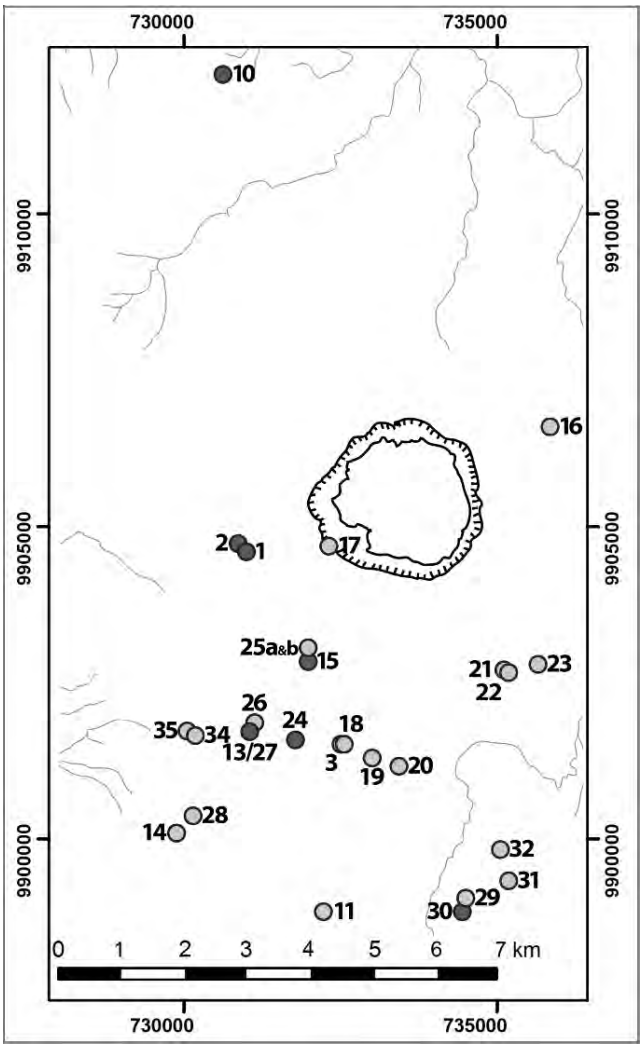

Figure 5.1. Location of the sites studied in this chapter, marked by dark gray circles. This map shows a partial section of the entire field area. For full map, see Figure 3.1.

Three variables must be considered when comparing trends in componentry: the unit, the grain size, and the site‟s distance from the vent. This chapter first examines all the data in general, then analyzes each of these variables in turn. The error of the componentry method for this study has been calculated at 0.89 % for -2.5 phi, 2.52% for -1.0 phi, 2.79% for 0.0 phi, 1.83% for 1.0 phi, 1.81% for 2.0 phi and 5.24% at 4.0 phi (Appendix 5.3). These errors are taken into consideration in the evaluation of the data discussed below.

COMPONENT DATA

This section covers all the component data in general, first by sample, and then by unit. Here the components are categorized as glass, crystal or other so that the broad trends can be examined.

By Sample

Grain type

U1 and U2a have a mode at -2.5 phi; and these grains are all glass, with the exception of one site (Figure 5.2). This exception belongs to a U1 sample in which three of the 35 grains are holocrystalline fragments, and one is a lithic fragment. Glass is present in all units at all sizes, but generally decreases in abundance at the smaller grain sizes until 4.0 phi, where it returns to dominance. For all the units, crystals are present at -1.0 phi and smaller sizes, becoming roughly equal in proportion to glass at 1.0 phi. The proportion of crystals that have adhering glass is 36 – 46% (Figure 5.3). The other category, encompassing lithic fragments, holocrystalline grains and glass-crystal aggregates, constitutes a minor component of all units at all sizes. At a mean of 5 wt %, U2b has the greatest proportion of grains in this category and at 1.5 wt % U1 the least.

The level of agreement varies between samples of the same unit (Figure 5.2). This is quantified in appendix 5.4.2, where the mean, upper and lower values for each unit at each grain size are given. Overall, U2b has the most agreement amongst its samples and U2a exhibits some of the greatest variance.

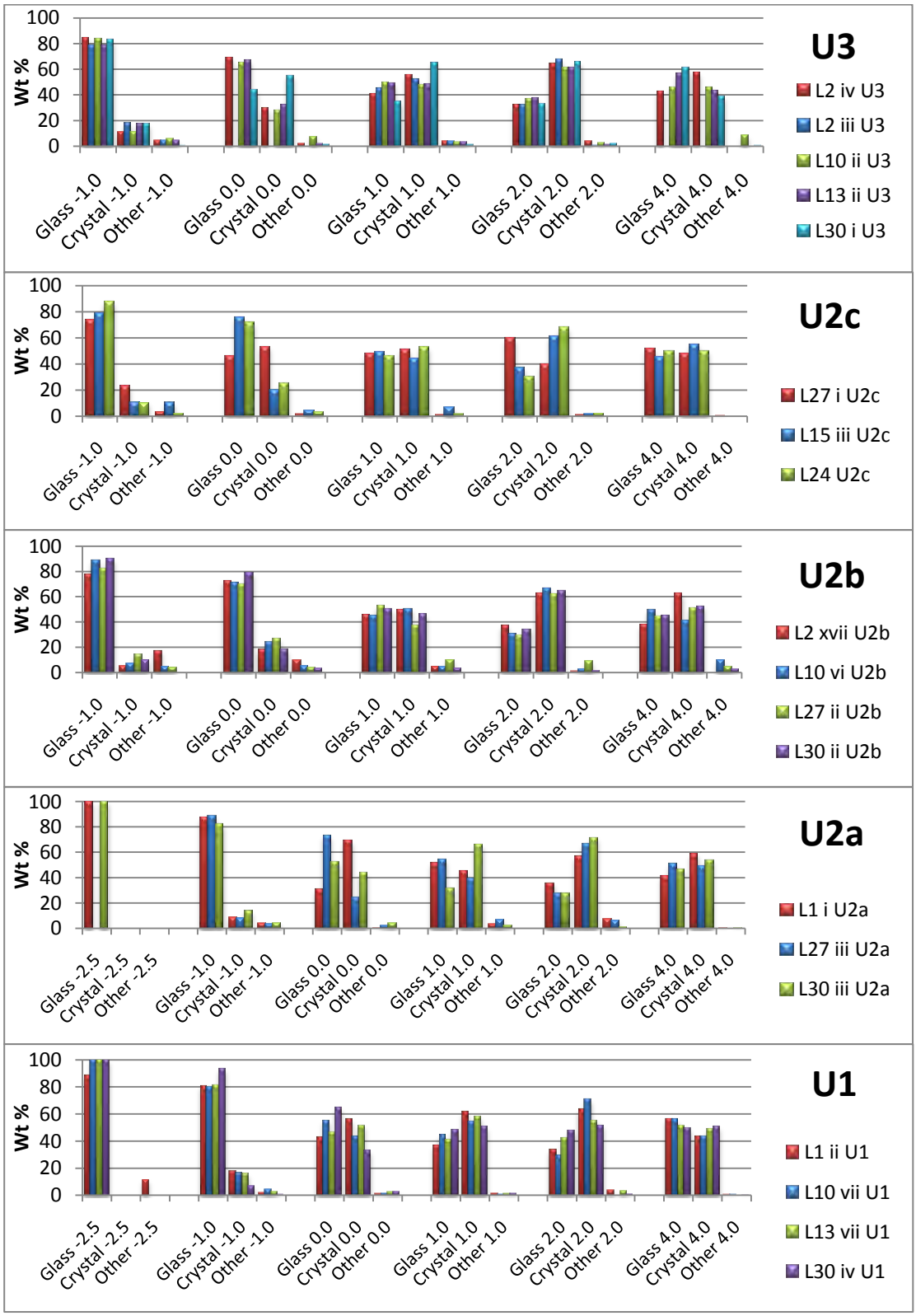

Figure 5.2. Complete suite of data, with grains categorized in terms of glass, crystal and other, where other includes lithic fragments.

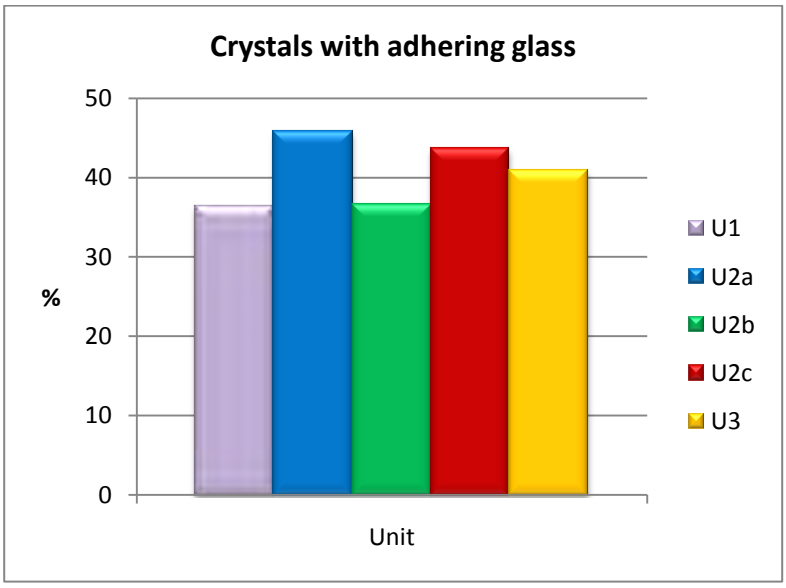

Figure 5.3. Percentage of all crystals that have adhering glass attached.

Staining

Some grains have a veneer of orange-colored dust and care was taken to distinguish this from grains that are stained orange. This was achieved by rinsing the grains in water to remove dust prior to assessment. The number of stained grains, across all units and sizes, is small (Figures 5.4 and 5.5). The number of stained grains is independent of grain size, but some units have more stained grains than others. U2b has the most stained grains, with a mean of 12 wt %, and U2c the least at 2.5 wt%.

Overall, 71 wt % of all stained grains are glass, 22.5 wt % crystals and only 4.5 wt % are lithic fragments. However, this partly reflects the different abundances of the grain types. When considered in terms of the proportion of each grain type, from all units, 67 % of lithic fragments are stained, compared with 8 % of glass and 6 % of crystals. Depending on the unit, however, there is a notable variation in these Figures (Figure 5.6). The lithic fragments in all units and the glass-crystal aggregates of U1 are

the only grain types to have >20 wt % stained. Also of note is the variability of the proportion of stained lithic fragments, ranging from 25 wt % in U2a to 91 % in U2b.

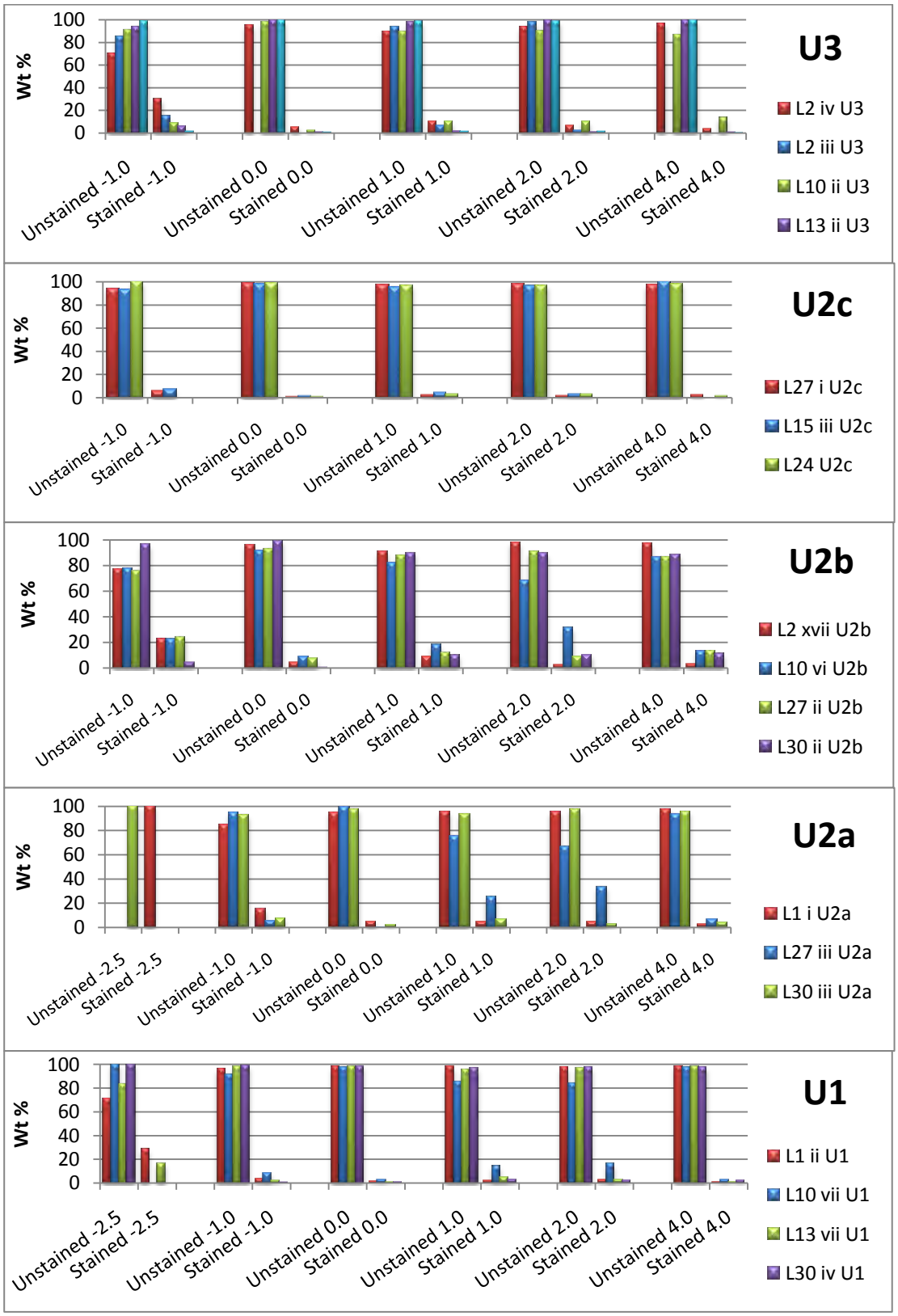

Figure 5.4. The complete suite of data, with grains categorized in terms of stained and non-stained.

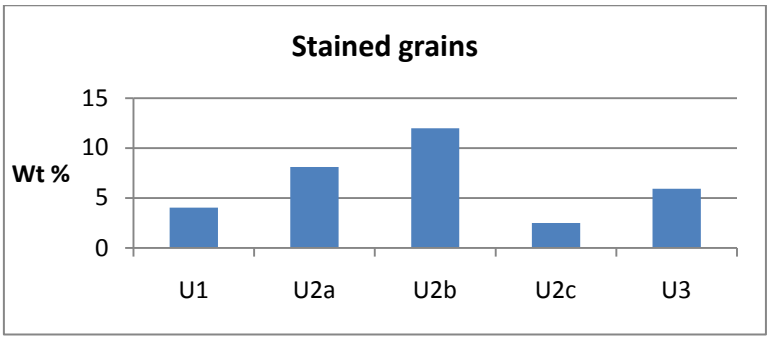

Figure 5.5. Weight percent of stained grains for each unit.

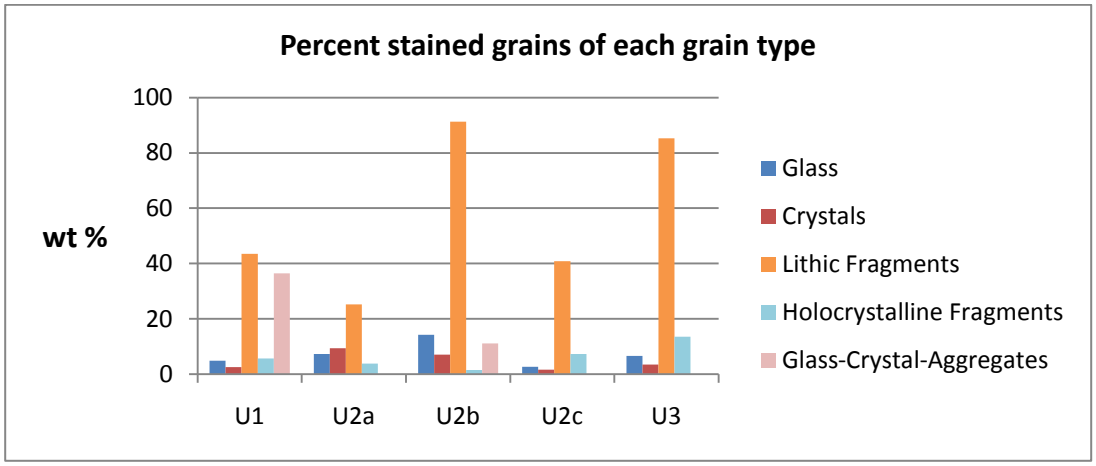

Figure 5.6. Weight percent of stained grains, in terms of grain type. Lithic fragments are the most commonly stained grain type, although there is great variation depending on the unit.

Unit mean componentry and grain-size distributions

To consider componentry in terms of grain-size, the mean of the samples from each unit is calculated and then the data from each phi size weighted with respect to the grain-size distribution (Figure 5.7). From these plots it becomes clear that the dominant modes, 1.0 and 2.0 phi, are similar in their componentry as well as their wt %

contribution to each unit. The 2.0 phi mode has proportionately more crystals than 1.0 phi, and, in all but U2b, 2.0 phi has the greater wt % of the two modes. Later in this chapter, the 1.0 and 2.0 phi modes are analyzed in more detail in order to determine the differences between the two.

Unlike the general componentry discussed above, the presence of stained and non-stained grains is not definitively dependent on grain size (Figure 5.8). For all units except U2c the 1.0 and 2.0 phi modes have the greater proportion of stained grains. Most of the stained grains of U1 are found at these two grain sizes. U2a has a few more stained grains at the other sizes too, and the proportion increases with U2b. U2c is almost without stained grains. Stained grains within U3 are again found at the 1.0 and 2.0 phi sizes, as well as at -1.0 phi. Whilst the 1.0 and 2.0 phi modes are associated with the stained grains, they are by no means the exclusive modes. When the overall low proportions of stained grains present in each unit is additionally considered, the data do not strongly indicate a grain-size-related trend that can be applied across the units.

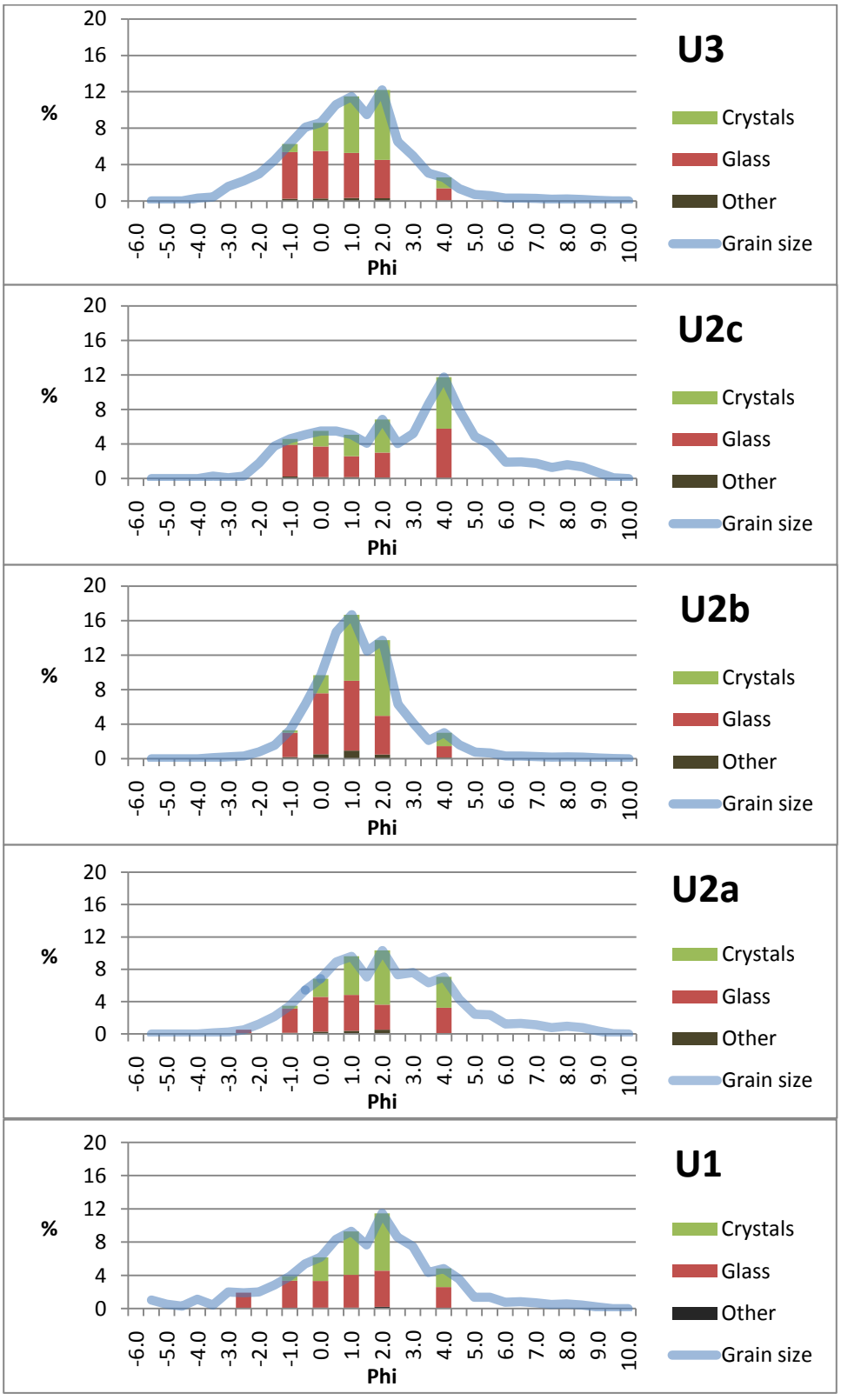

Figure 5.7. Mean componentry and mean grain-size distribution of each unit.

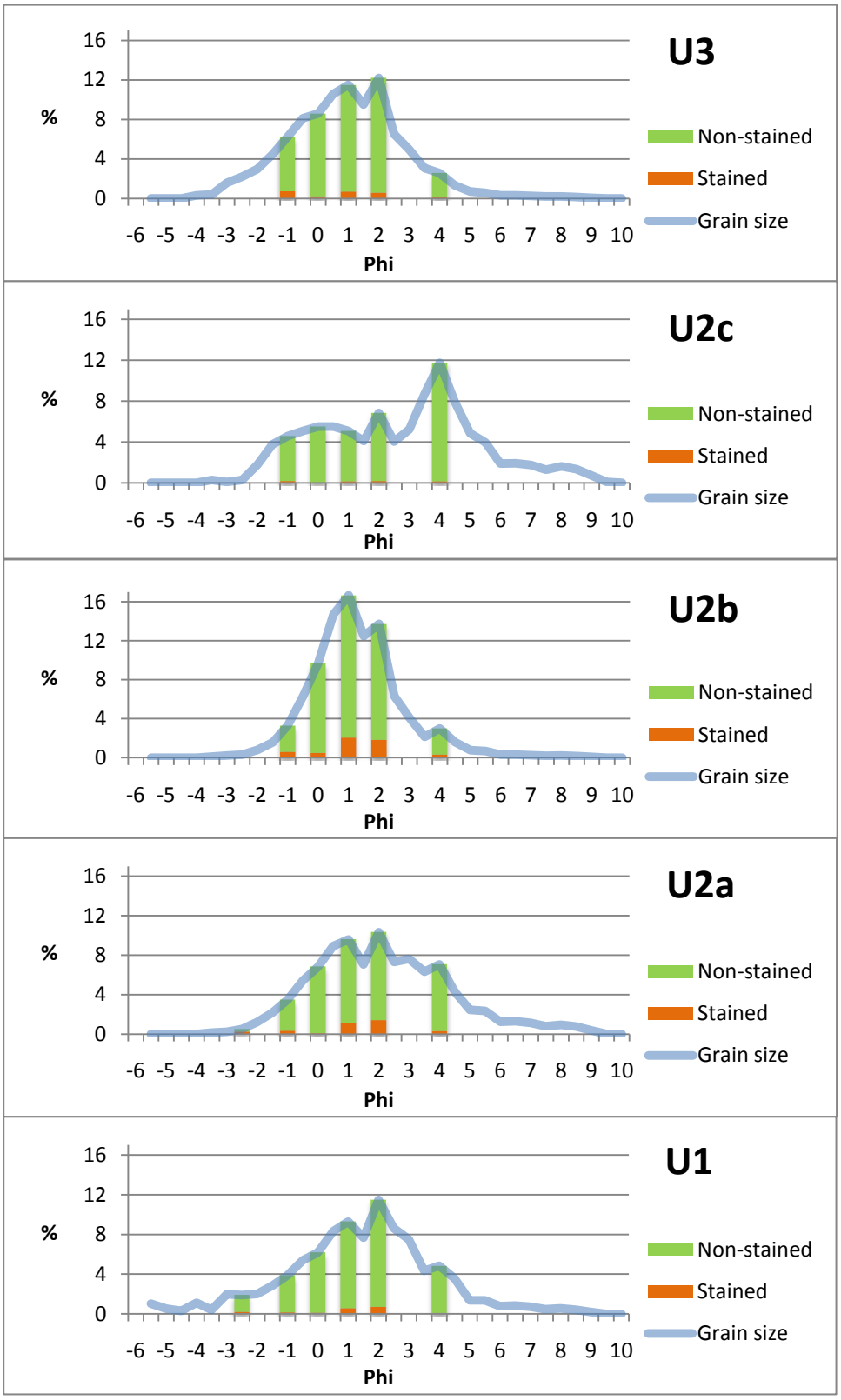

Figure 5.8. Mean proportion of stained and non-stained grains with respect to the mean grain size distribution of each unit.

MODE

As previously discussed, the general componentry of the 1.0 and 2.0 phi modes are very similar, the noticeable difference being that 2.0 phi, with the exception of U2c, is richer in crystals than 1.0 phi. However, as seen in the grain-size distribution graphs (Chapter 4), the modes are very distinct. A more detailed componentry classification of the units at Locality 13/27, selected for its medial location 4.5 km from the crater, examines the differences between the crystals that make up the two modes (Figure 5.9).

Felsic crystals dominate, and plagioclase feldspar is by far the most numerous at both grain sizes across all units (Figure 5.9). U1 has a similar percentage of crystals at 1.0 and 2.0, 41% and 42%, respectively, which falls within the 2.5% error (Appendix 5.3). The 2.0-phi fraction has more quartz, potassium feldspar, mafic crystal and other grains than 1.0 phi, and correspondingly less plagioclase feldspar.

U2a and U2b show the greatest difference in componentry between the grain sizes (Figure 5.9). At 1.0 phi, the proportion of glass, 54% for U2a and 53% for U2b, is higher than at 2.0 phi, 27% and 29%, respectively. In U2a, the remaining components increase in proportion at 2.0 phi, with the exception of potassium feldspar, which remains absent, and the „other" grains, which maintain approximately the same abundance. In U2b, the same relations hold true, with the addition of potassium feldspar, where it is present in similar proportions at both grain sizes. As seen in these Figures, the components of U2a and U2b are similar to each other. The difference is that U2b includes potassium feldspar, albeit at just 2%, and has more "other" grains. Also, at 1.0 phi, U2b has fewer mafic crystals, and at 2.0 phi less quartz than U2a. Otherwise, the componentry of U2a and U2b, at 1.0 and 2.0 phi, are very similar to each other.

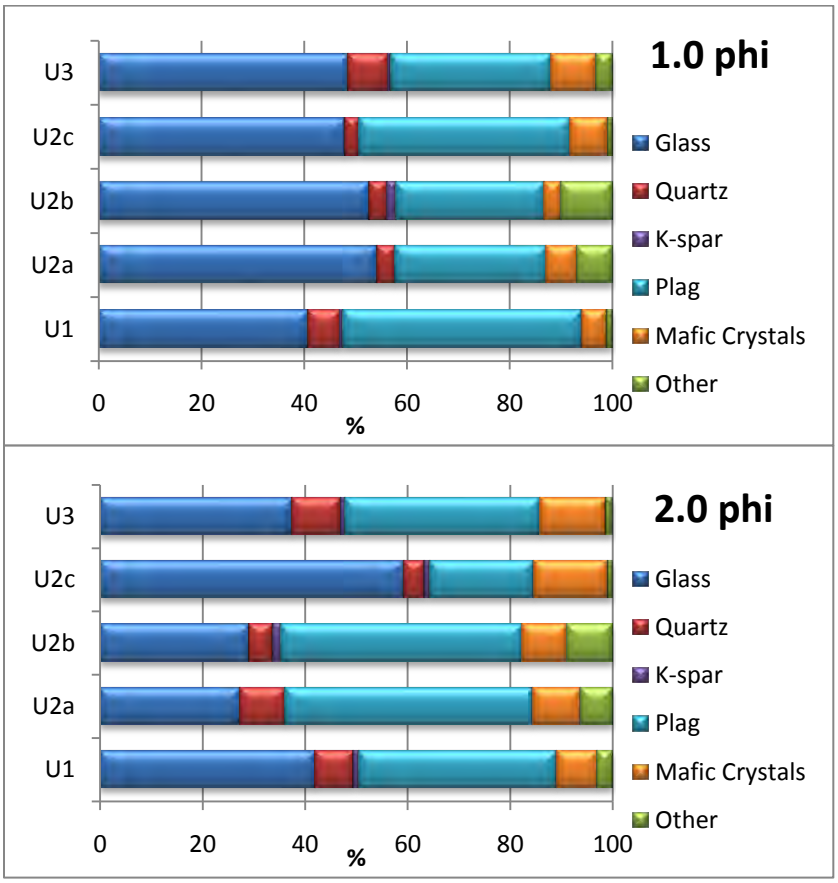

Figure 5.9. Detailed componentry of the crystals of L.13/27, comparing the 1.0 and 2.0 phi modes in all the units.

U2c has fewer crystals at 2.0 phi, both with respect to the lower units and in comparison to U2c at 1.0 phi. However, when considered in terms of grain-size distribution (Figure 5.7), where 2.0 phi is the larger of the two modes, this apparent decrease in crystals is not borne out in absolute numbers. Figure 5.7 shows that a proportional decrease in crystals occurs between 1.0 phi and 2.0 phi, but both crystals and glass increase in number at the smaller grain size. Therefore this apparent decrease in crystals more accurately reflects a shift in the relative proportions between components and not absolute values. Further comparison between the two modes of U2c shows an

increase in all components at the finer grain size, except plagioclase, which decreases by half, and other grains, which remain the same. Finally, U3 shows a decrease in glass and "other" grains at 2.0 phi, and an increase in all of the other components, compared to the 1.0 phi fraction.

From grain-size distribution data (Chapter 4), it is apparent that these two modes are distinct from each other. However, the componentry data so far have not shown them to be significantly distinctive. To look for more subtle trends, the glass types have been plotted in terms of a ratio with respect to white glass, the most abundant type, and similarly the crystals have been plotted with respect to plagioclase feldspar (Figure 5.10).

In terms of crystal type, U1 and U2c have large differences between the two modes, but the other three units are similar. For glass type, U2a and U2b exhibit varying data and the rest do not. However, the way in which the modes vary is not consistent. For example, in terms of glass type, the 1.0 phi mode of U2b has more grains with respect to white glass, whereas for U2a it is the 2.0 phi mode that exhibits dominance. The crystals of U2c have the greatest variation, and yet the relative proportion of crystals, in particular biotite and the other mafic minerals, does not vary. It is evident, therefore, that, whilst small variations are present, the component proportions do not definitively define the modes.

Another consideration is the shape of the grains. The dominant mineral, plagioclase feldspar, is considered in this respect. Due to its habit, plagioclase feldspar crystals may maintain a tabular form or be blocky in shape. The shape of 100 of these crystals at both 1.0 and 2.0 phi is examined (Figure 5.11). The proportion of the two grain shapes remains constant for all the units and both the modes.

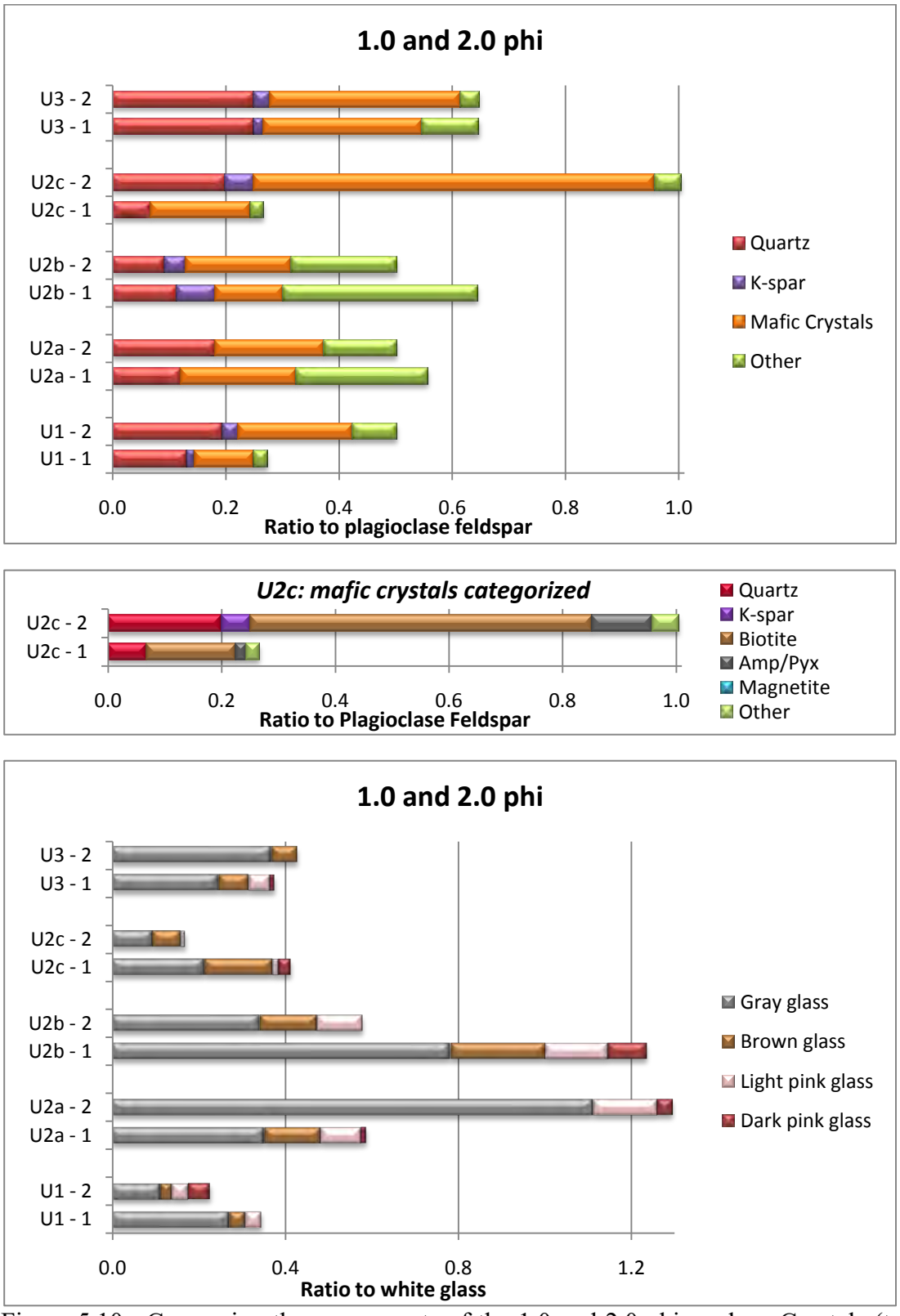

Figure 5.10. Comparing the components of the 1.0 and 2.0 phi modes. Crystals (top and middle) are given as a ratio to plagioclase feldspar, and glass (bottom) as a ratio to white glass. (Locality 13/27)

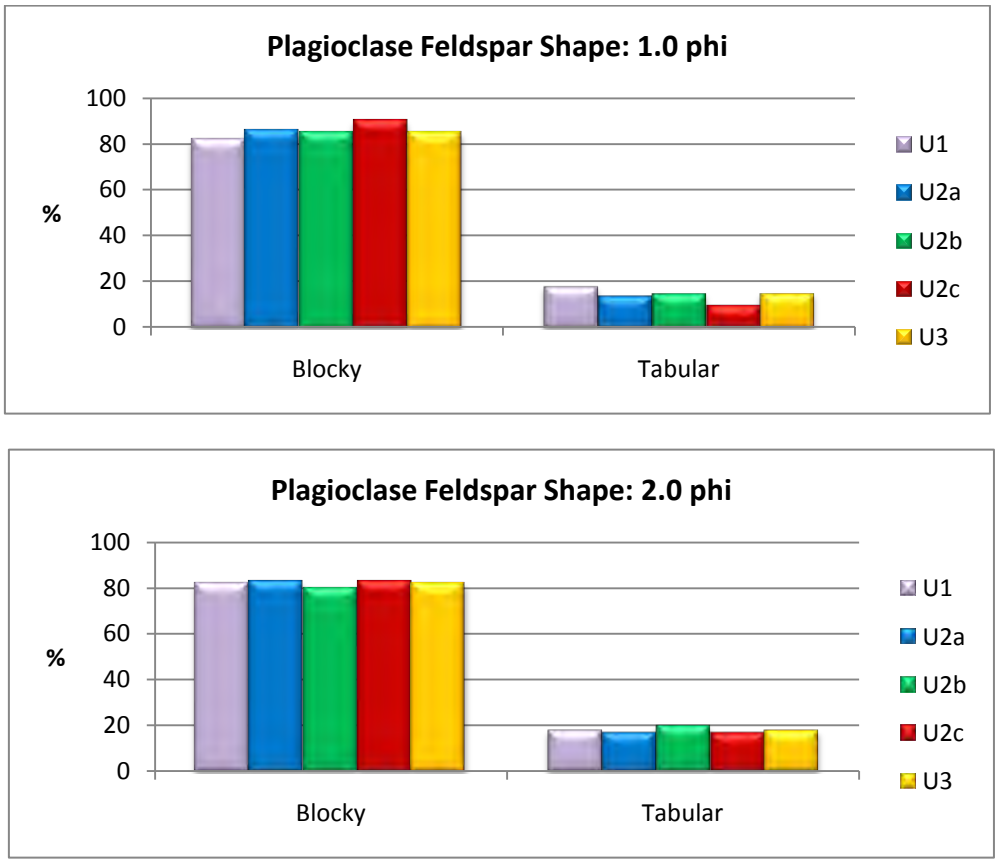

Figure 5.11. The shape of plagioclase feldspar grains in the 1.0 and 2.0 phi modes. (Locality 13/27)

The componentry of the 1.5 phi grain size is examined to link the 1.0 and 2.0 phi modes (Figure 5.12). These data show that at 1.0 phi, the proportion of glass is either greater than or approximately equal to that of the crystals, with the exception of U1. At 2.0 phi, with the exception of U2c, the proportion of crystals is higher than glass, indicating that, with respect to 1.0 phi, the 2.0 phi modal grain size is most likely a product of the crystal population, not the glass population. In U2c, the proportion of crystals remains approximately equal at all three grain sizes, whereas the proportion of glass it higher than crystals at 2.0 phi.

In conclusion, the presence of 1.0 and 2.0 phi modal grain sizes is a characteristic of these deposits. Componentry data suggest that the 2.0 phi mode is likely an artifact of the crystal population. However, componentry data have not shown there to be any systematic difference between the type or proportion of minerals in the 1.0 and 2.0 phi modes, meaning the question of why both exist so prominently is unresolved.

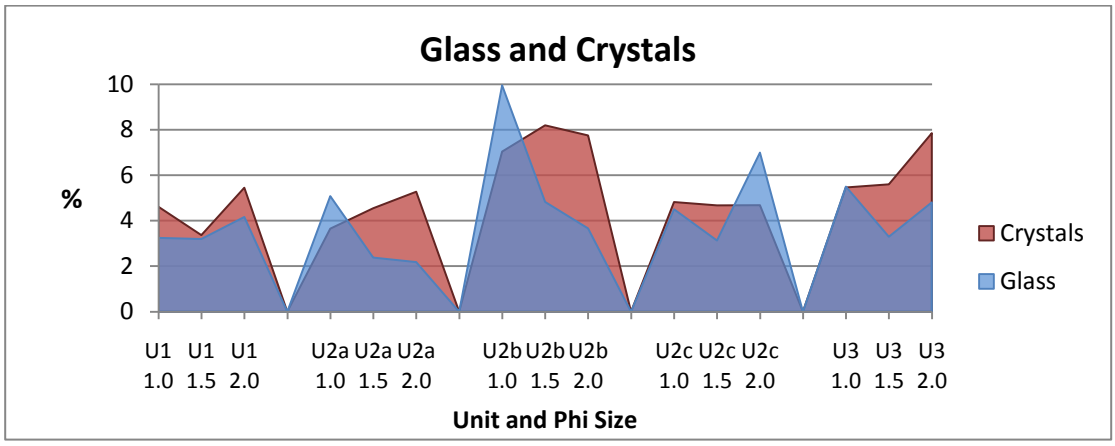

Figure 5.12. The proportion of glass and crystals in the 1.0, 1.5 and 2.0 phi modes. (Locality 13/27). Componentry is weighted to the weight percent of each mode based on the grain-size distribution data.

DISTANCE FROM VENT

In terms of general componentry, none of the units exhibit any distance-related trends: no systematic shifts in the components‟ abundance are apparent (Figure 5.13). This is exhibited in the way that the “other” grains remain minor, regardless of distance, and that the differences between the proportion of crystals and the proportion of glass is ≤13 % and does not change with distance in an orderly way. Therefore, more detailed componentry is employed to check for more subtle trends.

Where Figure 5.13 covered general componentry, Figure 5.14 separates the glass by color, and Figure 5.15 splits the crystals by mineral type. U1 exhibits a gradual increase in white glass with increasing distance from the vent (Figure 5.14). Gray and brown glass proportions remain fairly constant, with the exception of less gray glass present at the most distal site, and more brown glass at the 6.5 km site. The pink glasses are a minor component in all of U1.

The componentry of U2a does not show a relation between glass type and distance (Figure 5.14). The central locality has notably more gray glass than the other two sites, and less white glass. This does not fit a distance-dependent model, where a trend from proximal to distal sites would be expected. The brown and pink glasses show an association with distance, where brown glass increases and both pink glasses decrease with distance, but the contributions of these glasses to the overall deposit are small and the resultant trends therefore less significant.

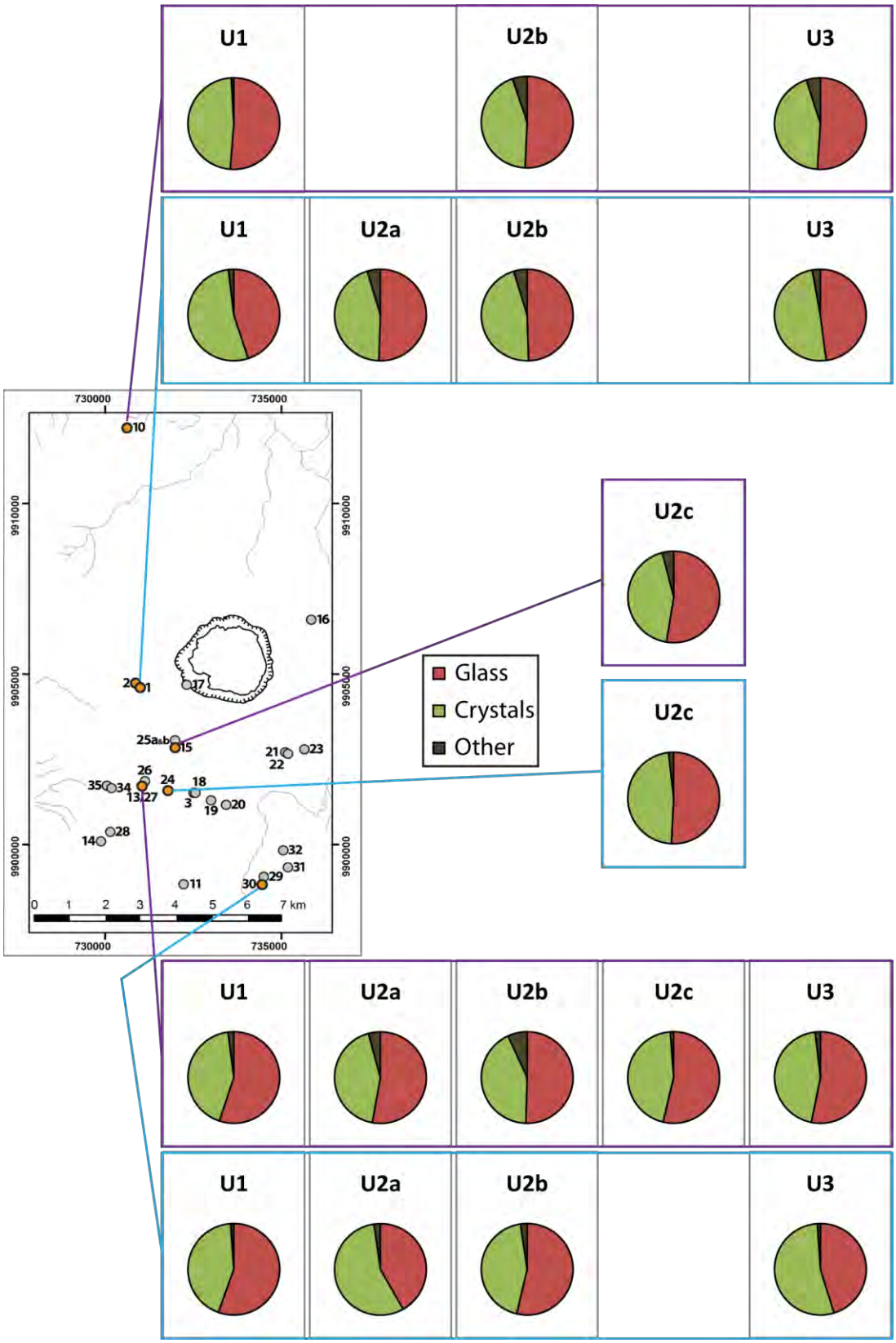

Figure 5.13. General componentry, with respect to distance.

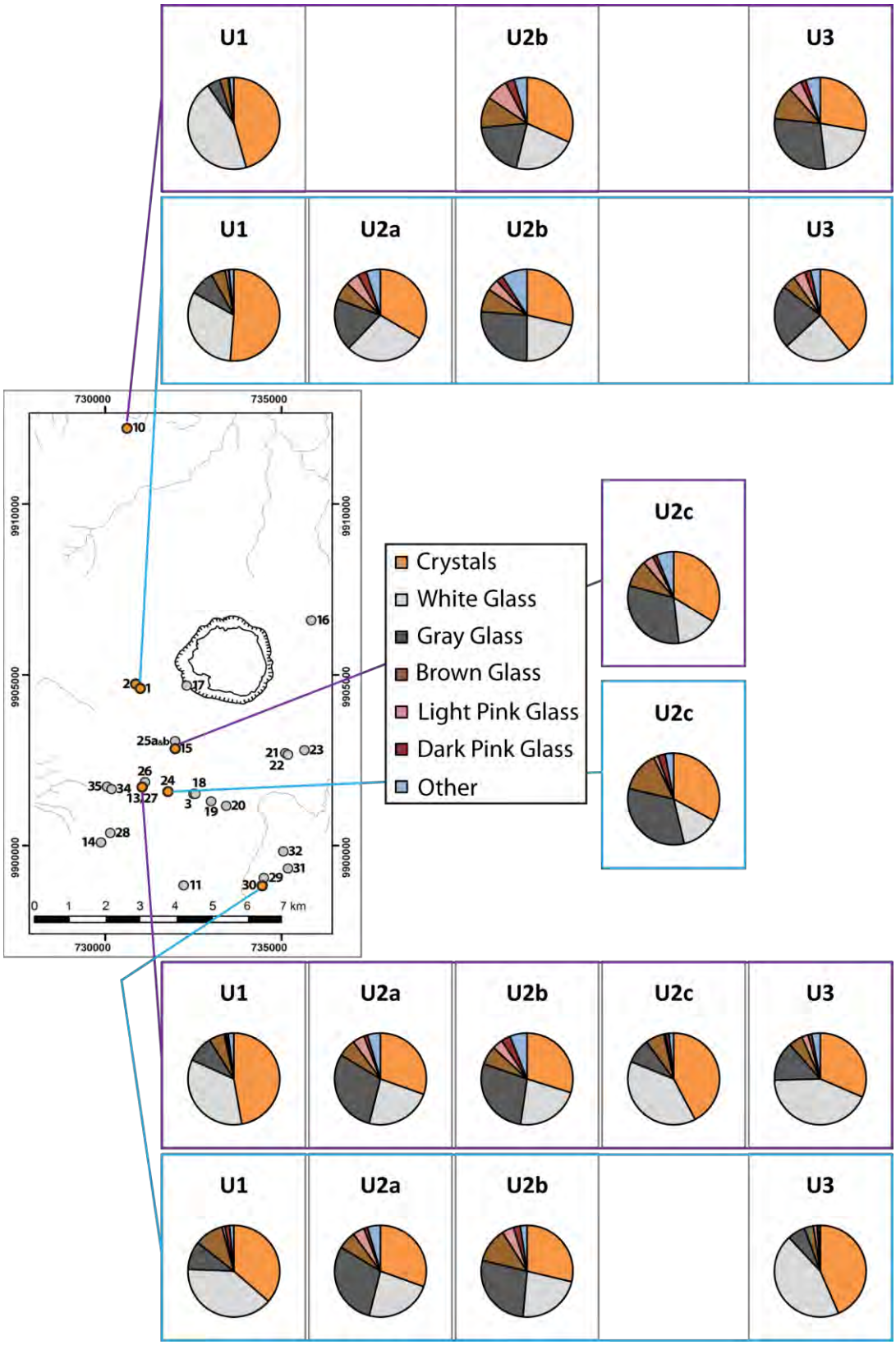

Figure 5.14. Detailed componentry of the vitric grains, with respect to distance.

U2b repeats the brown and pink glass trends of U2a (Figure 5.14). With respect to the white and gray glass, however, proportions remain close to constant at all sites, with the exception of a reduction in gray glass at the most distal locality.

The data for U2c indicate that distance may not be a strong influence. Two sites approximately 1 km apart are almost identical in their componentry, but one site just 0.5 km farther away has a very different gray:white glass ratio (Figure 5.14).

The componentry of U3 is similarly independent of distance, with the proximal and distal localities having more similar proportions of white and gray glass than the two central sites. The pink glasses are also more abundant at these two sites. Brown glass is most prominent at the distal site, but for this unit the overall trend with respect to distance is not linear.

In terms of crystal type, U1 has similar proportions of components across all the sites (Figure 5.15). Overall, the mafic crystals (including the separately listed magnetite and biotite) are more dominant at the proximal and distal sites, whereas felsic crystals remain the same throughout, except for an approximate 6 % drop at 6.5 km.

U2a shows an increase in felsic crystals and other mafic crystals (amphibole and pyroxene) with distance, whilst the holocrystalline fragments decline. Biotite remains roughly equal.

The componentry of U2b varies only slightly between the localities. Of note is the presence of the fragile glass-crystal-aggregates, limited to the most proximal site, and the presence of 7 wt % holocrystalline fragments at 5.5 km from the vent, three to four times more than in other outcrops of U2b.

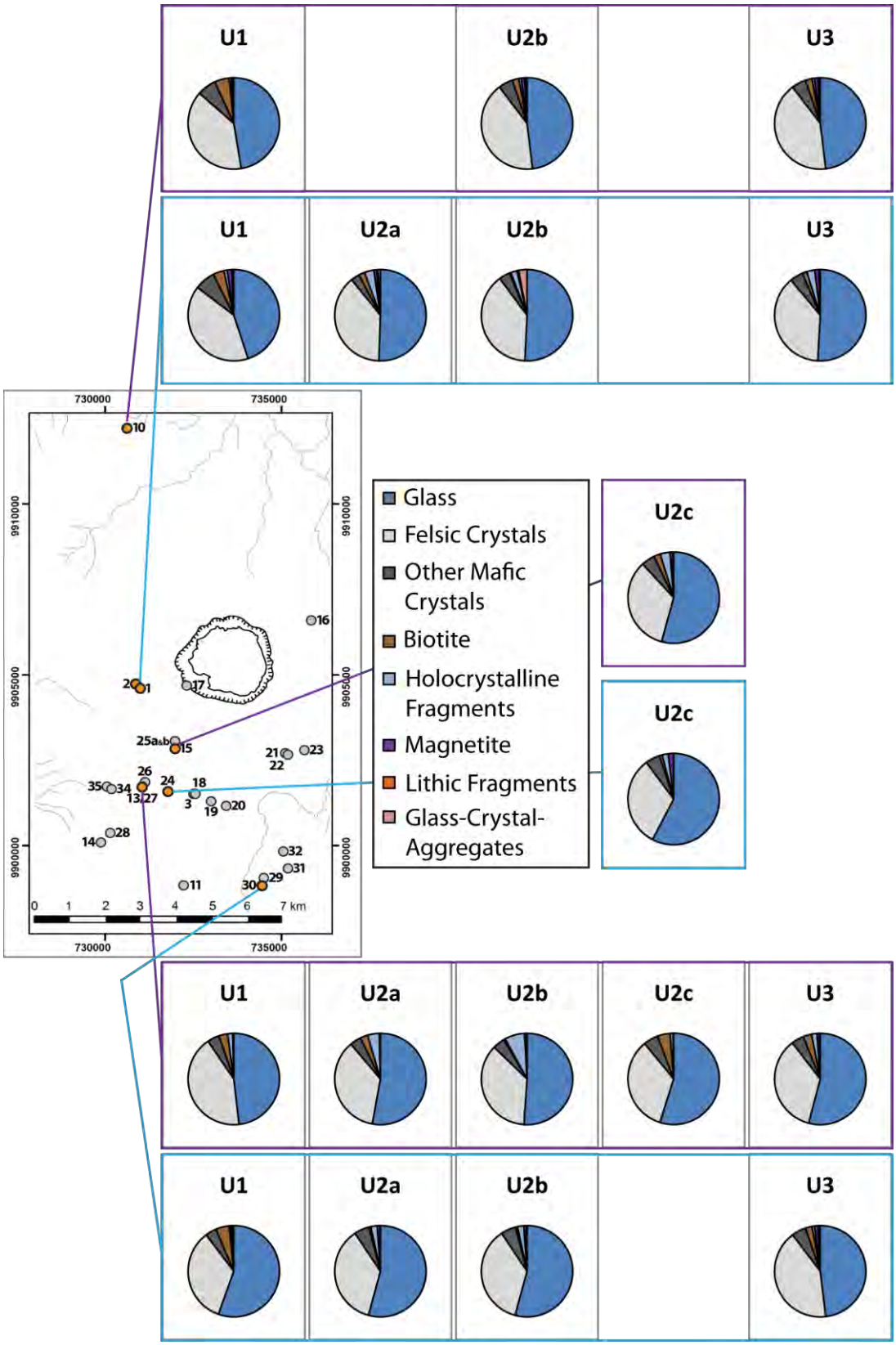

Figure 5.15. Detailed componentry of the non-vitric grains, with respect to distance.

The U2c sites are far more similar in crystal types than they are in terms of glass type. Closer sites have more holocrystalline fragments, and at the distal site biotite is more abundant.

U3 has a similar proportion of components, regardless of distance. Holocrystalline fragments are more numerous at the proximal and distal sites, and felsic crystals are less abundant at 2.5 km and 6.5 km. Other than that, little difference is noted between the sites. At all sites and units, lithic fragments are a minor component. They are present in all cases, but 1.2 wt %, from U3 at locality 10 (7.5 km), is the greatest contribution.

OVERALL COMPONENTRY OF THE UNITS

The overall componentry of each of the units indicates that they are all similar to each other in crystal and glass proportions (Figures 5.16). The differences become apparent, however, when the distribution of crystal types, glass types, and "other" grains is considered (Figures 5.17). In Figure 5.16 and 5.17, data on the composition of white and gray pumice obtained from Rosi et al. (2008), primarily from the fallout unit of U1, are provided for comparison with data from this study derived from the tephra of uppermost U1 to lowermost U3. In Figure 5.17, the weight percent of crystals is treated as a percent in order for approximate comparisons to be made. Figure 5.16 shows that the proportion of glass and crystals in the white pumice is very similar to that of the tephra from this study. Figure 5.17 shows that the abundance of crystal types from the gray pumice most closely resemble that of the tephra from this study.

U1 and U3 have more white glass than U2. The proportions of brown, light pink and dark pink glass vary with unit, with the most brown glass found in U2c, and the most

light and dark pink glass in U2b. Gray glass increases in dominance up sequence, until a decrease in U3. The "other" grains, the lithic fragments, glass-crystal-aggregates and holocrystalline grains, are minor components of U1 but have a greater presence in other units, with U2b having the most.

The proportion of felsic crystals remains the same, within 3.7 %, across all units. Biotite is most dominant in U1 and a minor component of U2b. Magnetite, lithic fragments and glass-crystal-aggregates are sparse in all units. Other mafic crystals (pyroxene and amphibole) are notable in each unit, with U1 having the most. The holocrystalline fragments are present in each unit, but particularly U2a and U2b.

This chapter considered componentry with respect to grain type and distance. The following chapter examines the grains themselves and the smaller-scale features that distinguish the deposits.

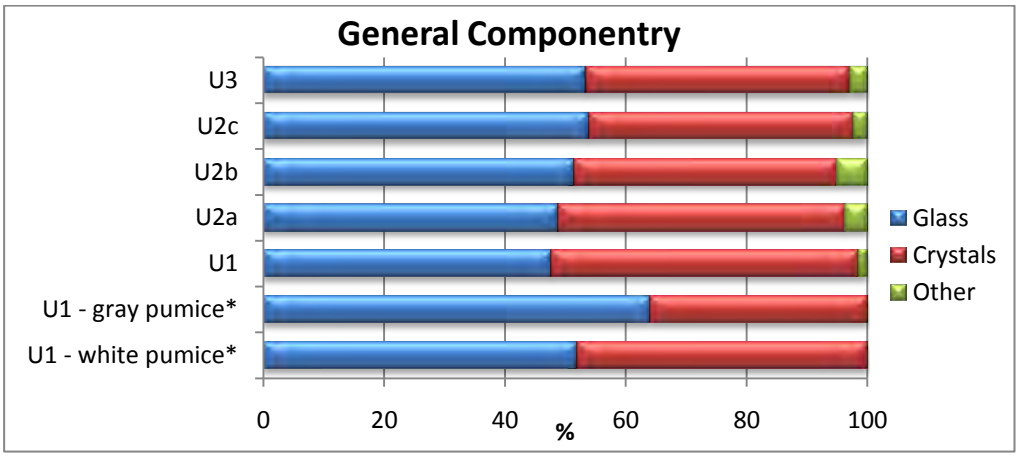

Figure 5.16. Overall componentry of the units, in terms of glass, crystals and other grains. * indicates data from Rosi et al. (2008)

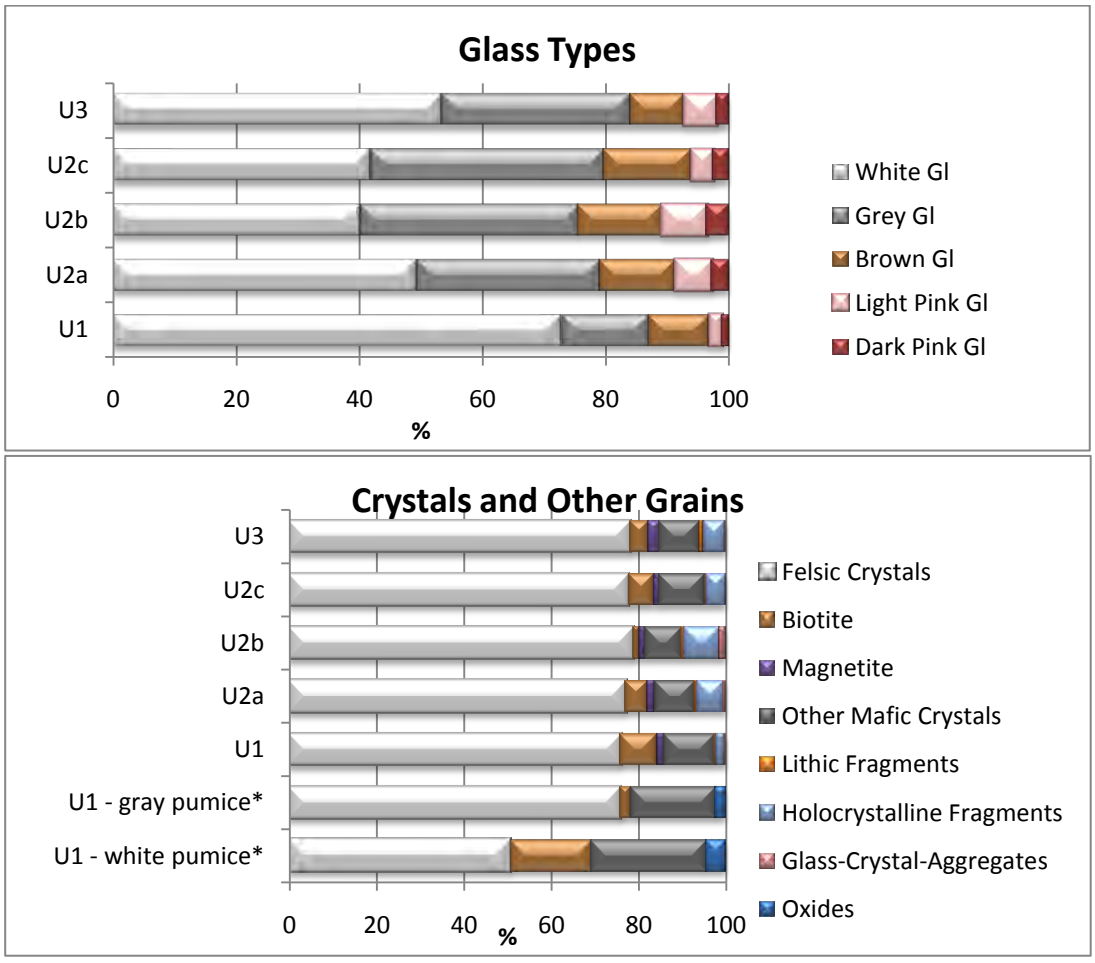

Figure 5.17. Overall componentry of the units, in terms of glass type only (top) and the crystal and "other" grain types only (bottom). * indicates data from Rosi et al. (2008)

CHAPTER 6

RESULTS: GRAIN MORPHOLOGY AND SURFICAL CHARACTERISTICS

The previous chapter considered the componentry of the different units. This chapter examines the grains themselves to determine the smaller-scale features that distinguish the deposits. This section of the study examines four subjects: grain texture, shape, staining and coating. Grain shape, together with surface texture, is often used to determine whether a grain is magmatic or phreatomagmatic in origin (Chapter 2). Another aspect of grain texture is vesicularity, for which white and gray glass, the two most dominant types, are examined. Finally, grain staining and the type of coating provide evidence of the conditions that affected the grains after they were created.

In these deposits, 1.0 and 2.0 phi are the main modal grain sizes seen. Because its larger size allows for grain features, such as surface staining, to be more easily identified visually the 1.0 phi size was selected for further analysis under the SEM. Due to its medial location, grains from locality 13/27 (Figure 6.1) were selected. For the grain shape analysis only, grains from a proximal site, locality 1 and 2, and distal site, locality 30, are also included (Figure 6.1) so that the results can be considered in terms of distance from the vent.

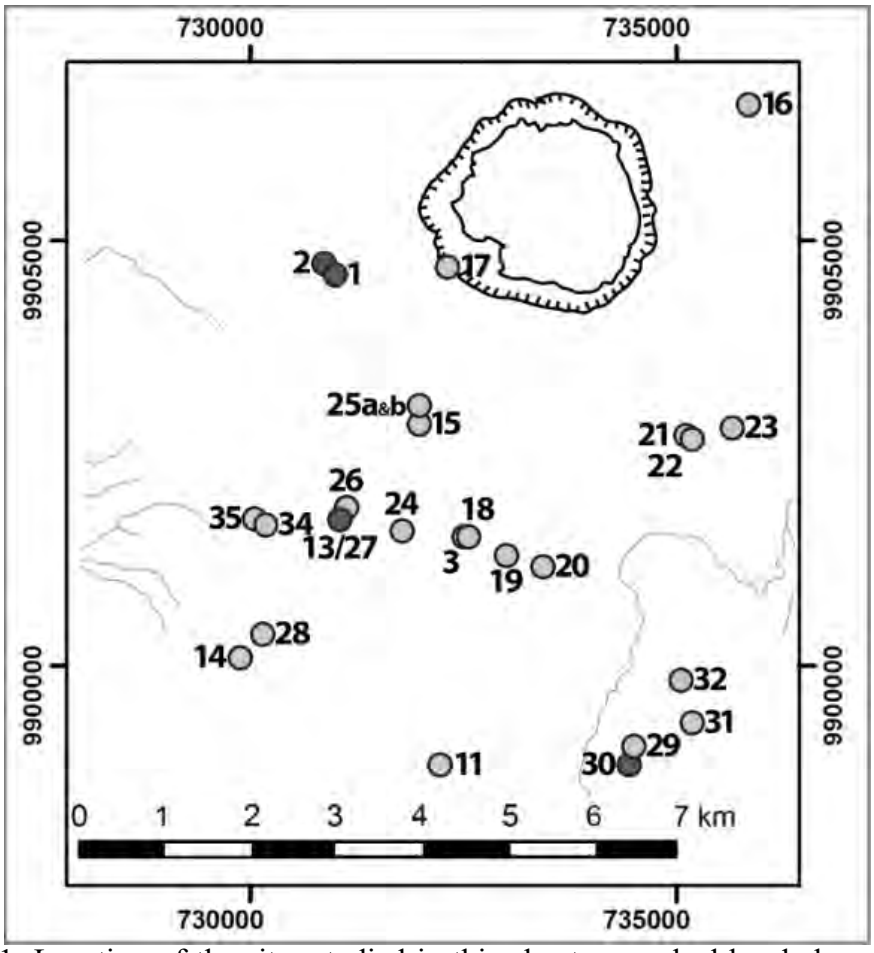

Figure 6.1. Location of the sites studied in this chapter, marked by dark gray circles. This map shows a section of the entire field area. For full map, see Figure 3.1.

GRAIN TEXTURE

Glass texture

The vesicularity of the different glass populations was categorized as either non-vesicular or dense, with no vesicles whatsoever, or vesicular, with any percentage of vesicles. Overall 59% of white glass grains are vesicular, compared with just 3% of gray glass (Figure 6.2). The brown and pink glasses, as well as all stained glasses, are not vesicular. Gray glass is almost exclusively non-vesicular (Figure 6.3). Only U1 and U2a contain vesicular gray glass, which accounts for 3 % and 4 % of the total of each unit, respectively.

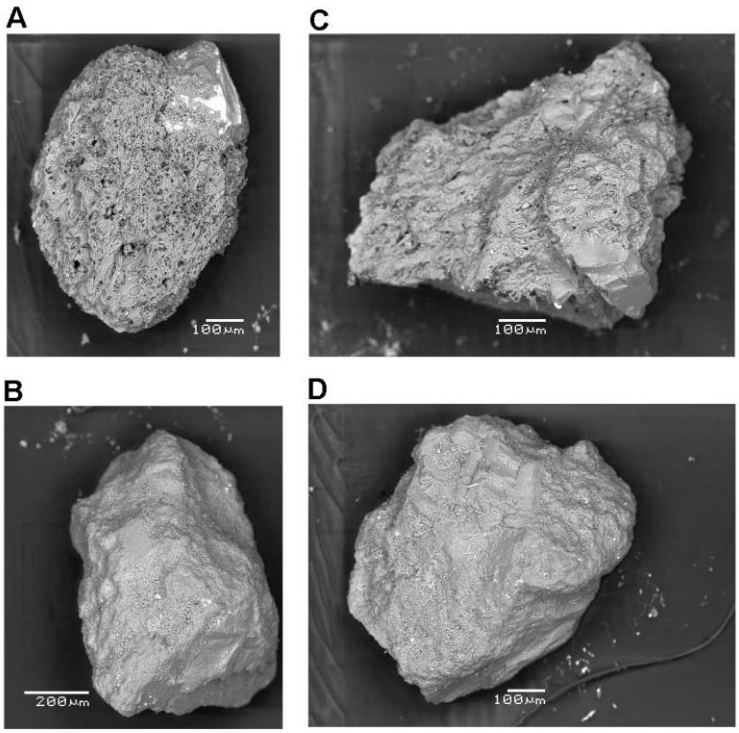

Figure 6.2. Examples of white and gray glass, both vesicular and non-vesicular. A) white vesicular; B) white non-vesicular; C) gray vesicular, D) gray non-vesicular. All from U1 at locality 30, except for B, which is from U2b at locality 30.

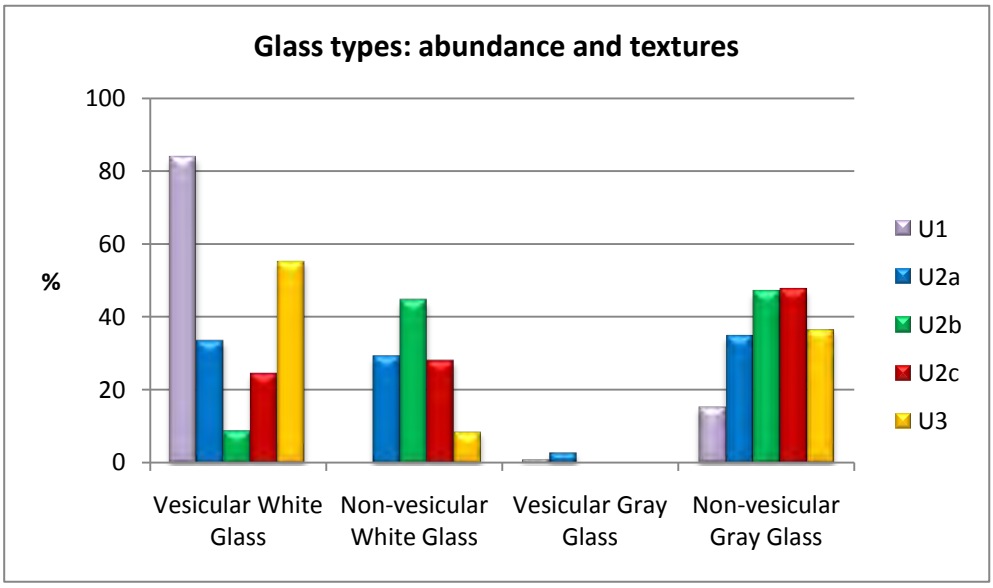

Figure 6.3. Glass texture variation with glass type and unit.

The proportion of gray glass remains similar across the units, between 46 % and 55 %, with non-vesicular gray glass by far the dominant texture (Figure 6.3). The distribution of vesicular and non-vesicular white glass, however, varies with each unit.

The white glass of U1 is all vesicular, and U3 has over six times as many vesicular grains as non-vesicular grains of white glass (Figure 6.3). U2a has similar proportions of vesicular and non-vesicular white glass, and in U2c the ratio is even closer to equal. U2b, however, is distinct, with non-vesicular grains of white glass approximately five times more abundant than vesicular grains.

The vesicularity of white glass varies with unit (Figure 6.4). Vesicularity was estimated visually (see Chapter 2), using charts of modal proportions (Best, 2003) of the type usually employed in igneous petrology. The range in values in the data set is narrow for U2c, with values within 10 %, to wide for U1 and U3, with values within 30 % (Appendix 6.6). Because of this range, both the mean and median values are calculated, so that the influence of any outliers would become apparent. The result is that the mean and median values are very similar. The trend of % vesicularity of the units matches that of the trend of % vesicular grains for white glass (Figure 6.3), in that vesicular U2b white glass also has the lowest vesicularity, and U1 and U3, which are dominated by vesicular grains, have the highest vesicularity.

Vesicle shapes are split into equant and elongate (Chapter 2). The proportion of each varies with the unit (Figure 6.5). The unit trend shows that the higher the vesicularity, and as described above the more abundant the vesicular grains (Figure 6.4), the more likely the vesicles are to be equant in form. The rare grains of vesicular gray glass have low vesicularities, 2% to 10 %, with vesicles that are equant in shape.

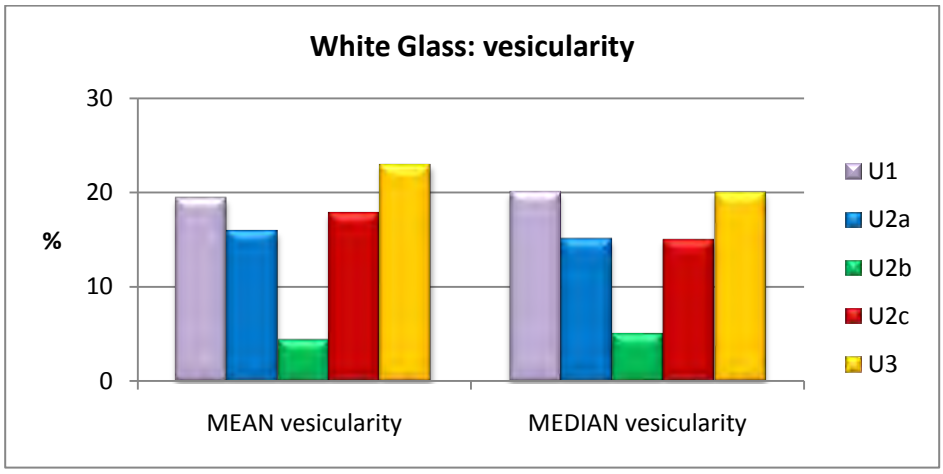

Figure 6.4. Mean and median percent vesicularity for white glass, estimated visually.

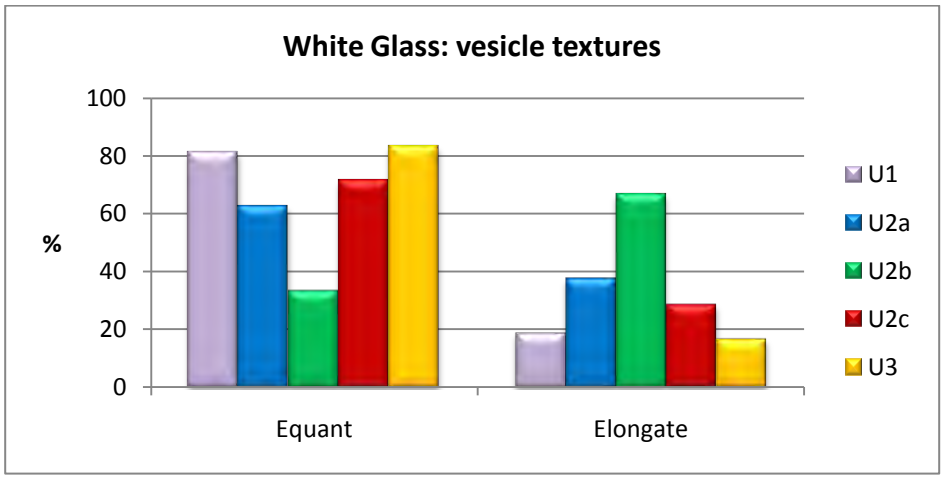

Figure 6.5. Proportion of grains with equant and elongate vesicles, by unit.

Other textures

Quench cracks, which can be the result of phreatomagmatic activity (Büttner et al., 1999), are absent from the deposits studied here (upper U1 to lower U3). In terms of other surficial features, none of the grains exhibit chemical pitting.

GRAIN SHAPE

The shape of glass grains is similar in all glass populations and units: all grains are blocky. As discussed in chapter 2, other studies describe shards and, in the presence of water, fluidal shapes and moss-like morphologies. Such morphological variety is absent from these deposits.

To quantify the degree of abrasion that grains have undergone, the circularity of white and gray glass from the three localities was calculated and considered in terms of unit, distance from the vent, and grain texture (Figure 6.6). These data are based on at least three grains of each color from each site and each unit. There is no obvious relation between circularity and distance for any of the glass types or units, nor for the mode of emplacement when comparing U2a, deposited by surges, to U2b, a fallout deposit. Non-vesicular white glass has consistently lower circularity values than the rest, indicative of the greatest rounding, which lie between 1.100 and 1.193. Non-vesicular gray glass ranges from 1.101 to 1.259, and vesicular white glass ranges from 1.117 to 1.443 (Figure 6.7). U1 and U2a have narrower circularity distributions than the three uppermost units.

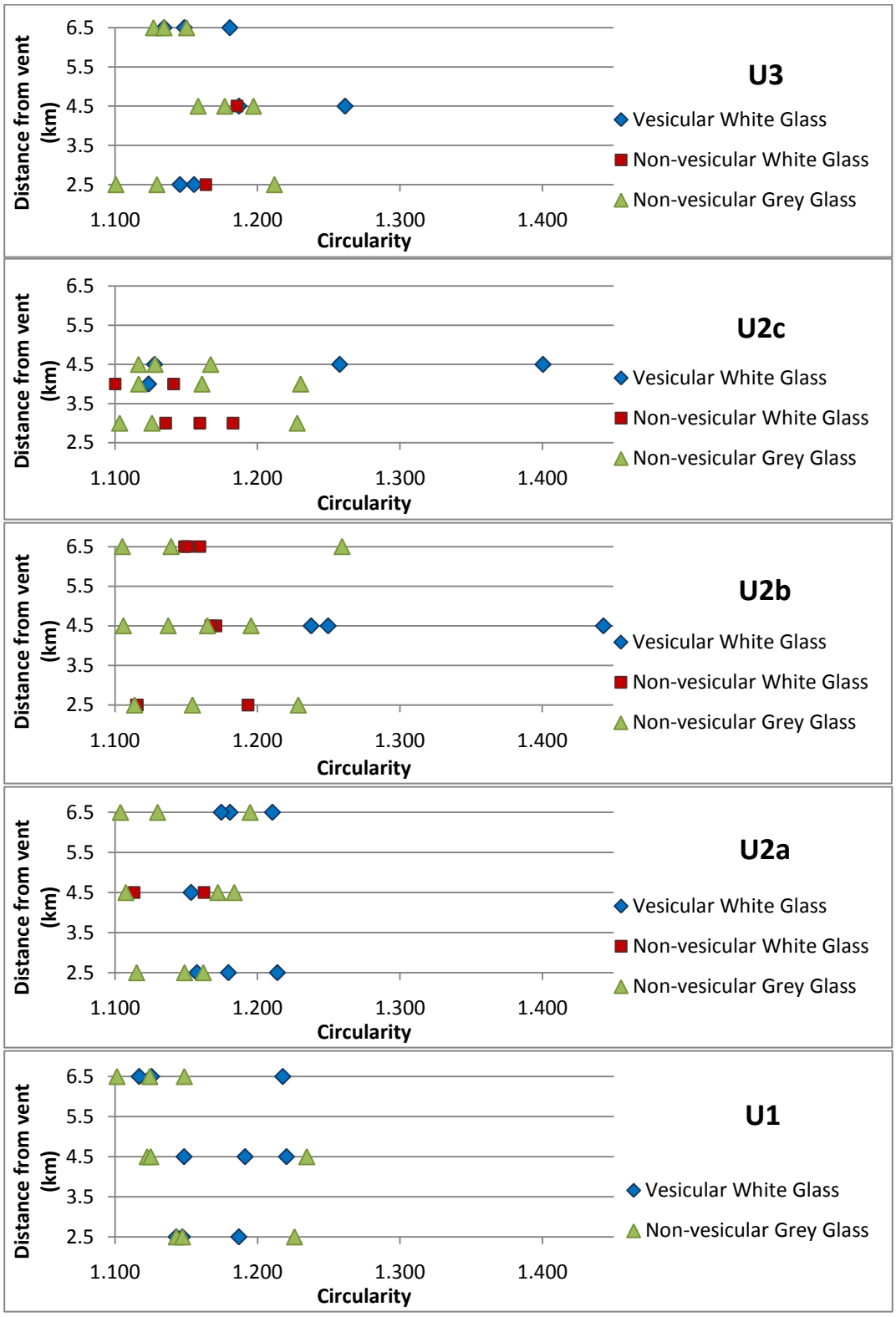

Figure 6.6. Circularity of white and gray glass. Higher numbers indicate greater angularity.

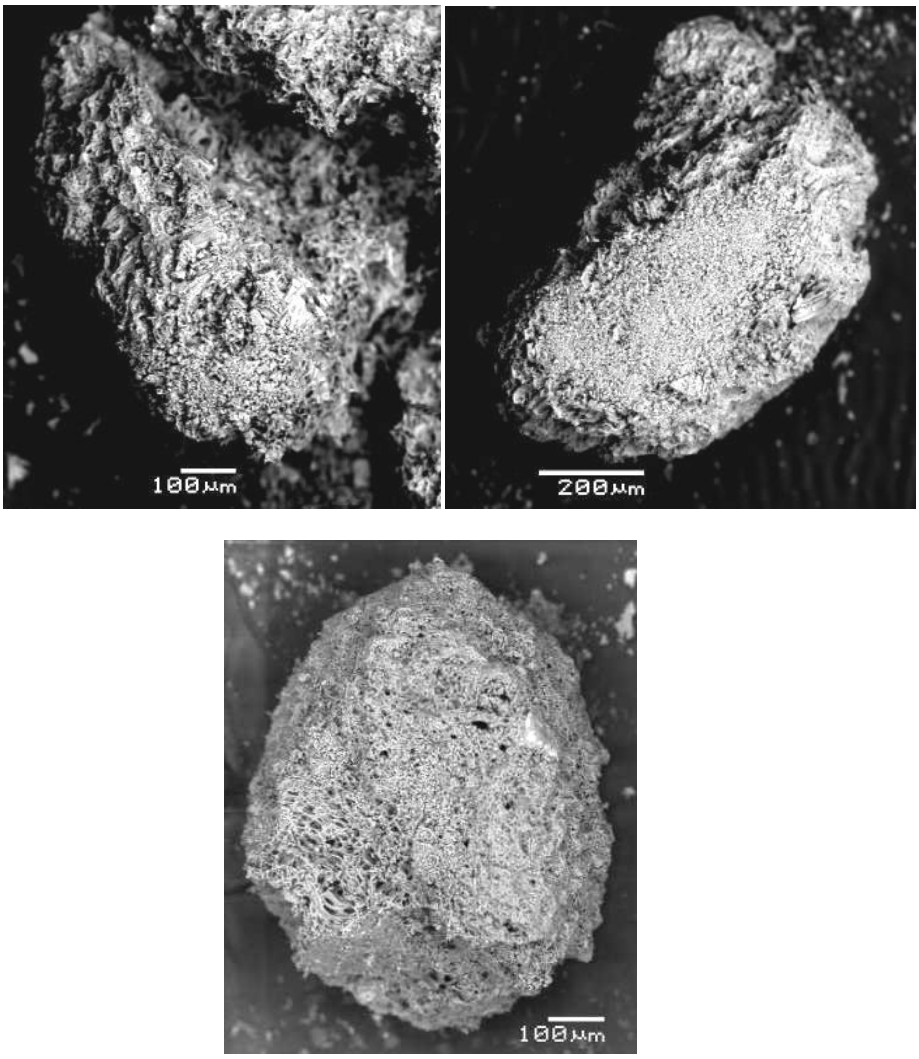

Figure 6.7. Circularity of the some of the most angular and most rounded grains. These are all vesicular white glass, taken from U2c, 4.5 km from the crater. The circularity values are: *Left* 1.4000, *right* 1.258, *bottom* 1.128.

GRAIN COATING

Very fine ash is the most common type of grain coating. This is where ash coats the grain almost completely (Figure 6.8), and not just where loose grains are caught in vesicles and cleavage planes. The presence of ash is not a diagnostic feature of any specific grain type, but ash-coated grains are twice as abundant in U2a as in U2c, the unit with the next largest population (Figure 6.9). U1 and U3, the plinian deposits, have the fewest ash-coated grains at 10 % and 9 % respectively. Very few grains are coated in glass. Of the four mineral grains with this feature, all are coated in vesicular glass. In summary, 74 % of all grains studied here are non coated.

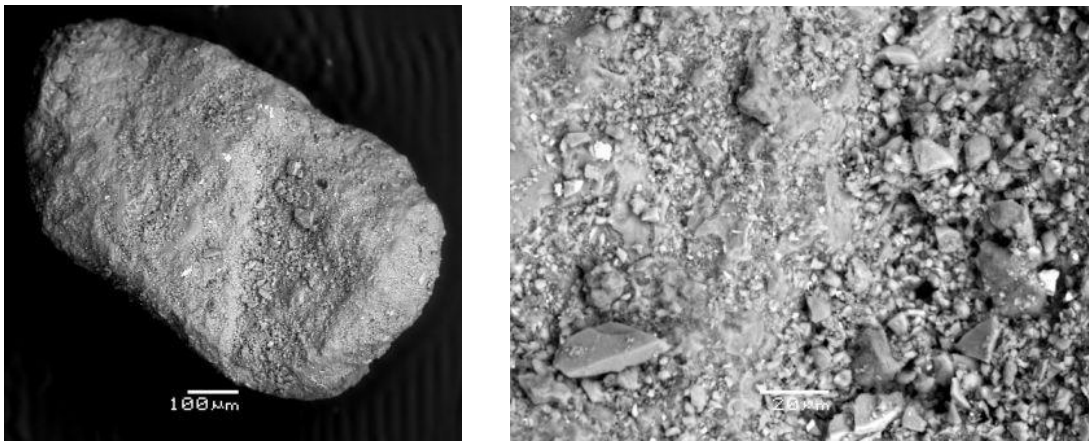

Figure 6.8. Example of a glass grain coated in ash, with a close-up image of the surface on the right. This grain is from U2a at locality 27.

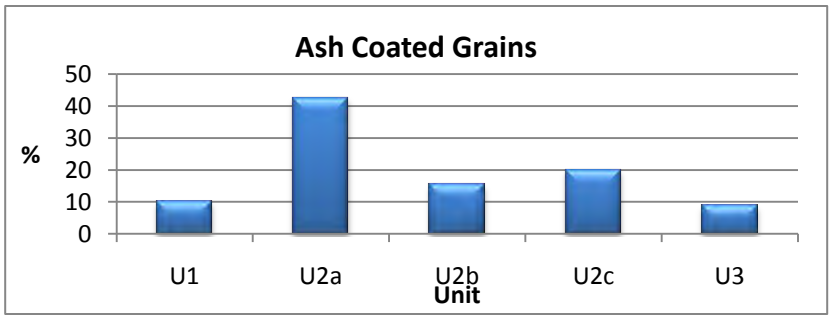

Figure 6.9. The proportion of grains that are coated in ash is significantly greater in U2a than any other unit.

CHAPTER 7

DISCUSSION

INTRODUCTION

This chapter first interprets the data presented in chapters 3 to 6. Then, a model of the Quilotoa 800 BP eruption is presented, and finally the implications for the eruption dynamics of dual eruptions are discussed.

Unit thickness, maximum clast size and stratigraphic data from Chapter 3 are used to infer changes in eruption style and intensity, as well as the depositional processes. Also noted is the presence of any evidence of post-depositional processes, such as erosion, as indicated by anomalous data.

Transport, whether within the umbrella cloud for fall deposits or along the ground within pyroclastic density currents, can influence the characteristics of the deposits. The influence of transport processes at Quilotoa is examined through isopach (Chapter 3), grain shape (Chapter 6), grain size (Chapter 4), and componentry (Chapter 5) data. If transport is an influence, then distance-dependent trends, derived from the comparison of proximal and distal sites, should be seen within these data sets.

Some processes occurring within the conduit are considered in this study using the vesicularity of the grains (Chapter 6). Vesicle abundance is used as an index of volatile content of the source magma of the glass. The proportion of lithic fragments, derived from componentry (Chapter 5), indicates the amount of country-rock erosion that took place. The abundance of stained grains (Chapter 5) reveals the degree of hydrothermal alteration that occurred within the conduit. The mechanical and chemical processes occurring within the vent are examined through grain shape and size data.

Milling within the vent affects both the shape (Chapter 6) and size (Chapter 4) of grains, by rounding and reducing grain diameter, respectively.

INTERPRETATION

The Eruption

All of the units in this study, from upper U1 to lower U3, are vitric and crystal rich (Figure 5.14). Free crystals, such as those crystals with adhering glass (Figure 5.3), can be sourced from the milling of larger glass fragments, but deposits that contain 44 - 51% free crystals also require an initial crystal-rich source magma. The proportion of the components is similar for all the units (Figure 5.14), indicating that they had the same source magma, and previous studies have indicated that that magma was particularly crystal-rich (Rosi et al., 2004; Mothes and Hall, 2008). The study of Rosi et al. (2004) determined that the white pumice had crystal contents of ~48 wt% and the gray pumice 29-36 wt%. The phenocrysts in the white pumice were 24.1 wt% plagioclase feldspar, 12.6 wt% amphibole, 8.9 wt% biotite, 2.1 wt% oxides, and minor quartz. In comparison, the crystals within the gray pumice had a similar proportion of plagioclase feldspar, 26.9 wt%, 7.1 wt% of amphibole and <1 wt% of biotite, oxides and quartz.

U1 to U3 of the 800 BP eruption of Quilotoa appear to be dry (Di Muro et al., 2008). Quench cracks, which can be the result of phreatomagmatic activity (Büttner et al., 1999), are absent from the deposits (upper U1 to lower U3), as are fluidal shapes and moss-like morphologies, which can also result from magma-water interactions (Heiken and Wohletz, 1985; Dellino and La Volpe, 1996; Büttner et al., 1999).

U1 and U3 are the deposits of two large plinian eruptions, between which U2 was deposited. U2 is primarily the product of a series of pyroclastic surges (U2a) and fallout from pulsatory eruptions (U2b), and hence is the product of discontinuous eruptions that were less explosive and less voluminous than the plinian eruptions preceding and succeeding it. Violent activity is characteristic of the previous eruptions of Quilotoa as

well as the 800 BP event (Hall and Mothes, 2008). Therefore, U2 represents a hiatus in the violent volcanic activity that produced the thick 800 BP plinian deposits of U1 and U3.

Upper Unit 1

Unit 1 as a whole consists of pyroclastic fall, flow and surge deposits. This study concerns uppermost U1, where the two subunits are laterally continuous beds of constant thickness on outcrop scale, characteristic of fallout deposits (Figure 7.1). The lower of the two, for example at locality 1, is a massive unit that is clast supported and dominantly (>90%) vitric lapilli >2 cm, which indicates a strong, sustained eruption column. Only two samples of the lower subunit were sieved (Chapter 4) and so the mean grain-size distribution of U1 is a reflection of the upper subunit. The upper subunit is a repeated sequence of well-defined coarse (-3 phi (8 mm)) and fine (-1 phi (2 mm)) planar beds, corresponding to repeated stronger and weaker eruption pulses that deposited larger and smaller grains, respectively. The uppermost part of U1 has an increased abundance of lithic fragments, likely indicating the erosion of the conduit or vent. The overall grain size of the upper subunit is finer than that of the lower subunit, indicating that the eruption intensity was reduced, which would make episodic activity more likely. The regular cycle of coarse and fine-grained beds is unlikely to be the product of wind direction. This is because changes in wind direction would have to be frequent and regular to deposit the observed repetitive sequence. Neither is the transition from the lower to the upper subunit the result of an increase in the efficiency of fragmentation producing smaller grains, because it would have been reflected in a high proportion of fine ash, which is not seen. This stratigraphy indicates that the strong eruption that

produced the sustained eruption column changed to a pulsatory style as the supply of magma and associated eruptive energy decreased.

Thickness data for the entire U1 were not collected as part of this study. However, for the sake of comparison with the other units, U1 is the thickest of the four units, with thicknesses of ~20 cm at a distance of ~21 km from the crater along the dispersal axis (Di Muro, 2002). Overall, uppermost U1 is poorly sorted, and has a mean grain size of 0.43 mm (1.23 phi). The individual coarse and fine-grained beds of the upper unit were not sampled separately (Chapter 4). Therefore, although each discrete bed was moderately sorted, sampling the upper subunit as one body, and therefore mixing the coarse and fine-grained beds, affected the apparent sorting, as indicated by the overall poor sorting of U1. Upper U1 clearly indicates the weakening of the eruption, as confirmed by the change from massive to bedded discussed above.

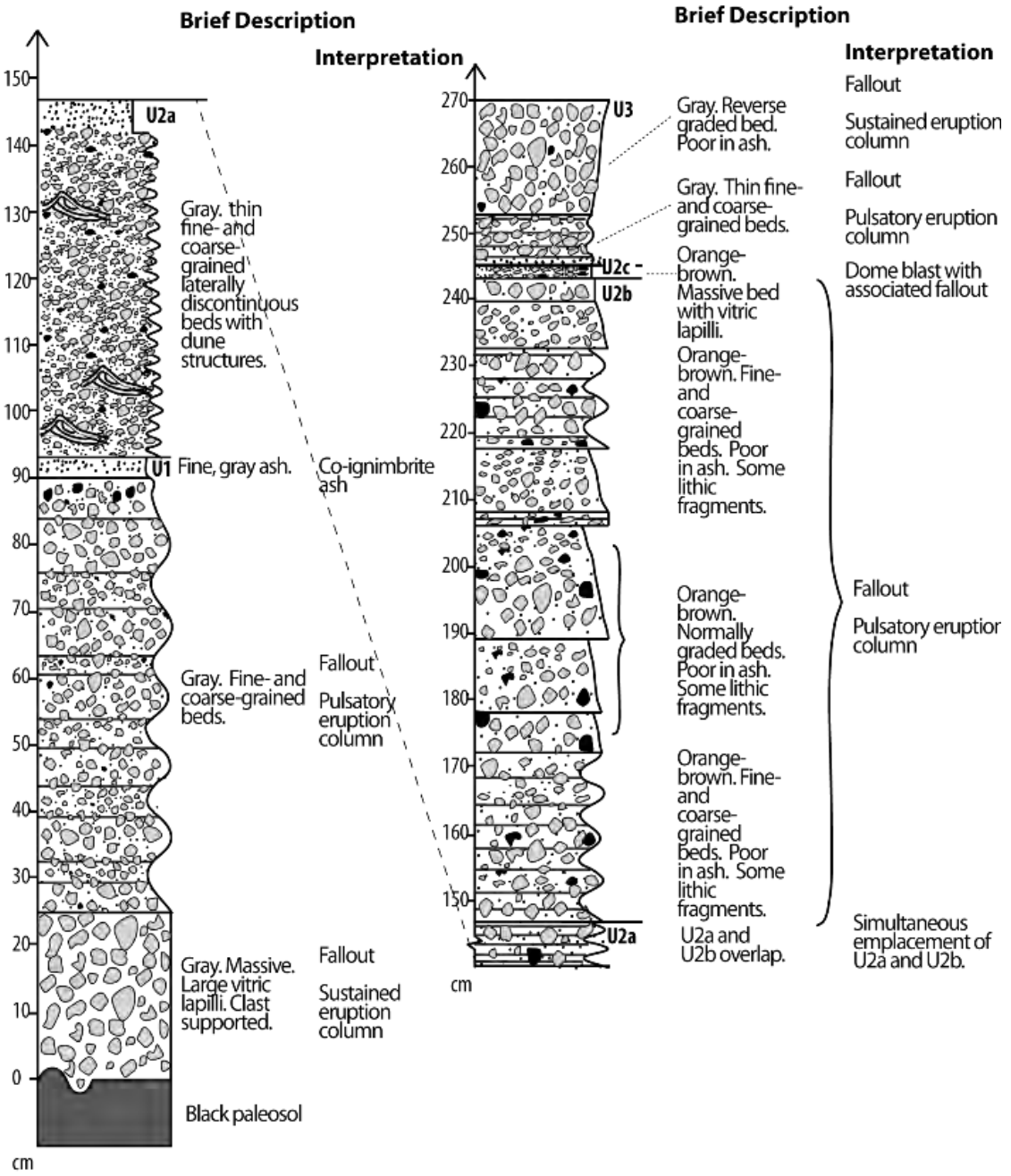

Figure 7.1. Interpretive stratigraphic section of the depositional units of the 800 BP Quilotoa eruption, from upper U1 to lower U3.

Unit 1/Unit 2a contact

The contact between U1 and U2a is sharp and marked by an increase in the proportion of ash (Figure 7.1). The underlying subunit is depleted in ash, so this thin ash bed is likely coignimbrite ash (Di Muro et al., 2008).

Unit 2a

U2a is a sequence of fine- and coarse-grained beds that form dune structures and pinch out laterally, illustrating that they were deposited by a series of pyroclastic surges of varying energy produced from weak eruptions (Figure 7.1). The interpretation of U2a as a surge deposit is confirmed by isopach data (Figure 3.10). The deposits are constrained by topography and are not found on the higher ridges, unlike the other units. Thickness variations between nearby sites, likely due to the varied infill of local topography, are also observed. The limited thickness of these beds, no more than a few cm, and the total unit thickness of ~1 cm at ~7.5 km from the crater, indicates that these surges were not voluminous. The largest clasts are 16 mm (-4 phi) in diameter (Figure 3.11). The grain-size distribution of the unit is broad except for the paucity of lapilli coarser than 4 mm (-2.0 phi) (Figures 4.1 and 4.3), and the mean grain size is 0.29 mm (1.80 phi) (Table 4.1), all showing that the surges were not very powerful.

Unit 2a/Unit 2b transition

At most localities, the contact between U2a and U2b is sharp. At the two most proximal localities (1 and 17), however, the contact between U2a and U2b is gradational, such that beds of U2b material are interlayered within uppermost U2a (Figure 7.1). The U2a beds form dune structures and pinch out laterally, and so, during this time, U2a was

still being deposited by surges. Beds of U2b, however, are laterally extensive like the main body of U2b, and hence are the product of fallout. This indicates that the final surges of U2a were weak, since the overlap is only seen at sites ≤ 2.6 km from the crater, and were emplaced at about the same time that U2b was beginning to be produced.

The grain-size distributions of the overlapping beds from Locality 17 show that most can be clearly attributed to either U2a or U2b (Figures 4.10 and 4.11). The same is true for locality 1. Therefore, a hybrid deposit was not the product of the overlap period but instead, conditions to deposit both U2a and U2b coexisted for a brief time. In order to confirm the punctuation of U2b fallout by U2a surges, it would be necessary to support the observation at locality 17 with additional proximal sites, where U2a-like beds appear within a generally reverse-graded sequence of U2b-like beds (Figure 4.12).

An important question is whether U2a and U2b were produced simultaneously from the same vent or from two separate vents. Production from the same vent is possible because the period of overlap is short; only 6 cm of tephra were deposited during that time at locality 1 located 2.6 km from the crater (Figure 7.1). Therefore a quick change in regime, from one producing U2a to one producing U2b, is possible. However, activity at two vents better explains the following observations. 1) U2a is gray in color and U2b is orange due to the presence of dust. It is unlikely that a single vent could transition between producing dust-covered and then non-dust-covered tephra on more than one occasion. 2) Whereas U2a is rich in fine ash, U2b is not. It is unlikely that batches of tephra, alternatively with and without fine ash, can be produced from the same vent. 3) The grain texture study (Figure 6.3) reveals that the glass of U2a and U2b are distinct. U2a glass is 4 times more likely to be vesicular than U2b glass, and is also 3.5

times more vesicular than U2b glass. Such fluctuations in the volatile content of the source magma are unlikely to occur in the same location during the short time period over which U2a and U2b were both deposited. Two separate vents best account for the production of the two distinctly different units. It is likely, therefore, that whilst U2b was being deposited from one eruption column, discrete eruptions from another vent emplaced the U2a surge deposits.

Unit 2b

U2b is a sequence of fine- and coarse-grained beds that are planar and laterally extensive, characteristic of a fall deposit (Figure 7.1). In the lower part of U2b the fine- and coarse-grained beds are massive. Farther up, the beds become thicker and normally graded. At the top, the sequence returns to thinner, massive, alternating fine- and coarse-grained beds. The presence of the repeated sequences of fine-and coarse-grained beds shows that the steadiness of the eruption column varied. The thicker, normally graded packages in the middle of the sequence are the product of longer-lived eruption columns.

The transition from discrete beds to graded beds marks an increase in the energy of the eruption. Deposits then return to discrete fine-and coarse-grained beds and are topped by a final 3-cm–thick (Locality 2), massive fine-grained bed, indicating that the eruption began to wane in energy until it stopped altogether. The deposits at the most distal U2b site, Locality 10, confirm the association of massive beds with more energetic eruptions, where massive U2b subunits are present and bedded U2b subunits absent (Figure 3.3).

U2b is the thickest U2 unit, with the greatest extent, and is not constrained by topography. It is present on ridges and in valleys beyond the basin closest to the crater

(Figure 3.12). The 10-cm isopach is at ~8 km from the crater to the south. However, 7.5 km to the north of the crater locality 10 has a thickness of 42 cm (Figure 3.12). This is consistent with U2b being a fall deposit. As a unit, it is more voluminous than U2a, which is approximately a quarter of the thickness of U2b where both are present. Isopleth data record the largest lapilli as 22.5 mm (-4.5 phi) in diameter, showing that the U2b eruption had more energy behind it than U2a, or had larger material to erupt (Figure 3.13). U2b is a moderately sorted deposit, with a mean grain size of 0.51 mm (0.97 phi) (Table 4.1), poor in both lapilli coarser than 4 mm (-2.0 phi) and fine ash (Figures 4.1 and 4.3).

The low vesicularity of the glass found in U2b, compared to the other units (Chapter 6), should have resulted in less efficient fragmentation and, thus, coarser grains. However, U2b is poor in lapilli. The other units of the 800 BP eruption (Figure 4.3), with the exception of U2a, have greater proportions of lapilli. The fragmentation of grains to lapilli size is common for the 800 BP magma body and the paucity of lapilli in U2b likely requires the influence of processes beyond fragmentation. This dearth of lapilli can be attributed to the efficient milling of coarse grains in the conduit to produce finer material (Rose and Durant, 2009). Only 37 % of the U2b crystals have adhering glass. This is a low value compared to the other units and so may require an increase in the mechanical removal of the glass, as would be achieved through the milling of the grains. The residence time of the grains within the conduit was long enough for pervasive hydrothermal alteration to occur (see The Conduit), and so likely also long enough for efficient milling to take place. The gases that caused the alteration would have also kept the grains in motion, causing them to interact with each other, resulting in the loss of

adhering glass and the milling of the larger grains into smaller sizes. The finer grains then increase the number of 1.0 and 2.0 phi-sized grains, resulting in these modal grain sizes being at their most abundant in U2b (Figure 4.3).

These observations indicate that U2b is likely not the product of fresh magma. The low vesicularity of the grains, which has been inferred to represent low volatile contents, should correspond to low fragmentation and therefore the production of coarse grains. However, coarse grains are absent from U2b. This may be due to the milling of the large clasts, and hence U2b is not the direct product of fresh magma. The extensive hydrothermal alteration of the grains, coupled with the need for a convective column from which grains can fall out ~8 km from the vent, indicates that gases did play an important role in the deposition of U2b, but were sourced externally from the dense, U2b material. Considering that time is required for the hydrothermal alteration that produced the orange dust, the source of the U2b grains predates the processes that oxidized and then deposited the unit.

U2b has the least fine ash of any of the units (Figure 4.3). The milling of the lapilli to smaller sizes would have resulted in an increase in the proportion of fine ash, but this is not seen in the deposits (Figure 4.3). If the wind carried the fine ash in one direction, it should be seen in some samples of U2b, but it is not. The fine ash could have been elutriated from the deposits. However, elutriation is usually the result of turbulent flow (Sparks and Walker, 1977), such as the flow within a pyroclastic density current. U2b is a fallout deposit and therefore the efficient elutriation of the fine ash portion, which would be required to produce the fine ash-poor grain-size distribution seen, is

unlikely, unless it occurred as a result of the turbulence within the conduit where the grains had collected and were milled.

Being of a smaller diameter, fine ash grains can travel farther before falling out of suspension. If this had happened to the fine ash of U2b, it should have been located within the field area between 8 km, the current limit of U2b, and 12 km, the maximum range of this study, due to U2b being emplaced by a relatively low column. However, no such fine-grained deposit is seen.

Unit 2b/Unit 2c contact

The contact between U2b and U2c is sharp. The fine ash of U2c is distinct from the coarse ash of U2b. In addition, vitric lapilli are only present above the contact.

Unit 2c

U2c is a single, poorly sorted, laterally extensive bed. The thickness and location of U2c outcrops are not constrained by topography (Figure 3.14.), consistent with U2c being a fallout deposit (Figure 7.1). U2c is poorly sorted with both lapilli mostly 4 mm (-2.0 phi) and smaller and a large proportion of ash. Unit thickness is ≤ 2.1 cm, with the 1 cm isopach ~ 7 km from the crater (Figure 3.14), and the largest lapilli are 11.5 mm (-3.5 phi) in diameter (Figure 3.15).

The vitric lapilli coarser than 4 mm (-2.0 phi) are fresh and dense. The non-vesicular texture indicates that the lapilli were sourced from degassed magma, which correspondingly is likely to have been effusively erupted or emplaced as a dome or plug. This correlates to a dome or a plug that was destroyed as it became the source for the lapilli. Since the glass is fresh and unaltered, unlike all the exposed dome rocks in the

caldera (locality 8), the dome was likely from the 800 BP eruption. If the lapilli of the older 14,770 BP eruption are also fresh, it could therefore be possible that the vitric lapilli of U2c were sourced from an older dome. However, the occurrence of vitric lapilli in a fine ash matrix is unique to the U2c unit of the 800 BP eruption and, since fragments of an older dome should have appeared in lower units, it is likely that the vitric lapilli of U2c are from a dome extruded during the 800 BP eruption.

The explosive destruction of the dome or plug would explain the limited extent of U2c, since a single blast will carry material only a short distance. It would also explain the large maximum clast size (Figure 3.15) in a predominantly fine ash unit. Additionally, U2c appears to be distributed in a SW direction (Figure 3.14). Although further field data would need to be collected to confirm, this may indicate the direction of the blast.

The fine ash of U2c requires high levels of fragmentation, commonly driven by high volatile contents (Zimanowski et al., 2003; Rose and Durant, 2009). However, open-system degassing beneath a dome (Fink and Anderson, 2000) inhibits high levels of fragmentation. Magma-water interaction can promote high levels of fragmentation (Büttner et al., 1999; Zimanowski et al., 2003), but no evidence of such interactions were found in U2c or any other deposits in this study (Chapter 6). Therefore, another mechanism is required to produce the large volumes of fine ash in U2c.

The textures of glass in the 1.0 phi size range (chosen because it is the modal grain size) of U2c indicate that the U2c magma was partially degassed (Figure 6.3). Dome-sourced lapilli (-2.0 phi in size) are dense, so the vesicular coarse ash of U2c must have been derived from a fresher, more volatile-rich, magma rising beneath the dome.

The partially degassed magma could still fragment to produce ash. Therefore it is most likely that the fine ash of U2c is sourced from the fragmentation occurring within the partly degassed vanguard magma of U3.

U2c is the product of a single discrete event and the observations fit that of a vulcanian eruption. Due to the small scale of the eruption, U2c is limited in extent and lacks the large clasts characteristic of vulcanian eruptions. However, the fall deposits from the 1975 eruptions of Ngauruhoe, New Zealand, are similarly limited, 3-4 cm thick <2 km from the vent, with a bimodal grain-size distribution (Morrissey and Mastin, 2000) which is also broadly seen in U2c. Vulcanian eruptions are sometimes precursors to larger plinian eruptions (Morrissey and Mastin, 2000), and U2c is the precursor to U3. Additionally, the dense vitric clasts of U2c are common products of vulcanian eruptions. The gases exsolved from the U3 magma at depth would have been trapped beneath the dome. With no evidence of magma-water interaction, the release of these gases is the most likely vulcanian eruption mechanism.

Unit 2c/Unit 3 contact

The contact between U2c and U3 is sharp, where brown ash gives way to gray ash. This indicates that U2c was a short-lived phenomenon, and if the product of a dome blast, the result of a single eruptive event (Figure 7.1). Vitric lapilli are present in lower U3 but, due to the change in the ash matrix, may have been deposited as a result of processes other than a dome blast, as discussed next.

Lower Unit 3

Lower U3 is laterally extensive and mantles topography, characteristic of a fall deposit (Figure 7.1). Overall, lower U3 is moderately sorted with a large mean grain size of 0.64 mm (0.64 phi) (Table 4.1), both of which require an energetic system to sort grains and carry larger clasts. The lower subunit is a repeated sequence of fine- and coarse-grained planar beds, indicative of a pulsatory eruption column. This gives way to the thicker upper subunit, which is coarse grained and reverse graded, possibly the product of an eruption column becoming sustained and more energetic (Figure 7.1).

Vitric U2c-like lapilli are present at the base of U3. U2c has a matrix of fine brown ash, whereas U3 has a matrix of coarse gray ash. Therefore, although the vitric lapilli at the base of U3 are probably from the same source as U2c, the emplacement mechanism is likely different. U2c is likely the product of a dome blast, and so it follows that the fragments that were not removed from the vent by the blast were later entrained by the U3 eruption column, and deposited at the base of the unit.

Thickness data of the entire U3 were not collected as part of this study. However, data from Di Muro (2002) show U3 thicknesses of ~3 cm at a distance of ~17 km from the crater along the dispersal axis. Therefore, U3 is thinner than U1 at similar distances, but is found in outcrops more distal than U2 (U2b in particular), indicating that the eruption that produced U3 was more powerful than that which emplaced U2. U3 includes fall deposits, but is predominantly the product of pyroclastic density currents (Di Muro et al., 2008). In terms of distance and thickness, it is clear that U1 and U3 were the main eruptions, and U2 the deposit of smaller eruptions of shorter duration during the hiatus.

Deposition

There is no evidence of significant erosion of any of the units. U2a is likely affected by some localized erosion where ephemeral streams removed some of the deposit, based on anomalously low thickness values in the region approximately 2.5 to 4.0 km south of the crater (Figure 3.12).

The emplacement of U2 was short, no more than several months. The duration of the hiatus between the two plinian eruptions is determined based on a number of observations. The top of U1 is marked in places by a coignimbrite ash, so there had to be enough time for the coignimbrite plumes to be generated, and the fine ash to fall out of suspension, before the surges of U2a were emplaced. An oxidized upper U1 surface, seen at some localities, indicates that the surface was exposed for some time prior to the emplacement of U2. The presence of phreatic blast deposits in the pyroclastic flow field demonstrate that there were at least a few days between the emplacement of U1 and U2 (Di Muro, 2002; Di Muro et al., 2008). Therefore, the time between the deposition of the U1 pyroclastic flows, from which the phreatic blasts were emitted, and the commencement of the deposition of U2 was short but at least a few days in length. Although the U2 deposits are typically only a few tens of cm thick they are thicker at the most proximal location, locality 17, where U2a is 48 cm thick and U2b 695 cm thick. It takes some time for nearly 7.5 m of tephra to be deposited as a number of discrete beds. There is no evidence of the presence of water, such as that which would result in phreatomagmatism, during or immediately after the hiatus to record that the crater lake reformed, as it did during the longer U3-U4 hiatus (Di Muro et al., 2008). It took less than three months for the crater lake at Mount Pinatubo to form after the June 15, 1991, eruption (Campita et al., 1996), and, with a lack of evidence indicating the presence of a

lake, the hiatus at rainy Quilotoa was no more than a few months in duration. Strong semi-annual rains are a characteristic of this locale (Vuille et al., 2000; Garreaud, 2009) so a hiatus of longer than about 5 months would be reflected in extensive erosion of U1. However, the lack of extensive erosion at the top of U1 (Di Muro et al., 2008) shows that this period of exposure was somewhat limited, and thus permits a postulated hiatus duration of weeks to months. The lack of soils also shows that the hiatus was not on the scale of years (Di Muro, 2002). Between U2a and lower U3, there are no major erosive surfaces, illustrating that the stratigraphic record can be treated as intact and hence the hiatus between Plinian eruptions was short in duration, linking the emplacement of U1 and U3 as the products of the same eruptive phase.

Transport

The spatial distribution of visited sites produced a paucity of data north of the crater. Therefore dispersion axes cannot be accurately determined. Isopach data indicate that the surges of U2a predominantly travelled south (Figure 3.10), U2b may have a NNW-SSE dispersion axis (Figure 3.12) and U2c is mainly deposited to the southwest of the crater (Figure 3.14). Similarly, without spatially complete isopach and isopleth data, unit volume and eruption column height estimates cannot be made using the prevailing methods (Pyle, 1989; Fierstein and Nathenson, 1992; Pyle, 1995). Some inferences as to the role of transport on the grain-size distribution and componentry of the deposits are presented here.

The most distal samples of U1, U2b and U3 were collected 8 km from the crater. As detailed in individual sections below, there is no apparent association between the grain-size distribution or componentry data and the distance an outcrop is located from

the vent. This implies that transport processes did not influence the deposition of the tephra. For sub-plinian and plinian eruptions, trends over a distance of 8 km might not be observable. A difference may be discernable over a distance of 12 km (Rose et al., 2008), but tens of kilometers may be required to define a trend (Sarna-Wojcicki et al., 1981; Paladio-Melosantos et al., 1996; Rose et al., 2008) in tall Plinian and sub-plinian columns. However, for the low, weak columns that likely emplaced U2b, 8 km should be sufficient to record any distance-related trend, if one was present.

Stratigraphy

All the units thin with distance from the crater (Figure 3.3). The transect also shows that U2a thins over a shorter distance than U2b (Figure 3.3.). This is consistent with the emplacement of U2a from surges and the emplacement of U2b from fallout. At Locality 25 U2a is absent, whereas 1 km farther away, at locality 26, U2a is present, perhaps as a result of the localized post-depositional erosion of U2a.

Grain-size distributions

The grain-size distributions of the units do not shift to smaller sizes with greater distance from the vent (Figure 4.6), as would be expected if the transportation of the grains was a major control on the grain size. The grain-size distribution curves mirror one another and the modal grain sizes do not change systematically with a locality‟s distance from the vent (Figures 4.6 and 4.7). Houghton et al. (2000) show that, in general, the influence of transport mechanisms on grain-size distributions is minor and the initial control of fragmentation on grain size is the greater control. To further explore

the relation between transport and grain-size distribution, the sorting, mean grain size of the units and weight percent of ash are considered below.

Whether the deposit was emplaced from fallout or by pyroclastic density current, the larger clasts would be deposited first, thus resulting in the average grain size becoming smaller, and sorting better, with distance from the vent. By the same mechanism, with the removal of the coarsest grains, the finer grains proportionately become a greater part of the deposit. If F1 is considered the weight percent of grains < 1 mm (0.0 phi), including coarse and fine ash, and F2 the weight percent of grains < 63 μm (4.0 phi), corresponding to fine ash (Walker, 1983; Papale and Rosi, 1993; Di Muro et al., 2008), then percentages should increase with distance, with F2 increasing at greater distances than F1 since the finest particles will fall out of suspension last. This relation might not apply, however, to the turbulent flow of pyroclastic density currents.

For all of the units, sorting does not change very much, if at all, over distance (Figure 4.9). This conforms with the observation that neither the grain-size distributions (Figure 4.6) nor the modes within them (Figure 4.7) change with distance. However, the mean grain size and F1 and F2 data indicate that transport does have some influence.

For upper U1, the predicted increase in wt % of F1 and F2 is observed (Figure 4.8) and, correspondingly, the mean grain size also gets smaller (Figure 4.9). The data for upper U1 match those of the top of U1 from the study of Di Muro (2002, 2008).

For U2a, F2 increases with distance, but F1 decreases with distance, likely reflecting the low energy of the surges so that even the coarse ash is deposited in proximal locations. The mean grain size remains approximately constant, a result of the poor sorting of the deposit.

The near-bimodality of U2b is shown by the mean grain size of U2b remaining constant. F2 also remains fairly constant, a likely result of U2b being poor in the finest-grained material at its source (Figure 4.3). F1 increases with distance as predicted, with a gradual shift, but not enough to change the modal grain sizes.

U2c data cover a short distance range. The mean grain size coarsens with distance. This may be explained by the source of the U2c lapilli being the explosion of a dome. With such a process, the lapilli are transported as projectiles, so the rules applied to grains held in suspension, either within a convecting cloud or a pyroclastic density current, do not apply. With a directed blast, coarser material will be transported farther along the blast axis, whereas, just off axis, smaller grains will not be transported as far. This could explain the apparent coarsening of the mean grain size of U2c with distance. F1 and F2 both decrease with distance, as a result of the low energy of the eruption, where even the finest grains are deposited close to the vent.

Finally, in lower U3 none of the parameters vary with distance. Lower U3 represents the initiation of the second plinian eruption, and such an intense eruption is unlikely to produce changes in grain-size distribution at locations ≤ 8 km from the vent.

The changes to mean grain size and the proportion of F1 and F2 with respect to distance are subtle, which is why they are not recorded in changed sorting values or shifted grain-size distributions. In conclusion, therefore, transport is a control on the grain-size distributions of the deposits, but only a minor one.

Grain shape

During transport in a current with significant grain-grain interaction, grains will become rounded through abrasion. Therefore, if transport is a major control on grain

shape, a shift from angular to rounded particles would be seen. Circularity can be used to approximate angularity (Chapter 2), and was calculated for 1.0 phi (0.5 mm) glass grains (Figure 6.6). None of the glass types for any of the units exhibited a relation between circularity and distance, indicating that the vent processes of fragmentation and milling are a far greater control on grain shape than abrasion during transport.

Componentry

The componentry of the units does vary with distance (Figures 5.11 - 5.13), but does not do so in a systematic manner. Therefore the change in the proportion of one component across the various sites cannot be attributed to the abrasion or removal of grains during transport, nor explained by differences in the settling velocities of the grains.

The Conduit

Glasses and volatiles

The type and texture of the glasses found within a unit are used to infer the conduit-based processes that occurred. The proportion of the different glass types, namely white and gray, varies between the units (Chapter 5). In terms of vesicularity, gray glass is dominantly dense. U1 and U2a have a few vesicular gray glass fragments, ≤ 4% of the total white and gray glass, with vesicularities between 2 and 10% (Chapter 6 and Figure 6.3). The low to non-existent vesicularity of the gray glass implies that it is either from a degassed source or a magma that had little gas to begin with. A low-volatile magma is unlikely because the source magma for all the units is dacitic and

crystal rich (Figure 5.14) (Rosi et al., 2004; Mothes and Hall, 2008). For a viscous, crystal-rich magma to be mobile and thus able to erupt, the volatile content had to be substantial.

The proportion of vesicular and non-vesicular white glass varies with each unit. The exsolution of dissolved volatiles is needed to drive the two plinian eruptions, and so it makes sense that all the white glass of U1 and 83% of the white glass of U3 is vesicular (Figure 6.3). U1 and U3 are from volatile-rich magmas, but U2 appears to be from a more degassed source. Approximately half of the white glass in U2a and U2c is non-vesicular (Figure 6.3), illustrating that around half of the source magma had completely degassed. Based on this, magma degassing occurred between the emplacement of U1 and U2a. With 80% of the white glass found in U2b dense and the rest partially vesicular (Figures 6.3 and 6.4), a low-volatile source is needed. It is likely therefore, that the U2b grains are the more-degassed product of an earlier eruption. Finally, following the emplacement of U2c, an increase in the flux of magma from depth at the start of the plinian eruption produced the mostly non-degassed white glass of U3.

The abundance of volatiles determines both the number of vesicular grains, as discussed above, and the vesicularity of each grain. Inter-unit trends in vesicularity match those for the number of vesicular grains (Figure 6.4), in that U1 and U3 have similar average vesicularity values that, at ~20 %, are the highest of the units. Next are U2a and U2c, with similar but lower (15 %) values. The glass found in U2b has vesicularities of only 5 %. These vesicularity data support the interpretation of the loss and subsequent redevelopment of a connection to a deep, volatile-rich magma source as the eruption cycle progressed from U1 to U3, as discussed above.

The shape of the vesicles themselves varies in the same way as vesicle density and the number of vesicular clasts. Approximately 80% of the U1 and U3 white glass grains have equant, rather than elongate, vesicles (Figure 6.5). This falls to 71% for U2c, 63% for U2a and 33% for U2b. Elongate vesicle textures are associated with lower vesicularities at Taupo volcano (Houghton et al., 2010), and this relation is borne out here.

In summary, the number of vesiculated white glass grains within a unit correlates positively with the vesicularity and the number of grains with equant vesicle shapes. As expected the mostly degassed magma produced the fewest and least vesicular grains. Additionally, the vesicles are predominantly elongate in form, possibly a result of the shearing of the magma along the conduit wall and resultant deformation of the vesicle shapes (Houghton et al., 2010). Therefore prolonged contact between the magma and the conduit wall, or compaction within a dome, resulted in the highest levels of degassing, and the elongation of residual vesicles.

Data obtained for this study do not allow the source of the different glass types to be fully determined. Work of others at Quilotoa (Rosi et al., 2004) and Mount Pinatubo (Polacci et al., 2001) have explained the coexistence of white and gray glass. Mingled pumices, where a mainly gray glass fragment includes white glass domains, indicate simultaneous production of both glass types at Quilotoa in the U1 deposits (Rosi et al., 2004) and at Mount Pinatubo in the 1991 eruption tephra (Polacci et al., 2001). At Quilotoa, the two pumice types are of a similar dacitic composition, but have different textures, with the white glass being richer in phenocrysts than the gray, in which the phenocrysts are fragmented and resorbed (Rosi et al., 2004). The mechanism that

produced both the white and gray glass at Quilotoa and Mount Pinatubo (Polacci et al., 2001; Rosi et al., 2004) requires that the white pumice represent is the original magma, from which the gray glass is produced when sheared along the conduit walls, causing the crystals to fragment. The origin of the two glass types may be debated, but it is clear that both formed simultaneously.

Modal grain sizes

The grain-size distribution data reveal three modal grain sizes common to all five units: 1.0, 2.0 and 4.0 phi (Chapter 4). Since each of the units had distinct emplacement mechanisms (see The Eruption), the presence of these common modes cannot be explained by shared transport processes. Therefore, these units likely share a common source or source processes. The composition of the magma remained dacitic and crystal-rich throughout the eruption (Figure 5.14) (Rosi et al., 2004; Mothes and Hall, 2008). One possibility is that different minerals tend to form crystals of a particular size, so that each mode is attributed to particular minerals. However, the componentry study (Chapter 5) showed that, when considering the componentry of the 1.0 and 2.0 phi modes, the mineral assemblages were not distinct. With a common magma source, the initial size of the phenocrysts within the magma could have remained fairly constant, and thus resulted in the deposition of free crystals also fairly consistent in size across all the units. This is because the size of phenocrysts within a magma is, among other things, a function of the cooling and degassing of the magma (Taddeucci et al., 2004). Large crystals are uncommon in volcanic systems, and the range of crystal sizes in pyroclastic deposits tends to be similar, regardless of the composition of the source magma. For example, at the Latera Volcanic Complex, Italy, crystal sizes typically range from 0 to 2.0 phi

(Taddeucci and Palladino, 2002); and at the similarly silicic Huaynaputina volcano, Peru, crystal sizes range from 0 to 3.0 phi (Adams et al., 2001). In the basaltic system of Fuego volcano, Guatemala, the main crystal-size range is 1.0 to 3.0 phi (Rose et al., 2008). Therefore, the modal sizes of 1.0 and 2.0 at Quilotoa are common crystal sizes. With a crystal-rich magma, there would be little space for further crystal growth as cooling and/or degassing continued, except perhaps as microlites as seen in the gray pumice of U1 (Rosi et al., 2004). Additionally, between upper U1 and lower U3, the time for such processes to occur is limited since even the longest time break, as represented by the hiatus, was likely no more than a few months (see Deposition).

The proportion of glass decreases with grain size, from approximately equal with crystals at 1.0 phi, to around half the abundance of crystals at 2.0 phi, then returning to an almost equal split at 4.0 phi (Figure 5.2). This may be result of the mechanical breakdown of glass into smaller sizes. Glass is less resistant than crystals. As the glass is broken the crystals within are released. The less resistant glass breaks down into smaller grain sizes than the crystals and so at 2.0 phi crystals dominate, whereas at 4.0 phi the proportion of glass is greater. This mechanical breakdown of glass is indicated by the number of crystals, at five grain sizes (-2.5, -1.0, 0.0, 1.0, 2.0 phi), that have adhering glass on them, the lowest being 36% for U1 (for all the grain sizes, weighted with respect to the grain-size distribution) and the highest 46 % for U2a (Figure 5.3). Therefore, this continual reduction in glass size is a common process and is reflected in the modal grain sizes of all the units.

Differences in the grain-size distributions of the units were discussed in the description of the production of each unit (this section). However, underpinning these grain-size distributions are the modal similarities of the units.

Two modes of note are 1.0 and 2.0 phi. These two modes, despite being close in size, are distinct populations. The componentry study (Chapter 5) considered the differences in glass type, crystal type, and crystal shape in order to determine the ways in which the two modes differ and therefore why they both exist. The study of the 1.0, 1.5 and 2.0 phi grain sizes showed that the 2.0 phi mode, with the exception of U2c, is most likely a product of the crystal population. Apart from this, the modes and their components are far more similar than they are different. The grain-size distributions showed that both modes are significant to all units, but it has not been determined why the two modes, so granulometrically distinct, are compositionally so similar.

Transport is no more than a minor control on the grain-size distribution data (modal populations, sorting, mean grain size, F1 and F2), grain shape or componentry of the deposits. Therefore, the shared characteristics within the deposits of a unit, regardless of outcrop location, have to be attributed to a common process, most likely fragmentation producing the initial grain population.

Hydrothermal alteration

The staining of grains and the generation of the orange dust, which gives U2b its characteristic color, are both the products of hydrothermal alteration. The orange color of the unit could solely be due to an abundance of lithic fragments, sourced from depth and stained as a result of alteration within the conduit. However, the componentry study shows that lithic fragments (stained and non-stained) are a minor part of all the deposits,

no more than 1.2 wt %, and so are not numerous enough to affect the outward appearance of a unit. Therefore it is the presence of the ubiquitous orange dust that is the cause of the color of U2b.

The fragmented material that would later be deposited as U2b sat in the conduit long enough to be hydrothermally altered. During this time, the material within the conduit was churned and milled (Rose and Durant, 2009), breaking down the grains into increasingly finer pieces. The orange hydrothermally altered grains, being already weakened, broke easily into very fine ash, the source of the dust that covers the remaining grains. The hydrothermal alteration occurring within the conduit is also reflected in the percentage of stained grains. U2b correspondingly has the most stained grains, 12 wt%, which is at least 1.5 times more than any other unit. However 12 wt% is a small fraction of the unit. So, although hydrothermal alteration is responsible for the staining of U2b grains, it is the orange dust that gives the unit its orange color, not the number of stained grains.

The volatiles responsible for the hydrothermal activity occurring during the preparation of U2b material also influenced a small part of the componentry. Glass-crystal-aggregates are grains held together by glass (Figure 2.3). The crystal-rich character of the Quilotoa magmas (Figure 5.14) (Rosi et al., 2004; Mothes and Hall, 2008) would produce a viscous system, which would make the flow of magma between crystals in order to bind them mechanically difficult. Additionally, while the bulk composition of the magma was dacitic, the liquid was rhyolitic (Rosi et al., 2004). Therefore the melt was very viscous and flow between the crystals even more unlikely. An alternative to the flow of melt between crystals is that hot volatiles, upon passing

through the loose material residing in the conduit, melted the glass shards, thus loosely fusing together the varied grain types with glass. Considering that a U2b site has the only "abundant" glass-crystal aggregates (Chapter 5), this mechanism correlates with the volatiles that are also responsible for the hydrothermal alteration and milling of the U2b grains.

The proportion of stained grains to non-stained grains remains low in all the units (Figure 5.4) with a maximum of 12 wt % in U2b. Despite being small in number, lithic fragments are the most commonly stained grain type (Figure 5.5). The staining of grains is seen in the presence of a thin orange-red layer around the grain, which is sometimes flaky. The percolation of hot volatiles through a system (Best, 2003) can alter the composition of a grain and/or precipitate other minerals as a coating. The staining of lithic fragments, therefore, is most likely the result of such hydrothermal alteration, usually occurring within the conduit where temperatures are higher than at the surface.

The percentages of the lithic fragments that are stained are U1 44%; U2a 25%; U2b 91%; U2c 41%; and U3 85%. Greater percentages of stained lithic fragments require the erosion of the conduit to have been either more extensive in one location, or to have occurred deeper within the conduit where hydrothermal alteration is more pervasive. The abundance of lithic fragments, stained or non-stained, is low (≤1.2 wt %) for all of the units. Therefore, variable conduit erosion is unlikely to be the mechanism behind the different percentages of stained lithic fragments, as this would be reflected in different abundances of lithic fragments, both stained and unstained, in each unit. Instead, deeper erosion is the likely cause. The erosion of the conduit and entrainment of lithic fragments most likely occurred at the fragmentation front, where the kinetic energy

generated by the exsolution of volatiles could fracture the country rock. Therefore, deeper fragmentation fronts would have entrained more stained lithic fragments.

The U1 fragmentation front was deep, as a result of a strong, long-lived eruption that required a high magma-volatile content. If the fragmentation front had been shallow, vesicular grains would likely be less common and less vesicular due to degassing. U2a is the product of weaker and shallower processes, resulting in the lowest percentage of stained lithic fragments for any of the units. U2b was emplaced by eruptions stronger than U2a but weaker than U1 and U3. Therefore, the erosion of the deep conduit is not likely the source of the 91% of the U2b lithic fragments that are stained. Instead, the flux of hot volatiles, which led to the hydrothermal alteration that produced the orange dust of U2b, is responsible for the staining of the lithic fragments. In comparison to U2b, U2c is a spatially limited unit indicative of a smaller eruption and has fewer stained lithic fragments, indicating that eruptive activity was confined to shallow depths. So, whereas shallow hydrothermal conditions operated during U2b, such conditions were absent during the production of U2c, and hence the abundance of stained lithic fragments in U2c is low. This requires that U2b and U2c had two different sources. The lithic fragments of U3 are predominantly stained. Orange dust and other stained grains are rare, implying U3 is not the product of shallow hydrothermal processes, like U2b. Therefore the higher abundance of stained lithic fragments in U3 may have come from deeper within the conduit. Alternatively, the U3 eruption could have tapped the stained lithic fragments from the shallowly hydrothermally altered vent or fumarole that produced U2b.

In summary, the proportion of lithic fragments is low in all units. However the proportion of stained lithic fragments varies by unit. The high percentage of stained

lithic fragments in U2b has been attributed to hydrothermal alteration, which also produced the orange dust characteristic of U2b. High percentages of stained lithic fragments may record the erosion of the conduit at depths conducive to hydrothermal alteration. However for U3 the source of the 85% of lithic fragments that are stained may additionally require the inclusion of grains produced as a result of the hydrothermal alteration that produced the dust and stained lithic fragments of U2b.

The Vent

The surface textures and coatings of grains reveal the vent-based processes that occurred. No chemical pitting (Heiken and Wohletz, 1985) is seen in any of the grains, nor are there any surface cracks indicative of magma interacting with water (Heiken and Wohletz, 1985; Dellino et al., 1990; Dellino and La Volpe, 1996; Büttner et al., 1999).

Coatings of ash are seen in all units and are independent of grain type. The proportion of ash-coated grains may be proportional to the F2 (grains smaller than 4.0 phi) population. U1 and U2b have low values of F2 and have the fewest ash-coated grains: 10% and 15%, respectively. U3 has more F2 material, but fewer ash-coated grains, 9%, than U1 and U2b. This can be explained when considering that lowermost U3 marks the initiation of a strong plinian eruption, and so it is feasible that the finest grain sizes, which would have otherwise coated the grains, remained in aerial suspension as the eruption column grew. U2a is ash rich and correspondingly 43% of its grains are coated in ash. U2c is even more ash rich, but only has 20% of its grains coated in ash. In this instance, the apparent relation between the proportion of ash-coated grains and F2 breaks down. The presence of an ash coating requires an abundance of fine ash, as well as an agent to adhere the ash to the grains. The agent, perhaps volatiles or precipitated

minerals, could be absent from U2c, and thus the relation between F2 and ash-coated grain abundance was not preserved. Therefore, although the abundance of F2 ash is important to the production of ash-coated grains, it alone is not sufficient to explain all the observations.

MODEL OF THE ERUPTION

Parameters

The two key objectives of this study are to determine why the eruption paused, resulting in a dual eruption instead of one large event, and to understand what U2, the deposit produced during and at the end of the hiatus, represents.

The model must fit a number of parameters. 1) The emplacement of each unit U2a by surges, U2b by fallout, and U2c is the product of a dome blast and the initial fragmentation of the U3 vanguard magma. 2) The apparent varying magma volatile contents of the units, based on the vesicularity data. 3) The eruption of U2b, despite being crystal-rich and poor in volatiles. 4) The hydrothermal alteration of U2b.

Description

Uppermost U1 was deposited by the intense phase of the plinian eruption during which pumice were deposited as a clast-supported unit. The magma was volatile rich, and the exsolved gases drove fragmentation and powered the eruption. As the eruption continued, the vesiculation and fragmentation fronts progressed deeper into the conduit (Figure 7.2a) (Di Muro et al., 2008). The erosion of the conduit resulted in the lithic fragments blocking the conduit, resulting in the cessation of plinian activity. An

increased abundance of lithic fragments at the top of the U1 sequence (Figure 3.2) (Di Muro et al., 2008) supports this interpretation. The blocking of the conduit was likely a gradual process as reflected in the switch of the sustained column to a pulsatory one, prior to the cessation of the U1 eruption. With the loss of the eruption column, the fine-grained material in suspension in the atmosphere was deposited as a thin ash layer at the same time as the coignimbrite ash from beyond the crater.

Gases from the magma below streamed through the blockage, carrying the pyroclasts that had been trapped above lithic block out of the vent where they travelled as surges, deposited as U2a (Figure 7.2b). It is possible that the conduit was not yet completely closed, allowing for limited fragmentation to occur above the barrier. This is based on the observation that the glass of U2a is more degassed than the glass of U1. If the pyroclasts of U2a were simply recycled U1 pyroclasts, the number of vesicular grains and the volume percent of vesicles, would be comparable to that of U1. The U2a surges deposited thin beds of poorly sorted ash within areas proximal to the crater and its local drainage basins.

The densest glass grains from the preceding U1 eruption would have been ejected from the vent at low velocities, if they were ejected at all (Carey and Sparks, 1986), and therefore many would have collected within the crater. Some of the low-vesicularity glass of U1 had collected with a fumarole or small vent within the crater. The rising U3 gases put the grains in motion, milling them into smaller pieces. Pyroclasts can retain heat for long periods of time, as illustrated by the elevated temperatures of the Mount St Helens pyroclastic-flow deposits two months after the eruption (Banks and Hoblitt, 1981; Rowley et al., 1981), and ignimbrite temperatures of 390°C 1 m below the surface at

fumaroles 1.5 years after the 1991 Mount Pinatubo eruption (Torres et al., 1996). The gas flux from the U3 magma continued, which kept the grains hot. Additionally, the mixture of heat and volatiles hydrothermally altered the grains within the conduit. As the milling continued, the weak grains were turned into an orange dust, which coated the rest of the grains. This was occurring simultaneously with the emplacement of U2a, as the main vent was beginning to be shut off.

With the main magma body still rising, the higher pressures and gas fluxes were great enough to allow the collected material to be carried up the conduit and out of the fumarole/vent where the retained heat allowed the material to convect within an eruption column (Figure 7.2c). The eruptions produced were pulsatory, since the collected pyroclasts inhibited the production of a sustained column, and dust-coated U2b was deposited as fallout. With this fumarole/second vent partially open, activity at the first vent waned. The final, smallest surges deposited material during the fallout of the first U2b material, possibly as a dome was beginning to be extruded over the first vent. It has been established that two sources are required to explain the overlap of the U2a and U2b deposits (see The Eruption).

Then activity at the main vent ceased, with the remaining shallow magma completing the extrusion of the dome, plugging the vent (Figure 7.2d). With the continued degassing of the ascending U3 magma, and the second vent/fumarole now the only outlet, the eruption became more vigorous. This periodically produced longer-lived eruptive pulses, as recorded by normally graded deposits.

The partially degassed vanguard magma of U3 began to fragment beneath the dome of the first vent. The flux of gas from the magma increased as the U3 magma

arrived at the near-surface, with the exsolved volatiles pressurizing the system. This pressure resulted in a vulcanian eruption that destroyed the dome over the first vent: the projectiles produced the lapilli and the fragmented U3 magma produced the voluminous fine ash of U2c (Figure 7.2e).

With the dome removed, the U3 eruption quickly commenced (Figure 7.2f). At first, it was pulsatory in style, perhaps due to residual lithic fragments still partially blocking the conduit. Then, with the decompression continuing and the magma flux to the first vent increasing, the obstacles were removed and the vent became fully open. U3 then quickly became a sustained eruption column. It is possible that activity also resumed at the small vent/fumarole from which U2b had been ejected. This is based on the observation that U3 has a high number of stained lithic fragments (Figure 5.6), comparable to that of U2b, and hence an additional hydrothermal source other than the altered walls of the conduit may be required.

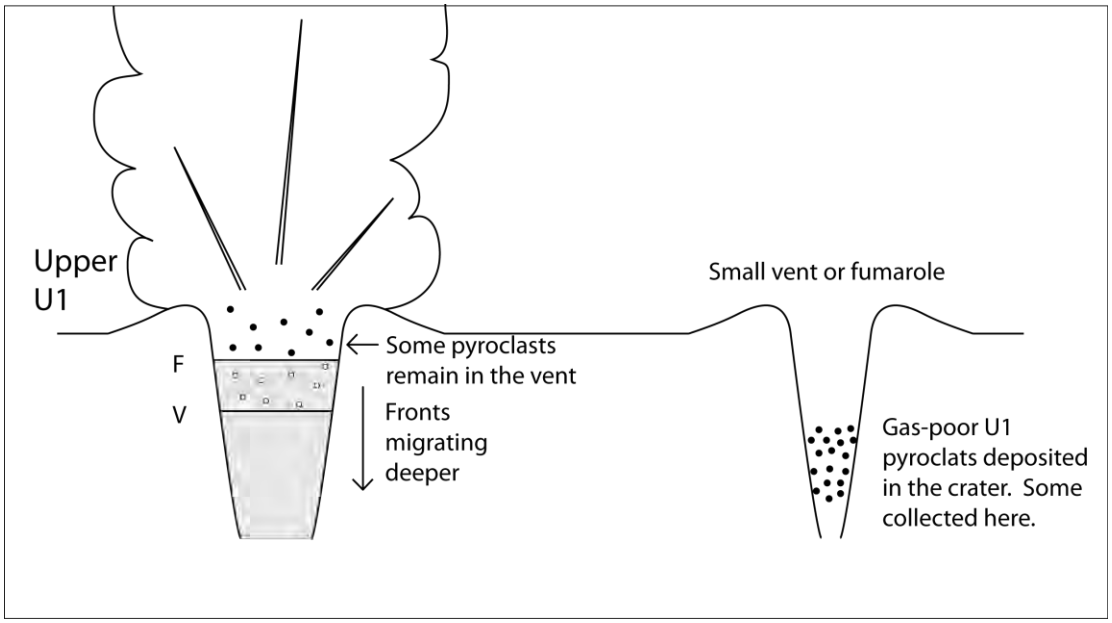

Figure 7.2a. Sketch model of the 800 BP eruption of Quilotoa. F = Fragmentation front, V = Vesiculation front. Fragmentation and vesiculation fronts migrate deeper as the eruption of U1 progresses. Material low in volatiles collects within the crater, some of which falls into a small vent or fumarole.

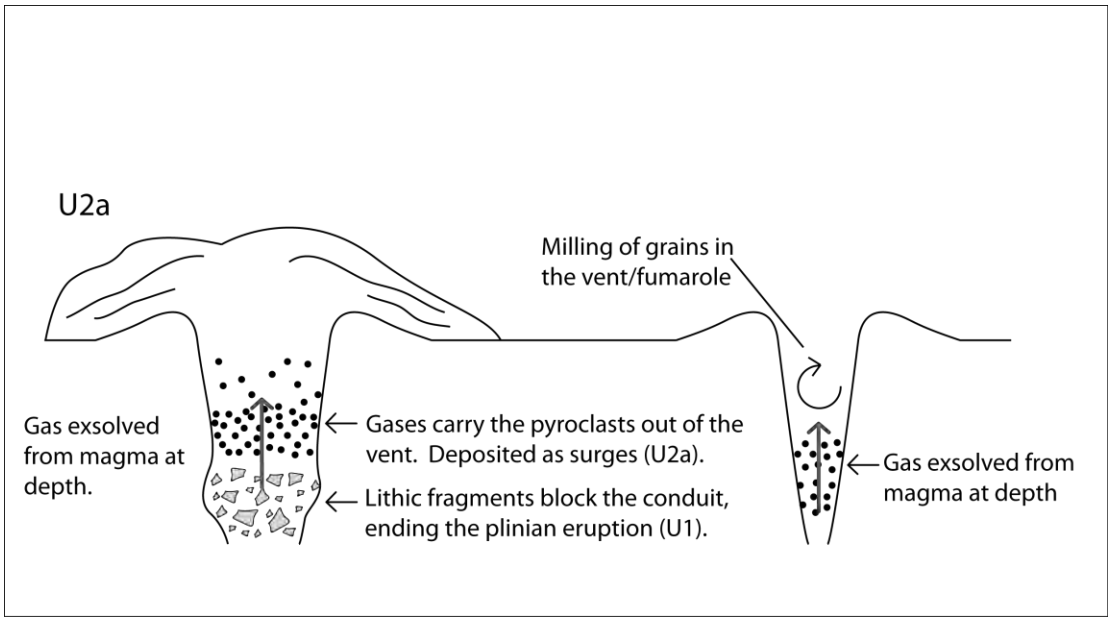

Figure 7.2b. Eroded country rock blocks the conduit, ending the plinian eruption. Gases exsolved from depth carry the remaining pyroclasts out of the vent, where they are emplaced as the surge deposits of U2a. Elsewhere, the material collected within the small vent/fumarole is milled as facilitated by the gases rising from the U3 magma at depth.

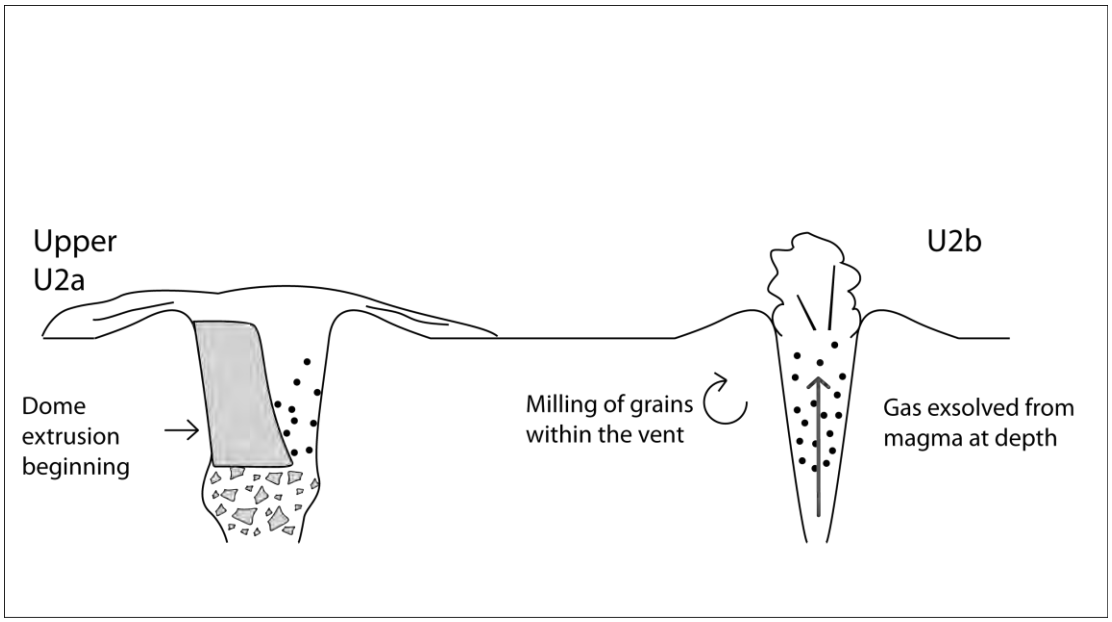

Figure7.2c. Dome extrusion at the main vent begins, partially blocking the vent. Below the small vent/fumarole gases from the magma at depth have exsolved and drive the eruption of U2b, which begins as U2a is ceasing.

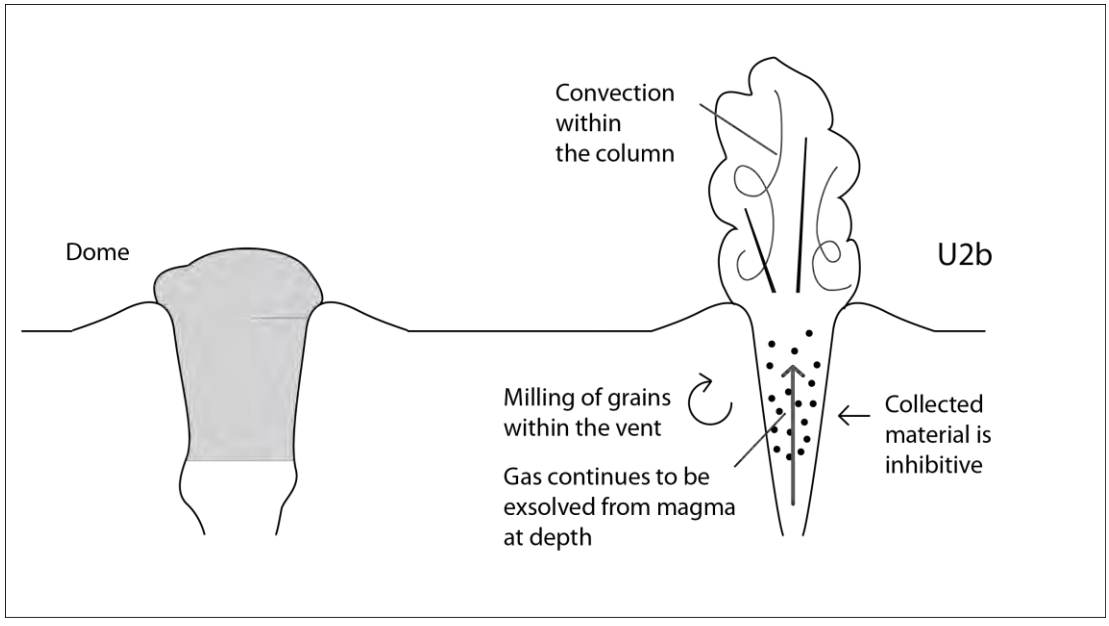

Figure7.2d. Dome emplaced over the first vent while U3 magma rises from depth. The eruption of U2b from the only active outlet intensifies.

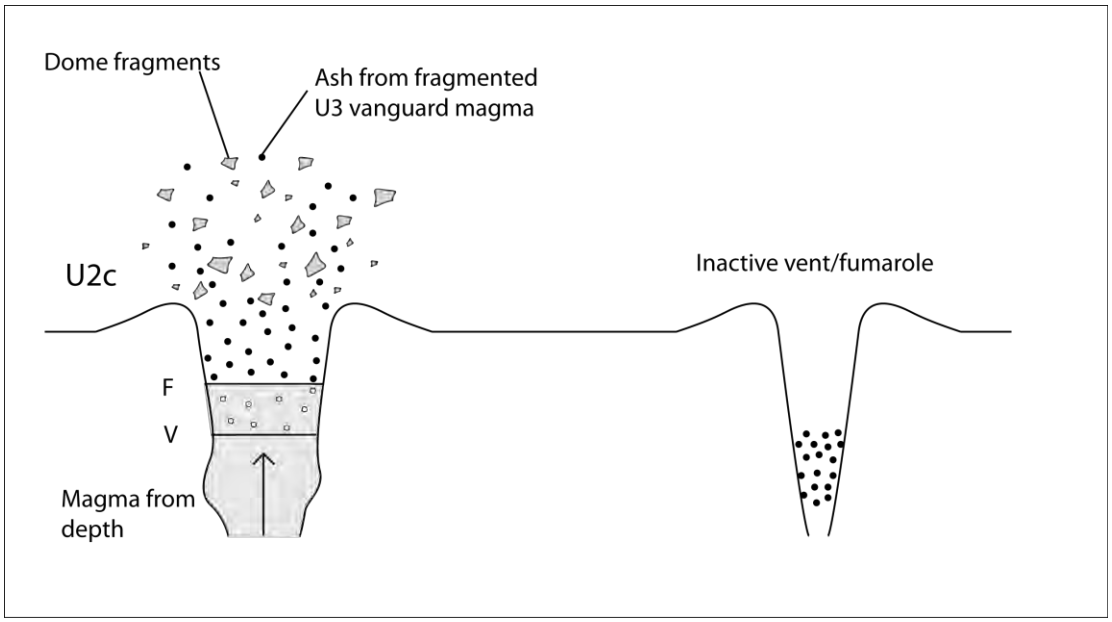

Figure 7.2e. Pressure from the magma at depth blows apart the dome over the main vent in a vulcanian eruption. Blast products and vanguard U3 magma form U2c.

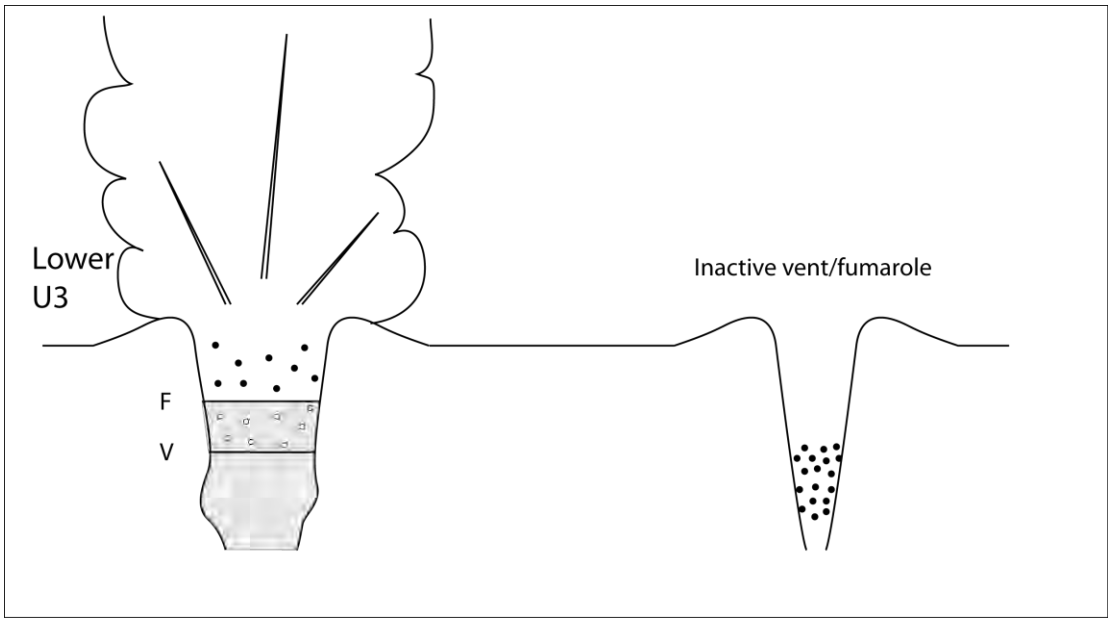

Figure 7.2f. With the dome removed, the eruption intensity increases and U3 is erupted.

Limitations

This model does have some limitations. The grain-size distribution of U2b is poor in the coarsest lapilli and fine ash (Figure 4.3). The lack of coarse lapilli has been attributed to the milling of the grains within the conduit, but the fine ash, produced as a result of the milling, is absent. It is feasible that the fine ash remained suspended in the atmosphere and was carried to distances beyond 8 km, deposited as layers too thin to be recognized as U2b. This is a viable explanation, as large proportions of fine ash from explosive eruptions are known to be deposited at great distances, and thick fine ash from the 800 BP Quilotoa eruption is found all over northern Ecuador (Mothes and Hall, 2008). Alternatively, if the elutriation of the fine material occurred within the conduit while the grains were being milled, which was at the same time U2a was being emplaced, the fine ash of U2b could have been interbedded with, and perhaps therefore lost within, U2a. If elutriated, it is likely that the fine ash was transported beyond the crater, as locality 17, the former crater rim site, is poor in fine ash (Figure 4.10). To test these hypotheses for U2b, a mildly explosive eruption, fieldwork focused on identifying the thin ash layers would be required.

To confirm that the vitric lapilli of U2c are from a dome formed during the 800 BP eruption, it is necessary to compare them to vitric lapilli of the 14,770 BP eruption. If the glass of the older lapilli is altered, then the fresh glass of the 800 BP lapilli had to be from a dome emplaced during that time, as presented in the eruption model.

Additionally, the processes behind the predominance of the 0.73 and 1.82 phi modal grain-sizes have not been identified. Although it has been determined that the 1.82 phi mode is likely associated with the crystal population, based on the higher proportion of crystals at 1.82 than at 0.73 phi, the two populations are not otherwise distinct in terms

of componentry and the reason why two nearby modal grain sizes exist has not been answered by this study.

IMPLICATIONS FOR THE ERUPTION DYNAMICS OF DUAL ERUPTIONS

With a body of eruptable magma at depth, which would later be deposited as U3, a mechanism is required to force the violent activity, characterized by the thick plinian deposits of U1, to stop. The erosion of the conduit was enough to prevent a continued eruption. Thus the system was capped, the plinian eruption ceased, and the activity entered a period of hiatus.

The 14,770 BP eruption of Quilotoa has an orange U2b-like bed, with a grain-size distribution similar to that of the 800 BP U2 unit. Therefore, a dual eruption is not unique but may have occurred at Quilotoa previously, perhaps even constituting the characteristic eruption style of Quilotoa volcano.

At Huaynaputina, Peru, the dacitic crystal-rich magma has been associated with the extrusion of domes and, in unit 4, the occurrence of small eruptions during a period of hiatus of the AD 1600 eruption (Thouret et al., 2002). This is similar to the 800 BP eruption of Quilotoa. Although more mafic in composition, the hiatus during the ~3,500 BP Pucón eruption of Volcán Villarrica, Chile (Parejas et al., 2010), shows that the occurrence of dual eruptions is not compositionally dependent, but can occur in basaltic-andesite systems.

This study was undertaken in order to understand the processes that can lead to dual eruptions, such as the two examples given above. This has implications for hazard mitigation, where it is necessary to determine whether a cessation of eruptive activity marks the end of the eruptive event, or is merely a short hiatus prior to a subsequent eruption of substantial magnitude.

CHAPTER 8

CONCLUSIONS

INTRODUCTION

The deposits of the 800 BP eruption of Quilotoa Volcano in the Ecuadorian Andes comprise four distinct units. These units have an estimated dense rock equivalent (DRE) volume of 4.9-5.5 km^3, based on proximal and medial deposits and excluding the distal deposits (Di Muro et al., 2008). Unit 1 and Unit 3 are the products of two large plinian eruptions. The deposits of Unit 2 were emplaced during the intervening hiatus period. Unit 4 represents renewed activity after Unit 3. The aim of this project was to determine why two large plinian eruptions took place within days to weeks of each other, with a pause in between, when a large amount of eruptable material was still available. To achieve this, uppermost Unit 1 to lowermost Unit 3 were studied.

FINDINGS

The conduit and the vent

All units are from a dacitic crystal-rich source (Figure 5.14) (Rosi et al., 2004; Mothes and Hall, 2008), and white and gray glass are the two dominant vitric components. Gray glass is almost exclusively dense, whereas the ratio of vesicular to dense glass varies in the white glass. The significance of the two different glass types has not been determined, but the magma appears to have been partially degassed during the production of U2a and U2c. This is reflected in both the number of vesicular grains and the vesicularity of the grains.

The inferred volatile content of the magma varies between units. However the units do share some common grain sizes, namely the modes at 0.73, 1.82 and 3.70 phi,

which indicate a common fragmentation processes for all the units. Glass is a minor component compared to crystals at 1.82 phi, and vesicularity varies widely among the units. For this reason, common crystal-size populations appear to be the most likely cause of these shared grain-size populations, with crystal size modes at about 0.73, 1.82 and 3.70 phi.

The low volume fraction of lithic fragments indicates that the vent and the conduit remained stable throughout the eruption, except at the top of U1 where the blocking of the conduit with eroded lithic fragments caused the emplacement of U1 to cease.

The grains of U2b were originally the product of the U1 eruption, but they remained in a nearby fumarole or small vent and were hydrothermally altered by volatiles flowing from depth. Milling of the grains produced orange dust, which is exclusively found on the grains of U2b. The same volatiles responsible for the alteration, exsolved from the ascending U3 magma, also helped keep the U2b grains hot, thus allowing them to couple with and heat the air in order to convect within short-lived eruption columns. U3 has a high number of lithic fragments that are stained. This can be attributed to the second plinian eruption having a deep fragmentation front, eroding the walls of the conduit at depth where the conduit is most likely to be hydrothermally altered. Alternatively, the U3 eruption could have tapped the stained lithic fragments from the shallowly hydrothermally altered vent or fumarole that produced U2b.

Transport

Transport processes had a very limited influence upon the characteristics of the deposits, other than a general thinning with distance. Changes in componentry are not related to distance, nor is the circularity of the grains or the sorting of the deposits. Some

units exhibit some relation between mean grain size, weight percent of ash and distance, but a link between overall grain-size distributions and modal grain-size populations is not discernable.

Deposition

U2a is the only unit that was possibly affected by post-depositional erosion, based on anomalously low thicknesses in some areas where the flow of ephemeral streams may have removed some of the deposits. Otherwise the stratigraphy of upper U1 through to lower U3 appears to be complete.

ERUPTION PROGRESSION

Uppermost U1 fallout was emplaced from a sustained eruption column. The erosion of the conduit capped the system, inhibiting and eventually stopping the progression of the eruption. Some of the most gas-poor grains of U1 did not travel beyond within the crater, some collecting within a fumarole or small vent.

Building pressures beneath the main vent resulted in intermittent eruptions that emplaced the surge deposits of U2a. With the main vent still mostly obstructed, gas began to escape via a fumarole or small secondary vent. Material within the conduit there was continually milled into smaller grain sizes.

Gases from the ascending U3 magma at depth pressurized the material, expelling it from the conduit, where convection driven by the heat of the grains produced a pulsatory eruption column. At the same time, activity from the main vent ceased as the dome capped the system. With one outlet and the continued rise of the U3 magma, the high gas flux caused the pulsatory columns to increase in vigor, depositing the fallout

unit of U2b. However, the vent was never fully open to permit a sustained eruption column.

Volatiles from the continually rising U3 magma increased pressures in the system, resulting in the destruction of the dome covering the first vent as a result of a single vulcanian eruption. The dome fragments are seen as lapilli in U2c and the fragmented vanguard U3 magma the ash. With the first vent fully open, the second plinian eruption ensued, depositing U3.

FUTURE WORK

There is a dearth of field data to the north of the crater. An extensive drive-through did not reveal any more outcrops. Therefore, a future field season, which would require a lot more time to overcome the topographic accessibility issues, should target this region so more complete isopach and isopleth maps can be drawn. The gathered data can be used to further characterize U2 in terms of volume and column height. Additionally, more distal sites > 8km should be sought so that the apparently limited extent of U2 can be confirmed in all directions, but to the north in particular.

Distal U2b sites should be sought to confirm that, as postulated, the missing fine ash was elutriated and deposited as what is likely a thin bed. The deposits of locality 17, the former crater rim site, are poor in fine ash (Figure 4.10), and therefore it is unlikely that the missing U2b fine ash was deposited within the crater. Additionally, U2a deposits should be examined, as it is possible that the fine ash of U2b was instead deposited at the same time that U2a was emplaced. Sites lacking data on U2c, because the unit was not initially recognized, should be revisited. This is so that the isopach and isopleth maps for

U2c can be more tightly constrained. A unidirectional distribution of the thickest beds and the largest clasts would reinforce the model of a dome blast being the source of U2c.

The search for a mechanism behind the simultaneous production of white and gray glass needs to be revisited. The proportion of these glasses varies between the units of the deposit, but, until their source is better understood, inferences as to different conduit-based processes cannot be made.

Lastly, I recommend that a similar study be undertaken to examine the 14,770 BP (Q-II (Hall and Mothes, 2008)) deposits of Quilotoa. The units have similar field characteristics to those of the 800 BP eruption. If similarities between the deposits are found, it could confirm the idea that dual eruptions are not odd or random occurrences, but typical of particular volcanoes or volcanic systems. This, in turn, would imply that conditions specific to the plumbing systems of particular volcanoes produce dual eruptions. Such a study would greatly contribute to the understanding of these phenomena, globally as well as at Quilotoa volcano, so that, for modern eruptions, the end of an eruption can begin to be distinguished from a pause in activity.

REFERENCES

Adams, N. K., de Silva, S. L., Self, S., Salas, G., Schubring, S., Permenter, J. L., and Arbesman, K., 2001, The physical volcanology of the 1600 eruption of Huaynaputina, southern Peru: Bulletin of Volcanology, v. 62, no. 8, p. 493-518.

Aguilera, E., Chiodini, G., Cioni, R., Guidi, M., Marini, L., and Raco, B., 2000, Water chemistry of Lake Quilotoa (Ecuador) and assessment of natural hazards: Journal of Volcanology and Geothermal Research, v. 97, p. 271-285.

Angermann, D., Klotz, J., and Reigber, C., 1999, Space-geodetic estimation of the Nazca–South America Euler vector: Earth and Planetary Science Letters, v. 171, p. 329-334.

Austin Erickson, A., 2007, Phreatomagmatic Eruptions of Rhyolitic Magma: A Case Study of Tepexitl Tuff Ring Serdan-Oriental Basin, Mexico: Northern Arizona University, 234 p.

Bacon, C. R., 1983, Eruptive history of Mount Mazama and Crater Lake Caldera, Cascade Range, U.S.A.: Journal of Volcanology and Geothermal Research, v. 18, p. 57-115.

Banks, N. G., and Hoblitt, R. P., 1981, Summary of temperature studies of 1980 deposits, *in* Lipman, P. W., and Mullineaux, D. R., eds., The 1980 eruptions of Mount St. Helens, Washington. Geological Survey Professional Paper 1250.

Best, M. G., 2003, Igneous and Metamorphic Petrology: Malden, MA, Blackwell publishing, 729 p.

Büttner, R., Dellino, P., and Zimanowski, B., 1999, Identifying magma-water interaction from the surface features of ash particles: Nature, v. 401, p. 688-690.

Bursik, M., 1998, Tephra dispersal, *in* Gilbert, J. S., and Sparks, R. S. J., eds., The physics of explosive volcanic eruptions: Geological Society Special Publications: London, The Geological Society.

Campita, N. R., Daag, A. S., Newhall, C. G., Rowe, G. L., and Solidum, R. U., 1996, Evolution of a small caldera lake at Mount Pinatubo, *in* Newhall, C. G., and Punongbayan, R. S., eds., Fire and Mud: eruptions and lahars of Mount Pinatubo, Philippines: Quezon City and Seattle, Philippine Institute of Volcanology and Seismology and University of Washington Press, p. 1126.

Carey, S., and Bursik, M., 2000, Volcanic plumes, *in* Sigurdsson, H., Houghton, B. F., McNutt, S. R., Rymer, H., and Stix, J., eds., Encyclopedia of volcanoes: San Diego, Academic Press, p. 1417.

Carey, S., Maria, A., and Sigurdsson, H., 2000, Use of fractal analysis for discrimination of particles from primary and reworked jökulhlaup deposits in SE Iceland: Journal of Volcanology and Geothermal Research, v. 104, no. 1-4, p. 65-80.

Carey, S., and Sparks, R. S. J., 1986, Quantitative models of the fallout and dispersal of tephra from volcanic eruption columns Bulletin of Volcanology, v. 48, p. 109-125.

Cioni, R., D'Oriano, C., and Bertagnini, A., 2008, Fingerprinting ash deposits of small scale eruptions by their physical and textural features: Journal of Volcanology and Geothermal Research, v. 177, p. 277-287.

de Rosa, R., 1999, Compositional modes in the ash fraction of some modern pyroclastic deposits: their determination and significance Bulletin of Volcanology, v. 61, p. 162-173.

Dellino, P., Frazzetta, G., and La Volpe, L., 1990, Wet surge deposits at La Fossa di Vulcano: Depositional and eruptive mechanisms: Journal of Volcanology and Geothermal Research, v. 43, no. 1-4, p. 215-233.

Dellino, P., Isaia, R., La Volpe, L., and Orsi, G., 2001, Statistical analysis of textural data from complex pyroclastic sequences: implications for fragmentation processes of the Agnano-

Monte Spina Tephra (4.1 ka), Phlegraean Fields, southern Italy: Bulletin of Volcanology, v. 63, no. 7, p. 443-461.
Dellino, P., and La Volpe, L., 1996, Image processing analysis in reconstructing fragmentation and transportation mechanisms of pyroclastic deposits. The case of Monte Pilato-Rocche Rosse eruptions, Lipari (Aeolian islands, Italy): Journal of Volcanology and Geothermal Research, v. 71, p. 13-29.
Dellino, P., and Liotino, G., 2002, The fractal and multifractal dimension of volcanic ash particles contour: a test study on the utility and volcanological relevance: Journal of Volcanology and Geothermal Research, v. 113, p. 1-18.
Di Muro, A., 2002, The transitional dynamics of sustained Plinian eruptions. PhD Thesis.: University of Pisa, 223 p.
Di Muro, A., Rosi, M., Aguilera, E., Barbieri, R., Massa, G., Mundula, F., and Pieri, F., 2008, Transport and sedimentation dynamics of transitional explosive eruption columns; the example of the 800 BP Quilotoa plinian eruption (Ecuador): Journal of Volcanology and Geothermal Research, v. 174, p. 307-324.
Fierstein, J., and Nathenson, M., 1992, Another look at the calculation of fallout tephra volumes: Bulletin of Volcanology, v. 54, p. 156-167.
Fink, J. H., and Anderson, S. W., 2000, Lava domes and coulees, *in* Sigurdsson, H., Houghton, B. F., McNutt, S. R., Rymer, H., and Stix, J., eds., Encyclopedia of volcanoes: San Diego, Academic Press, p. 1417.
Folk, R. L., 1974, Petrology of sedimentary rocks: Austin, Hemphill, 182 p.
Garreaud, R. D., 2009, The Andes climate and weather: Advances in Geoscience, v. 22, p. 3-11.
Gómez-Tuena, A., and Carrasco-Núñez, G., 1999, Fragmentation, transport and deposition of a low-grade ignimbrite: The Citlaltépetl Ignimbrite, Eastern México: Bulletin of Volcanology, v. 60, no. 6, p. 448-464.
Gutscher, M.-A., Malavieille, J., Lallamand, S., and Collot, J.-Y., 1999, Segmentation of the North Andean margin: impact of the Carnegie Ridge collision: Earth and Planetary Science Letters, v. 168, no. 3-4, p. 255-270.
Hall, M. L., and Mothes, P. A., 2008, Quilotoa Volcano - Ecuador: An overview of young dacitic volcanism in a lake-filled caldera: Journal of Volcanology and Geothermal Research, v. 176, p. 44-55.
Hall, M. L., Samaniego, P., Le Pennec, J. L., and Johnson, J. B., 2008, Ecuadorian Andes volcanism: A review of Late Pliocene to present activity: Journal of Volcanology and Geothermal Research, v. 176, p. 1-6.
Hay, R. L., 1959, Formation of the Crystal-Rich Glowing Avalanche Deposits of St. Vincent, B.W.I: The Journal of Geology, v. 67, no. 5, p. 540-562.
Heiken, G., and Wohletz, K., 1985, Volcanic ash, Los Alamos series in basic and applied sciences: Berkeley, University of California Press, 246 p.
Herd, R. A., Edmonds, M., and Bass, V. A., 2005, Catastrophic lava dome failure at Soufrière Hills Volcano, Montserrat, 12-13 July 2003: Journal of Volcanology and Geothermal Research, v. 148, no. 3-4, p. 234-252.
Holasek, R. E., Woods, A. W., and Self, S., 1996, Experiments on gas-ash separation processes in volcanic umbrella plumes: Journal of Volcanology and Geothermal Research, v. 70, no. 3-4, p. 169-181.
Hooten, J. A., 1999, Phreatomagmatic Diatremes of the Western Hopi Buttes Volcanic Field, Navajo Nation, Arizona,: University of Arizona, 140 p.
Houghton, B. F., Carey, R. J., Cashman, K. V., Wilson, C. J. N., Hobden, B. J., and Hammer, J. E., 2010, Diverse patterns of ascent, degassing, and eruption of rhyolite magma during the

1.8 ka Taupo eruption, New Zealand: Evidence from clast vesicularity: Journal of Volcanology and Geothermal Research, v. 195, no. 1, p. 31-47.
Inman, D. L., 1952, Measures for describing the size distribution of sediments: Journal of Sedimentary Research, v. 22, no. 3, p. 125-145.
Jaupart, C., 1998, Glass loss from magmas through conduit walls during eruption, *in* Gilbert, J. S., and Sparks, R. S. J., eds., The physics of explosive volcanic eruptions: Geological Society Special Publications: London, The Geological Society.
Mader, H. M., 1998, Conduit flow and fragmentation, *in* Gilbert, J. S., and Sparks, R. S. J., eds., The physics of explosive volcanic eruptions: Geological Society Special Publications: London, The Geological Society.
Morrissey, M. M., and Mastin, L. G., 2000, Vulcanian Eruptions, *in* Sigurdsson, H., Houghton, B. F., McNutt, S. R., Rymer, H., and Stix, J., eds., Encyclopedia of volcanoes: San Diego, Academic Press, p. 1417.
Mothes, P. A., and Hall, M. L., 2008, The plinian fallout associated with Quilotoa's 800 yr BP eruption, Ecuadorian Andes: Journal of Volcanology and Geothermal Research, v. 176, p. 56-69.
Orsi, G., Gallo, G., Wohletz, K., Yu, E., and Bonani, G., 1992, A comprehensive study of pumice formation and dispersal: the Cretaio Tephra of Ischia (Italy): Journal of Volcanology and Geothermal Research, v. 53, p. 329-354.
Paladio-Melosantos, M. L., Solidum, R. U., Scott, W. E., Quiambao, R. B., Umbal, J. V., Rodolfo, K. S., Tubianosa, B. S., Delos Reyes, P. J., Alonso, R. A., and Ruelo, H. B., 1996, Tephra falls of the 1991 Eruption of Mount Pinatubo, *in* Newhall, C. G., and Punongbayan, R. S., eds., Fire and mud: eruptions and lahars of Mount Pinatubo, Philippines: Quezon City and Seattle, Philippine Institute of Volcanology and Seismology and University of Washington Press, p. 1126.
Papale, P., and Rosi, M., 1993, A case of no-wind plinian fallout at Pululagua caldera (Ecuador) - implications for models of clast dispersal: Bulletin of Volcanology, v. 55, no. 7, p. 523-535.
Parejas, C. S., Druitt, T. H., Robin, C., Moreno, H., and Naranjo, J. A., 2010, The Holocene Pucn eruption of Volcan Villarrica, Chile: deposit architecture and eruption chronology: Bulletin of Volcanology, v. 72, no. 6, p. 677-692.
Polacci, M., Papale, P., and Rosi, M., 2001, Textural heterogeneities in pumices from the climactic eruption of Mount Pinatubo, 15 June 1991, and implications for magma ascent dynamics: Bulletin of Volcanology, v. 63, no. 2, p. 83-97.
Pyle, D. M., 1989, The thickness, volume and grainsize of tephra fall deposits.: Bulletin of Volcanology, v. 51, p. 1-15.
-, 1995, Assessment of the minimum volume of tephra fall deposits: Journal of Volcanology and Geothermal Research, v. 69, p. 379-382.
Rasband, W. S., 1997-2009, ImageJ: Bethesda, Maryland, U. S. National Institues of Health.
Rolandi, G., Barrella, A. M., and Borrelli, A., 1993, The 1631 eruption of Vesuvius: Journal of Volcanology and Geothermal Research, v. 58, no. 1-4, p. 183-201.
Rose, W., Self, S., Murrow, P., Bonadonna, C., Durant, A., and Ernst, G., 2008, Nature and significance of small volume fall deposits at composite volcanoes: Insights from the October 14, 1974 Fuego eruption, Guatemala: Bulletin of Volcanology, v. 70, no. 9, p. 1043-1067.
Rose, W. I., and Durant, A. J., 2009, Fine ash content of explosive eruptions: Journal of Volcanology and Geothermal Research, v. 186, no. 1-2, p. 32-39.

Rosi, M., 1998, Plinian eruption columns: particle transport and fallout, *in* Freundt, A., and Rosi, M., eds., From magma to tephra: Modelling physical processes of explosive volcanic eruptions: Developments in volcanology: Amsterdam, Elsevier, p. 318.

Rosi, M., Landi, P., Polacci, M., Di Muro, A., and Zandomeneghi, D., 2004, Role of conduit shear on ascent of the crystal-rich magma feeding the 800-year-b.p. Plinian eruption of Quilotoa Volcano (Ecuador): Bulletin of Volcanology, v. 66, p. 307-321.

Rowley, P. D., Kuntz, M. A., and Macleod, N. S., 1981, Pyroclastic-flow deposits, *in* Lipman, P. W., and Mullineaux, D. R., eds., The 1980 eruptiuons of Mount St. Helens, Washington. Geological Survey Professional Paper 1250.

Sarna-Wojcicki, A. M., Shipley, S., Waitt, J., Richard B, Dzurisin, D., and Wood, S. H., 1981, Areal distribution, thickness, mass, volume, and grain size of air-fall ash from the six major eruptions of 1980., *in* Lipman, P. W., and Mullineaux, D. R., eds., The 1980 eruptiuons of Mount St. Helens, Washington.

Scott, W. E., Hoblitt, R. P., Torres, R. C., Self, S., Martinez, M. L., and Nillos, J. T., 1996, Pyroclastic flows of the June 15, 1991, climactic eruption of Mount Pinatubo, *in* Newhall, C. G., and Punongbayan, R. S., eds., Fire and Mud: eruptions and lahars of Mount Pinatubo, Philippines: Quezon City and Seattle, Philippine Institute of Volcanology and Seismology and University of Washington Press, p. 1126.

Sheridan, M. F., Wohletz, K. H., and Dehn, J., 1987, Discrimination of grain-size subpopulations in pyroclastic deposits: Geology, v. 15, no. 4, p. 367-370.

Sparks, R. S. J., Self, S., and Walker, G. P. L., 1973, Products of Ignimbrite Eruptions: Geology, v. 1, no. 3, p. 115-118.

Sparks, R. S. J., and Walker, G. P. L., 1977, The significance of vitric-enriched air-fall ashes associated with crystal-enriched ignimbrites: Journal of Volcanology and Geothermal Research, v. 2, no. 4, p. 329-341.

Sruoga, P., Llambías, E. J., Fauqué, L., Schonwandt, D., and Repol, D. G., 2005, Volcanological and geochemical evolution of the Diamante Caldera-Maipo volcano complex in the southern Andes of Argentina (34°10'S): Journal of South American Earth Sciences, v. 19, no. 4, p. 399-414.

Taddeucci, J., and Palladino, D., 2002, Particle size-density relationships in pyroclastic deposits: inferences for emplacement processes: Bulletin of Volcanology, v. 64, no. 3, p. 273-284.

Taddeucci, J., Pompiliob, M., and Scarlato, P., 2004, Conduit processes during the July–August 2001 explosive activity of Mt. Etna (Italy): inferences from glass chemistry and crystal size distribution of ash particles: Journal of Volcanology and Geothermal Research, v. 137, p. 33-54.

Tatsumi, Y., and Eggins, S., 1995, Subduction Zone Magmatism, Frontiers in Earth Sciences, Blackwell Science.

Thorpe, R. S., and Brown, G. C., 2003, The field description of igneous rocks, Geological Society of London Handbook: Chichester, John Wiley and Sons, 154 p.

Thouret, J.-C., Jasmine, D., and Eissen, J.-P., 1999, Largest explosive eruption in historical times in the Andes at Huaynaputina volcano, A.D. 1600, southern Peru: Geology, v. 27, no. 5, p. 435-438.

Thouret, J.-C., Juvigné, E., Gourgaud, A., Boivin, P., and Dávila, J., 2002, Reconstruction of the AD 1600 Huaynaputina eruption based on the correlation of geologic evidence with early Spanish chronicles: Journal of Volcanology and Geothermal Research, v. 115, p. 529-570.

Torres, R. C., Self, S., and Martinez, M. L., 1996, Secondary pyroclastic flows from the June 15, 1991, ignimbrite of Mount Pinatubo, *in* Newhall, C. G., and Punongbayan, R. S., eds., Fire and Mud: eruptions and lahars of Mount Pinatubo, Philippines: Quezon City and Seattle,

Philippine Institute of Volcanology and Seismology and University of Washington Press, p. 1126.
Valentine, G. A., 1998, Eruption column physics, *in* Freundt, A., and Rosi, M., eds., From magma to tephra: Modelling physical processes of explosive volcanic eruptions: Developments in volcanology: Amsterdam, Elsevier, p. 318.
van Hunen, J., van den Berg, A. P., and Vlaar, N. J., 2002, On the role of subducting oceanic plateaus in the development of shallow flat subduction: Tectonophysics, v. 352, no. 3-4, p. 317-333.
Vuille, M., Bradley, R. S., and Keimig, F., 2000, Climate Variability in the Andes of Ecuador and Its Relation to Tropical Pacific and Atlantic Sea Surface Temperature Anomalies: Journal of Climate, v. 13, no. 14, p. 2520.
Wadge, G., Herd, R., Ryan, G., Calder, E. S., and Komorowski, J. C., 2010, Lava production at Soufriere Hills Volcano, Montserrat: 1995-2009: Geophysical Research Letters, v. 37, p. 5.
Walker, G. P. L., 1971, Grain-size characteristic of pyroclastic deposits: Journal of Geology, v. 79, p. 696-714.
-, 1983, Ignimbrite types and ignimbrite problems: Journal of Volcanology and Geothermal Research, v. 17, no. 1-4, p. 65-88.
White, J. D. L., and Houghton, B. F., 2006, Primary volcaniclastic rocks: Geology, v. 34, no. 8, p. 677-680.
Wilson, C. J. N., and Walker, G. P. L., 1985, The Taupo Eruptions, New Zealand I. General aspects: Philosophical transactions of the Royal Society of London. A, v. 314, p. 199-228.
Wilson, L., Sparks, R. S. J., and Walker, G. P. L., 1980, Explosive volcanic-eruptions .4. The control of magma properties and conduit geometry on eruption column behavior: Geophysical Journal of the Royal Astronomical Society, v. 63, no. 1, p. 117-148.
Wohletz, K., 2007, SFT (Sequential Fragmentation/Transport) Regents of the University of California.
Wohletz, K. H., Sheridan, M. F., and Brown, W. K., 1989, Particle-size distributions and the sequential fragmentation transport-theory applied to volcanic ash: Journal of Geophysical Research-Solid Earth and Planets, v. 94, no. B11, p. 15703-15721.
Wolfe, E. W., and Hoblitt, R. P., 1996, Overview of the Eruptions, *in* Newhall, C. G., and Punongbayan, R. S., eds., Fire and Mud: eruptions and lahars of Mount Pinatubo, Philippines: Quezon City and Seattle, Philippine Institute of Volcanology and Seismology and University of Washington Press, p. 1126.
Woods, A. W., 1998, Observations and models of volcanic eruption columns, *in* Gilbert, J. S., and Sparks, R. S. J., eds., The physics of explosive volcanic eruptions: Geological Society Special Publications: London, The Geological Society.
Zimanowski, B., Wohletz, K., Dellino, P., and Büttner, R., 2003, The volcanic ash problem: Journal of Volcanology and Geothermal Research, v. 122, p. 1-5.